# A Study of the Consolidation Process of Cu from Powder to Plate by Compression Shearing Method

TOHOKU UNIVERSITY
Graduate School of Engineering

# A Study of the Consolidation Process of Cu from Powder to Plate by Compression Shearing Method

# (圧縮せん断法による
# 銅粉末の薄板への固化成形プロセスに関する研究)

A dissertation submitted for the degree of Doctor of Philosophy (Engineering)
Department of Mechanical Systems and Design

by

Sho TAKEDA

January 16, 2018

# A Study of the Consolidation Process of Cu from Powder to Plate by Compression Shearing Method

Sho Takeda

## Abstract

There are various inhibitions to making sustainable development in human society, such as depletion of reserve resources, environmental pollution, mass production, and mass consumption. To overcome these problems, developing new materials and proposing new materials operation methods are required in the field of materials science.

One method for developing such metal materials that the author is focusing on is a novel powder molding technique called the compression shearing method at room temperature (COSME-RT). COSME-RT is a molding method in which metal powder is consolidated into a thin plate material by applying biaxial forces at room temperature and an ambient atmosphere. The most notable feature of this method is that it can fabricate materials without heat treatment. Therefore, with this method, it is possible to fabricate materials that are vulnerable to heat.

There are some issues to be solved before COSME-RT can be put into practical use. For example, the consolidation mechanism of metal by COSME-RT is a key issue that has not been clarified in detail yet. A major reason behind the lack of progress in mechanism clarification is the difficulty in controlling and visualizing the process of COSME-RT. To solve this issue, the author attempts to clarify the bonding mechanism of powder particles by COSME-RT by controlling the shearing force applied to the powder particles and controlling the COSME-RT process.

In Chapter 1, the social and industrial backgrounds of materials and their molding methods are introduced. There are several requirements for materials in industrial use, and COSME-RT appears to be one solution for meeting these requirements. The objective of the author's thesis is proposed in this chapter.

Chapter 2 introduces the experimental details. In this chapter, experimental and analytical methods are explained; such as a COSME-RT apparatus and a linear tribometer, analytical instruments, and the raw materials used for experiments, such as copper (Cu) powder. After the experimental details have been presented, two experimental approaches to control the forming process of materials by COSME-RT are proposed in Chapter 3 and Chapter 4. These approaches are intended to achieve the objective presented in Chapter 1.

In Chapter 3, the method of suppressing a shearing force applied to the powder particles by dispersing solid lubricant particles in the pure Cu powder particles is explained. This explanation allows for understanding of the effect of the shearing force on the consolidation process of copper by COSME-RT. Molybdenum disulfide ($MoS_2$) powder is used as a dispersed solid lubricant. The Cu/$MoS_2$ samples are formed under several shearing distances and their microstructures are observed. The microstructural change related to the reduction of the applied shearing force is discussed. From this experiment, it is suggested that the dispersed $MoS_2$ powder particles suppress the progress of the consolidation process of the Cu powder by dissipating the applied shearing force. Therefore, the

applied shearing force appears to be an important factor in promoting metal consolidation by COSME-RT. In addition, the author successfully controls the extent of consolidation of COSME-RT by dispersing $MoS_2$ into a Cu matrix.

In Chapter 4, a unidirectional friction experiment is performed to clarify the mechanism of interparticle bonding from a new point of view. Friction experiments that repeatedly makes spherical sliding contact on the uniaxially compressed Cu powder samples in the local area are used as a tool for visualizing the timeline information of interparticle bonding during the compression shearing process. In this experiment, the stress applied to the sample decreases from the surface to its inside. Bonding conditions of the powder particles change in the depth direction of the sample. The relation between the normal loads applied, the number of sliding cycles, and the microstructural change of the powder particles is investigated by morphological and cross-sectional observations of the uniaxially compressed pure Cu powder samples after the friction experiments. The results of structural observations clarify that the normal load $P$ had a greater effect on the deformation of the powder particles than the number of the sliding cycles $N$. A numerical analysis using Hamilton's model reveals that the tensile stress applied to the powder particles along the sliding direction is the most effective stress to the interparticle bonding process.

In Chapter 5, the findings obtained from the previous experiments and the previous research results are considered and the mechanism of materials consolidated by COSME-RT is discussed. The results of the experiments suggests that the bonding process of the powder particle proceeds in the order of, (1) plastic deformation, (2) initial crystal refinement to micro size, (3) bonding by local sliding between powder particles, (4) crystal refinement to sub-micro size. In addition, the results suggest that the shearing force causes the local sliding between the powder particles, and the bonding process proceeds because of this sliding. In conclusion, a new consolidation model of pure Cu from powder to plate by COSME-RT is proposed.

Finally, the summary of my research findings and the future perspectives of this study are stated in the Chapter 6, "General conclusion and perspective". As the result of this study, the author successfully obtained new knowledge about the consolidation process of Cu from powder to plate using COSME-RT, especially regarding a new model of powder particle bonding by COSME-RT.

The author attends a double doctoral degree program between the Graduate School of Engineering, Tohoku University, Japan and Laboratoire de Tribologie et Dynamique des Systèmes, École Centrale de Lyon, France. The research project of this thesis is based on the collaboration of these two research institutes.

# Contents

# List of figures

# List of Tables

# Chapter 1
# Introduction

The main objective of this study is to understand the consolidation mechanism of the metal powder to thin plate by the method using biaxial force, termed as a compression shearing method. It means that understanding the bonding mechanism of the metal powder particles by applying two axes forces.

The aim of this chapter is to present a general overviews about materials and their molding methods by reviewing the literatures.

Chapter 1 starts with a social background of metal materials and their molding methods. The requirements from the industrial society to metal materials and the problems of liquid-state material molding method are mainly described.

Subsequently, as the solutions of these problems, several solid-state molding methods of metal materials are presented. Features, advantages, and drawbacks of the methods are introduced.

Then, a novel molding technique, a compression shearing method are mainly explained. By introducing previous studies of this method, it is described that the compression shearing method will be one of the solutions to meet the requirements for materials.

However, the consolidation mechanism of materials by this method is not clarified yet. Finally, I propose that the way to clarify the material consolidation mechanism by the compression shearing method from the point of view of the contact mechanism.

## 1.1 Social background

Presently, there are many problems that jeopardize the sustainable development of human society, such as circulatory product development to solve mass consumption and mass disposal, alternative element strategies to cope with depletion of resources, reduction of environmental pollutant, overcoming poverty and hunger, and treatment and prevention of intractable diseases. To solve these problems, development of new materials and materials utilization processes are required. For instance, for elements that have low reserves such as rare earth elements and whose production countries are also limited, elemental strategy projects aiming at reduction of their usage and development of alternative metals exhibiting similar functionalities has been started [(1-1)]. Therefore, not only a high strength is obvious

required but also functional properties are also highly desirable for metal materials to be used in ever-demanding technologies. To make improvement on such requirements, several methods to mold metals have been attempted.

Firstly, there are two main ways to mold metal materials, that is the liquid processing and the solid processing.

## 1.2 Liquid and solid processing

### 1.2.1 Liquid processing

The liquid processing is the process using a liquid metal, generally it called as a molten metal [1-2]. The liquid processing is a casting method in other words. The principle of a casting method is as shown in Fig. 1-1 although there are various kinds of methods such as a sand casting, a die casting, and a lost wax casting. The mold with desired shape is prepared, and the molten metal is poured into it and is filled. By cooling the mold and the metal, the material has the transferred shape of the mold is formed. A material formed by a casting method is called as a casting material or just a casting. Starting materials of the almost metal products are casting materials. The casting materials are processed to the final shape by performing a removal processing such as a cutting and a polishing, and a plastic working such as a rolling and a stamping.

The material with the shape close to the final product can be fabricated by a casting method because it can transfer the complex shapes from the molds. However, the casting method needs a high temperature process because it use the molten metal, and a high temperature process leads the some problems. For instance, the casting method needs enormous energy for a high temperature process. The melting point of steel, which is the most widely used metal material, is around 1400 to 1600 Celsius degrees, and a lot of energy is required for high temperature process. In addition, the casting method is not suited for fabrication of metal/metal or metal/non-metal composite materials because a chemical reaction between different materials produces compounds having undesirable properties.

From these facts, the solid state processing appears to be better in the point without high temperature process. Even during the solid state processing such as a powder metallurgy, the process temperature increases several hundred Celsius degrees, but it is lower than molten temperatures. Therefore, the solid state processing appears to be one of solutions for the problems caused by the high temperature process during the metal molding processing.

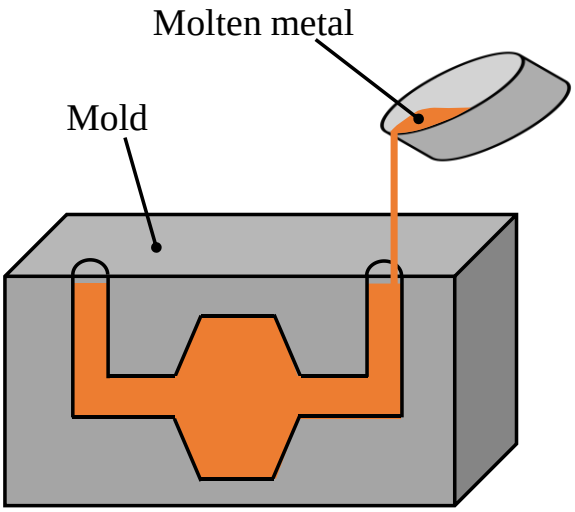


**Fig. 1-1 Schematic illustration of casting.**

## 1.2.2 Solid processing

The solid processing is the metal molding method using a solid metal for the starting material. For the solid processing, there are methods using bulk or plate materials as starting materials such as a rolling and an extrusion molding and methods using a powder material such as a powder metallurgy and a cold spray.

Fig. 1-2 shows the schematic illustration of the rolling method [1-2]. First, the bulk material is bitten between a pair of parallel rolls rotating by the friction at high temperature or at room temperature. Thereafter, the thickness of the material is reduced by the compressive force from the rolls and the material is stretched in the length direction. Thereby, the sheet material, the bar material, and the tube material are fabricated.

The rolling method and the extrusion molding methods using a casting material as a starting material shown in Fig. 1-2 have the same problems as the casting method in that the molding of composite materials is difficult. For instance, in the rolling method, layered composite materials can be fabricated by using laminated plate materials of different materials, but it is difficult to form composites having homogeneously dispersed particles in a matrix material.

Therefore, I focused on the methods using a powder material as a starting material. By this kind of methods, composite materials and alloy can be fabricated by using a mixed powder of different materials as a starting material.

In the next section, I describe methods using a powder material as a starting material in detail.

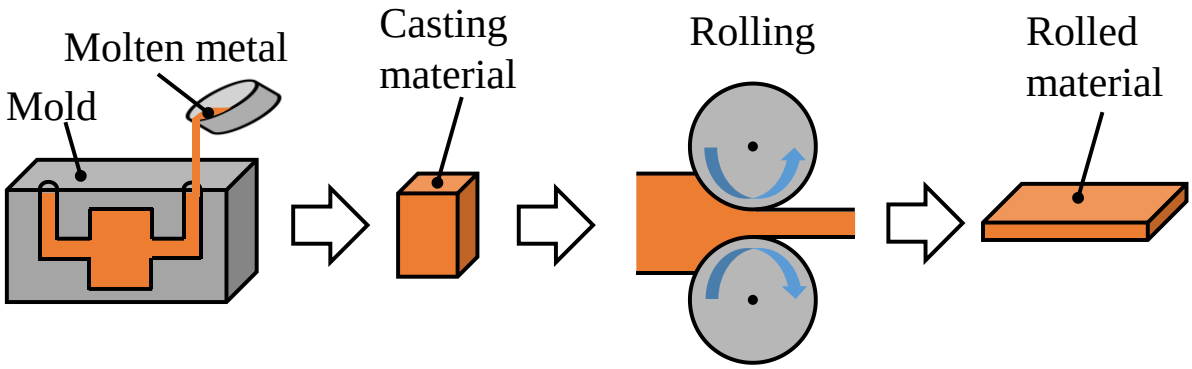


**Fig. 1-2 Schematic illustration of rolling method.**

## 1.3 Overview of metal powder molding methods

### 1.3.1 Diffusion process (Powder metallurgy)

Most common method to mold powder material to bulk material is a powder metallurgy. The powder metallurgy is the method to mold the bulk material from powder material. Fig. 1-3 shows the schematic illustration of the powder metallurgy process. First, the feedstock powder is put into the mold. A compressive stress is applied to the powder thought the mold, then the compressed material is fabricated. The final form is consolidated by sintering and cooling this compressed material [1-3, 1-4].

The powder metallurgy easily can mold composite materials by using a mixed powder as a feedstock, and it is also used to mold unique materials which have high melting points or composites consists of materials which have totally different melting points [1-5]. The powder metallurgy is characterized as follow. It can bond the powder particles each other by heating them to the temperature below their melting point. In the early stage of the powder metallurgy process, oxide films covering powder particles are fractured by heating so that the particles are partly bonded, then a constricted joint called as a neck is formed. The areas of the joints expand and the powder becomes a dense material by continuing the heating process.

Although the powder metallurgy can form a dense material, it is also possible to fabricate a porous material by controlling the conditions of the heating process. Porous materials formed by the powder metallurgy which are used as bearings with self-lubricating properties by impregnating lubricating oils [1-6]. Usually, additives improve abrasion resistance or formability of materials, or powder of alloys is used as a starting material. However, attention is needed when fabricating pure metal material by the powder metallurgy. Especially at sintering of pure metal materials such as pure Cu, powder particles melt without forming necks. Therefore, fabrications of porous pure metal materials are difficult under a non-pressurized environment.

In addition, the powder metallurgy methods can be divided into several methods by the difference of powder mixing and sintering methods.

As a one of typical mixing methods of feedstock powders, Fig. 1-4 shows the schematic illustration of a mechanical alloying method. Powders of different materials and hard balls are put into a mixing container, and the powders are stirred by rotating the container. The pulverization, work hardening, or alloying of different kinds of powders are occurred by the collision energy generated when the balls collide to the powder particles.

As the name suggests, the mechanical alloying was developed as a method to fabricate an oxide dispersion-strengthened alloy by Benjamin in 1970 [1-7]. Materials fabricated by the mechanical alloying exhibit excellent mechanical properties due to dispersion strengthening by finely and homogeneously dispersed reinforcements and strengthening by work hardening and crystal grain refinement. Powder particles alloyed by the mechanical alloying is usually needed to be formed to a bulk material by sintering in order to use as a practical material. Recently, the mechanical alloying technique is also applied to the fabrication of the composite materials, and the researches for improvement of material strength by dispersing various ceramics in the metal matrix materials have been attempted [1-8].

As a one of typical sintering methods, Fig. 1-5 shows the schematic illustration of a spark plasma sintering method (SPS). SPS is the spark sintering processing developed by Dr. Kiyoshi Inoue of Japax Inc. in 1962 [1-9, 1-10].

In the SPS, the oxide films of the powder particles are removed by discharging a spark between the powder particles, and the particles are bonded by Joule heat. The SPS has been widely used because of its short sintering processing time, because rapid heating and cooling processes are possible.

In these powder metallurgical techniques, not only the development of composites aimed at material reinforcement but also the development of a metal-based solid lubricant-dispersed composite material by using a powder metallurgy has been attempted [1-11, 1-12, 1-13].

It has been clarified by Suzuki et al. that a steel (SUS304)-based molybdenum disulfide ($MoS_2$)-dispersed sintered composite material exhibited excellent tribological property in a vacuum at a high temperature of 450°C [1-11].

In addition, the development a Cu-based $MoS_2$-dispersed composite material has been attempted [1-12]. According to the article published in 2003, the compound of Cu and $MoS_2$, $CuMo_2S_3$ is produced during the molding process even the sintering is performed in a nitrogen atmosphere which is an inert gas to prevent an oxidation of $MoS_2$ and the wear resistance of the material is degraded (Fig. 1-6).

As described above, in the powder metallurgy, a tribological property of a material can be improved by dispersing a lubricant in a matrix material. However, it is sometimes necessary to disperse a relatively large amount of lubricant considering the decrease of lubricant due to the chemical reaction because the lubricant chemically deteriorates with the matrix metal material [13]. When the amount of the lubricant

which is softer than matrix material increases, the amount of matrix material is relative decreased and the material strength of the composite will be degraded. Therefore, there appears to be a trade-off relation between a tribological property and a material strength of a composite material formed by the powder metallurgy.

Hence, even the powder metallurgy fabricates the materials at the temperature lower than the melting point of the materials, sometimes the material properties is deteriorated by heating process depending on the combination of the starting materials.

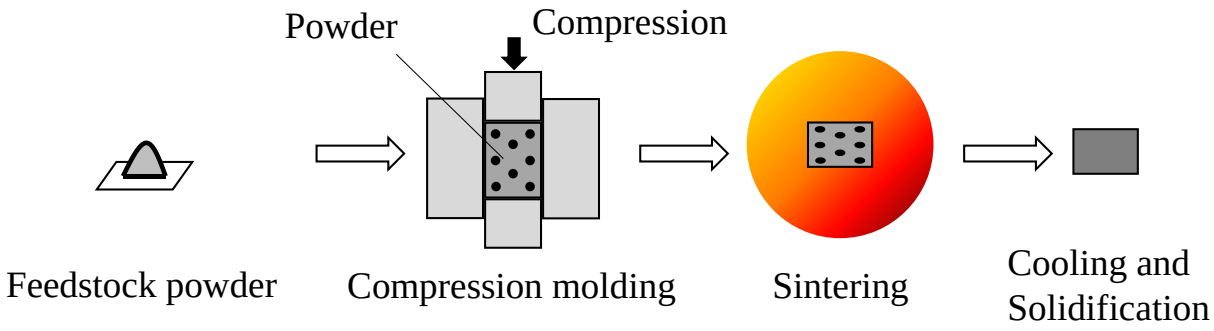


**Fig. 1-3 Schematic illustration of powder metallurgy.**

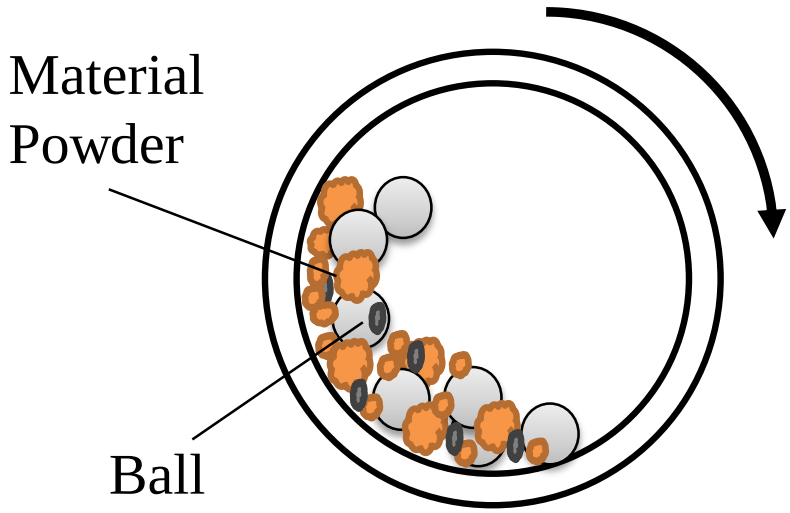


**Fig. 1-4 Schematic illustration of mechanical alloying.**

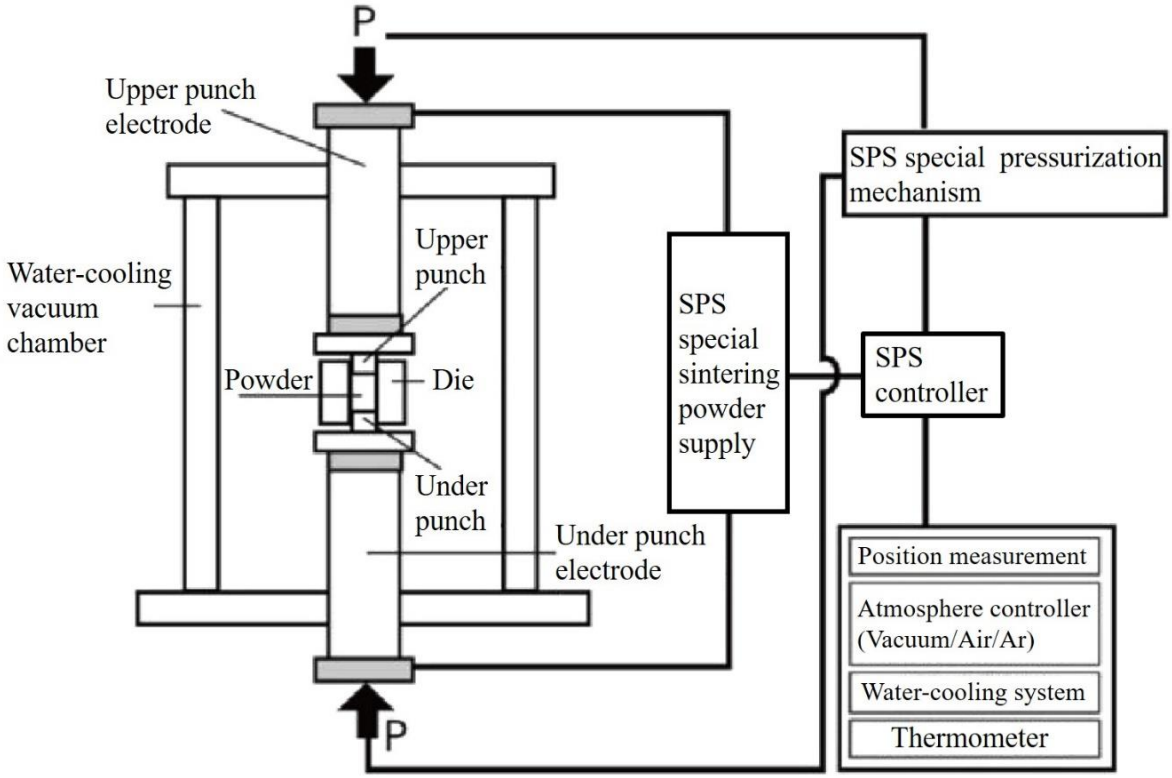


**Fig. 1-5 Schematic illustration of SPS method [1-10].**

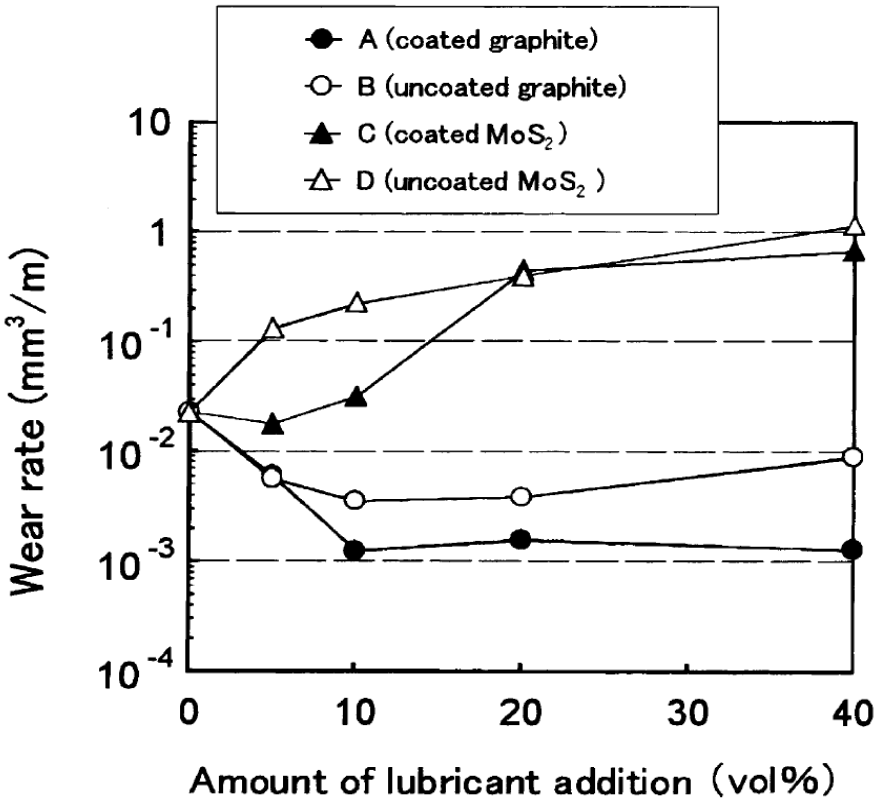


**Fig. 1-6 Relationship between amounts of lubricants (Graphite and $MoS_2$) addition and wear rate of composite materials (Cu/Graphite and Cu/$MoS_2$) [1-12].**

## 1.3.2 Plastic deformation process

### 1.3.2.1 Cold spray

Cold spray is a deposition method in which the minute powder particles with 10 to 50 μm diameter are imping at high velocity (300 to 1200 m/s) on the substrate [1-14, 1-15, 1-16]. Fig. 1-7 shows the schematic illustration of the cold spray method. In this method, the powder particles are accelerated by a supersonic gas jet at a high temperature, but it is usually lower than the melting point of the powder material (Fig. 1-8). Therefore, cold spray is one of solutions for the problems caused in the conventional thermal spray processes.

The principle of deposition of metal by the cold spray has been considered as follows. Firstly, the oxide films and/or contamination on the substrate surface are removed by the impact when the powder particles collide with the substrate. The powder particles are deformed by the impact and the oxide films around the particles are removed. Then, the clean metal surfaces of the substrate and the particles are bonded by metal bonding each other. Cold spray can deposit not only metals but also non-metal materials such as polymers and ceramics.

However, the cold spray has some issues. Although it can form relatively thick layer over 10 mm on the substrate, it is usually used as a coating method and it is difficult to form self-supported bulk or plate. In addition, the process proceeds under lower temperature than conventional thermal spray processes, but the temperature is several hundred Celsius degree and it is still higher than oxidation temperature of non-metal material such as a kind of sulfides like $MoS_2$. It means that fabrication of the composite material consists of non-metal material is sometimes difficult by using the cold spray.

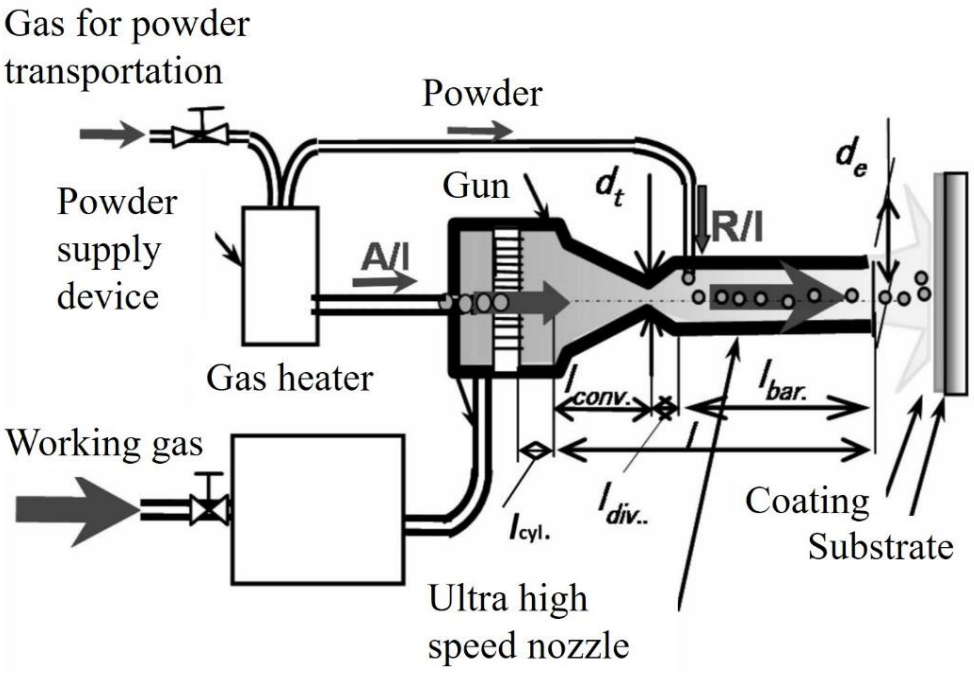


**Fig. 1-7 Schematic illustration of cold spray method [1-14].**

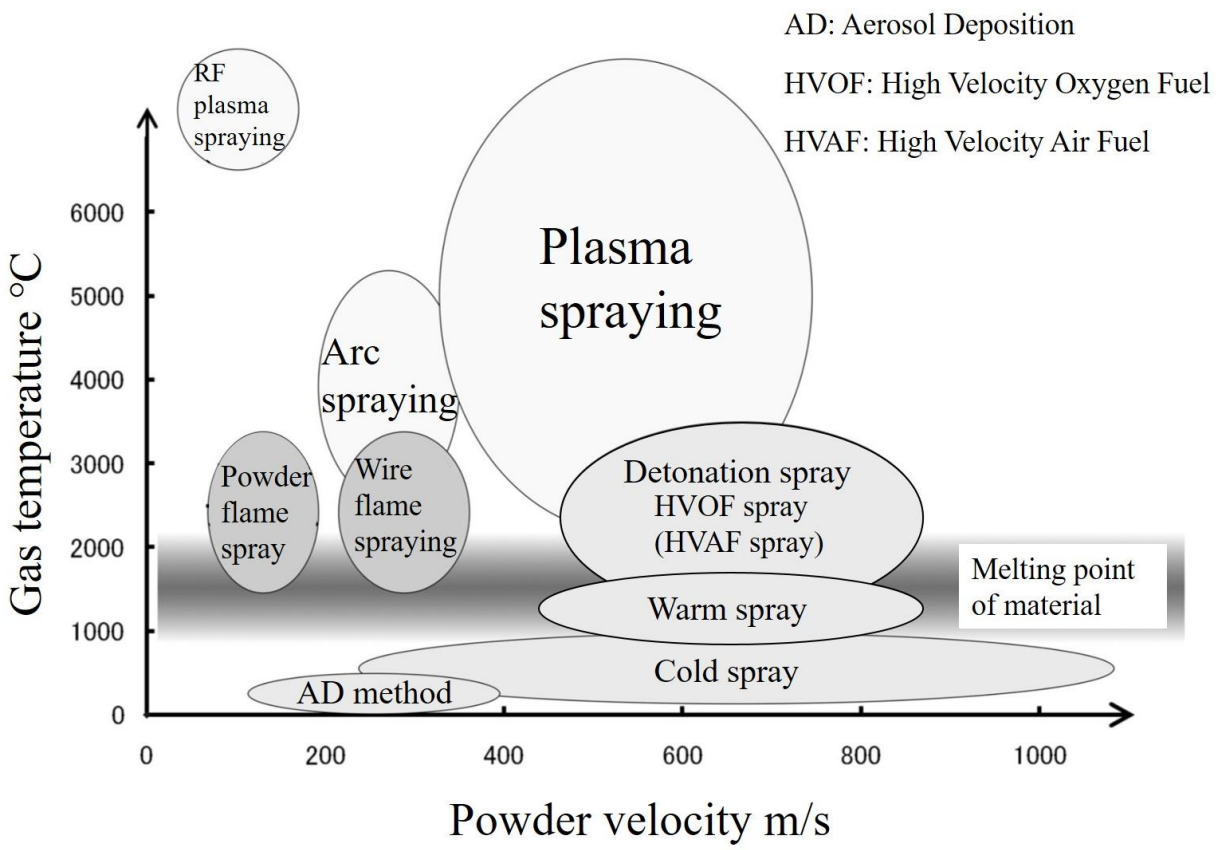


**Fig. 1-8 Relation between powder velocity and gas temperature on several thermal spray methods [1-14].**

### 1.3.2.2 Friction stir process (FSP)

The Friction Stir Process (FSP) [1-17] is a method in which the friction stir welding (FSW) [1-18, 1-19] is applied to the material surface modification technique. FSW is the technique to bond the materials, usually metal plates. The cylindrical tool with a protrusion at the tip is inserted to the junction by pressurizing while rotating it, and the materials are bonded each other by generating a plastic flow around the junction.

FSP is especially used for forming composite material. Fig. 1-9 shows the schematic illustration of the fabrication process of composite materials by FSP. Firstly, make the groove on the metal material and fulfill the dispersant in the groove. Then, the composite is formed by applying FSW on the dispersant.

As a major feature of FSP, it can perform partial compounding. This composite area does not peel off unlike the coating such as that formed by thermal spraying. Moreover, unlike other methods, it can be proceeded by using existing apparatuses such as a milling machine and without heating input from the outside. Morisada et al. attempted partial compounding of SiC into Mg alloy (AZ31), and it has been clarified that SiC particles promotes refinement of crystal grains and improves mechanical strength of Mg alloy [1-20, 1-21].

However, there are some issues. For example, the forming thickness is limited. The material becomes high temperature by the friction between material and the tool even though there is no heat input from the outside. In addition, the plastic flow of the material is complicated and not homogeneous.

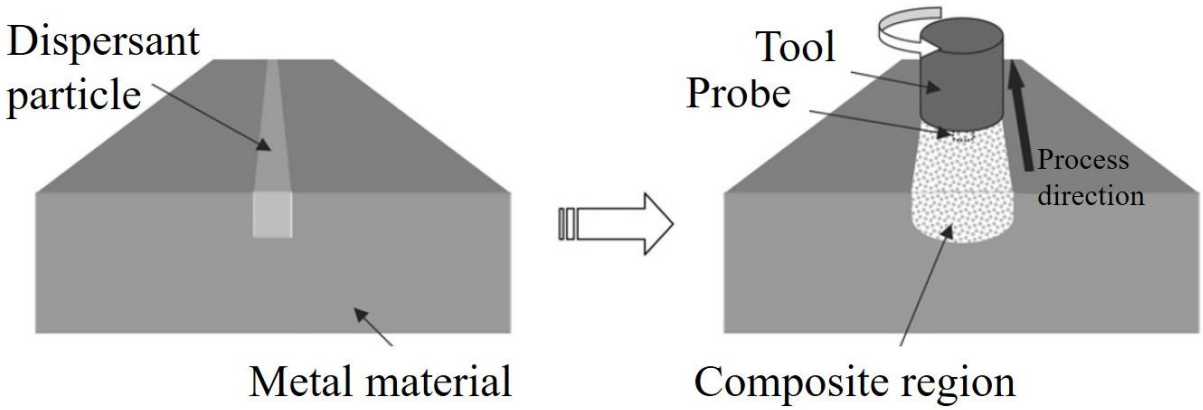


**Fig. 1-9 Schematic illustration of surface composite by FSP [1-20].**

### 1.3.3 Mechanical mixing

During the friction between two surfaces, there is a lot of phenomenon such as abrasion and chemical reaction at the contact surface. The mechanical mixing is the one of this phenomena. During the friction, the counter materials are sometimes fragmented by applying compression and shearing forces, and the fragments, that is, wear debris are mixed each other or enters the material and these are mechanically mixed. In other case, the elements from the environment such as ambient or lubricants are mixed into the material. These mixed material forms the layer on the contact surface. [1-22, 1-23]

Fig. 1-10 is an example of the mechanically mixed layers [1-22]. Fig. 1-10 shows the TEM image of longitudinal section of an oxygen free high conductivity copper block after sliding against 440C steel ring. After the long distance friction test, the nanocrystalline mixed layer was formed on the contact surface of Cu. It appears that wear debris of steel was mixed into the Cu sample and composite layer was formed.

In some situations, wear debris did not mixed into a counter material but form a layer on a contact surface by itself. Fig. 1-11 shows the optical micrographs of (a) Iridium (Ir) contained diamond like carbon (DLC) coating on the JIS SUS316L stainless steel substrate and (b) counter NF 100C6 bearing steel pin (equivalent to JIS SUJ2 or AISI 52100) after 2000 cycle ball-on-flat reciprocating friction test [1-24]. As shown in Fig. 1-11, the DLC coating was worn and a tribofilm (layer) was observed on the ball. By an energy dispersive X-ray spectrometry analysis, this layer consisted of large amount of Ir and few carbon. This results suggested that during the friction between Ir-DLC and steel pin, wear debris of Ir was selectively transferred on the steel pin and form the layer.

This phenomenon was also observed during the friction between Cu-DLC and Brass [1-25], Cu- and Ag-DLC and SUJ2 [1-26].

This process is interesting as a solid-state processing technique, however, the process is restricted to the sample surface and it is almost just a surface modification.

In contrast, this consolidation process of the wear debris by compression and shearing force is similar as a novel powder molding method termed a compression shearing method and it can consolidate metal plate materials.


**Fig. 1-10 TEM image of the cross-section of wear track showing ultrafine-grained mechanically mixed layer and elongated subgrains [1-22].**

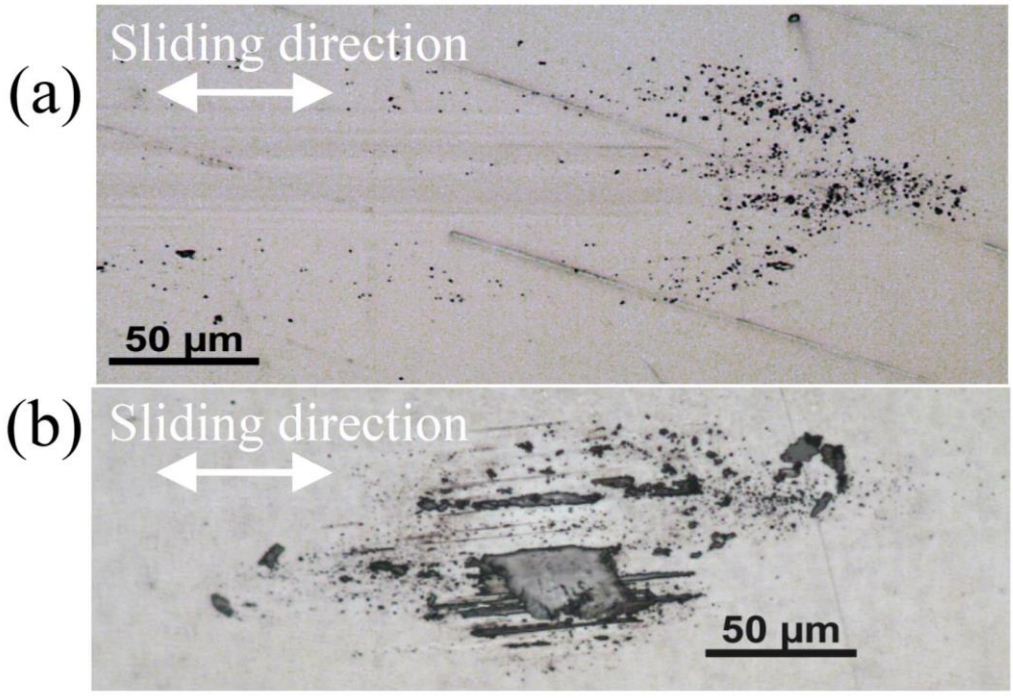


**Fig. 1-11 Optical micrographs of (a) Ir-DLC coating on SUS plate and (b) corresponding steel pin after 2000 cycles test [1-24].**

## 1.4 Material strengthening technique, severe plastic deformation (SPD)

I took on the molding methods of metal materials into consolidation as methods to develop metals with excellent material properties. As a result, composite materials should exhibit both high strength and excellent functionality, but it turned out that there are some problems in development of composites by conventional methods. In addition, metal / non-metal composites using non-metal material with lower material strength than metal host matrix appears to have lower strength than only metal material. Therefore, to obtain both high strength and excellent functional property, the way to strengthening the materials is required. I focus on severe plastic deformation (SPD) as a method to strengthening the metal materials.

Severe plastic deformation (SPD) is basically the method for the material hardening. It is well known as Hall-Petch's relation that metal materials having fine crystalline structures show excellent strength, toughness, and fatigue properties [1-27, 1-28]. In the SPD, the crystal grain sizes of the material become finer and the material strengths such as a tensile strength increase by applying a huge strain to the material. The equal channel angular pressing (ECAP) [1-29] and the accumulative rolling bonding (ARB) [1-30] are one of typical SPD methods.

Fig. 1-12 shows the schematic illustration of ECAP method. The metal material is inserted to the angled path in the mold by applying compression. The huge strain is applied to the material by passing the material through this path many times, and the crystal grain of the material become finer.

ECAP method is the oldest SPD, and the clarification of the principle of ECAP method and application of ECAP to developments of composite materials have been attempted actively. For instance, the development of a Magnesium (Mg) alloy-based SiC particle-dispersed composite material has been attempted by using Mg alloy cutting chip as a starting material [1-31]. It was difficult to make composite by using other methods such as a mechanical alloying because Mg or its alloy are easily ignite. ECAP can fabricate Mg-based composites without any ignitions of materials because it doesn't need high temperature process in ECAP and its process proceeds relatively slowly. ECAP is excellent in recyclability because cutting chips can be used as starting materials.

ARB method is a SPD method using conventional rolling apparatus. Fig. 1-13 shows the schematic illustration of ARB method. Firstly the plate material which is starting material is cut into two plates, and these surfaces are wire brushed and degreased. Then, these plates are accumulated and rolled with heating. By repeating these processes, huge strain is applied to the material and the grain size of the material become finer.

ARB has been used for fabrication of the composite material owing to its feature that the two materials are laminated and formed into a single plate. For instance, Ohsaki et al. attempted the development of Cu-Ag eutectic alloy and Cu/Zr laminated composite by ARB [1-32]. This article published in 2007 clarified that the layer of amorphous alloy was formed the interface of Cu and Zr by

the diffusion of Cu atoms due to the application of large strain and the heating.

Although the SPD appears to be useful as a metal strengthening method, it requires multiple processing. Furthermore, it is generally necessary the heating process to reduce the deformation resistance of the material. Therefore, the crystal grain coarsening by the dynamic recrystallization during heating process is concerned, and temperature is needed to be carefully controlled so that material does not deteriorates.

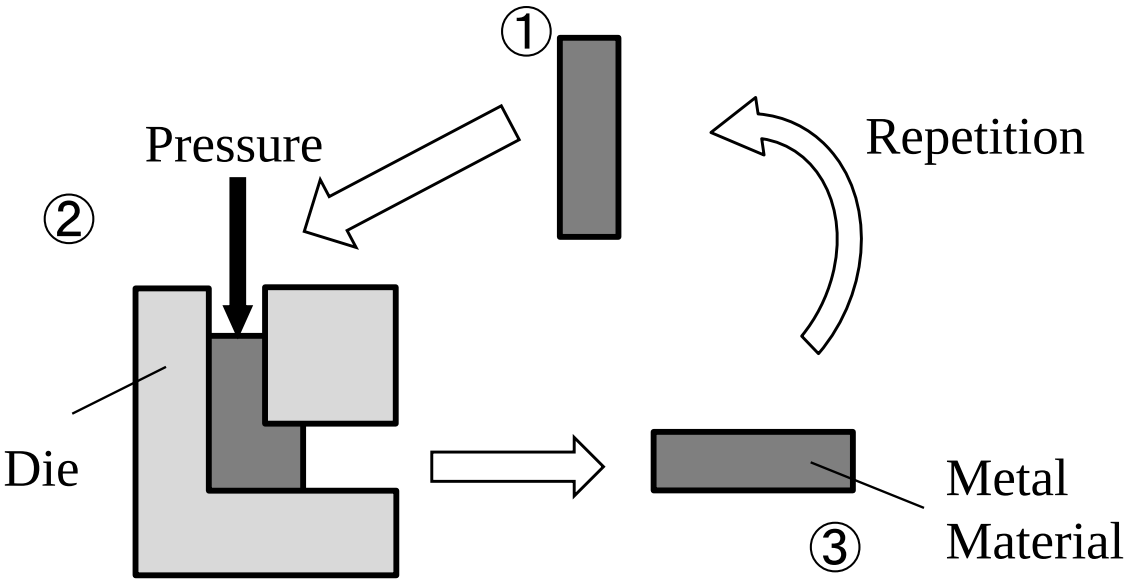


**Fig. 1-12 Schematic illustration of ECAP method.**

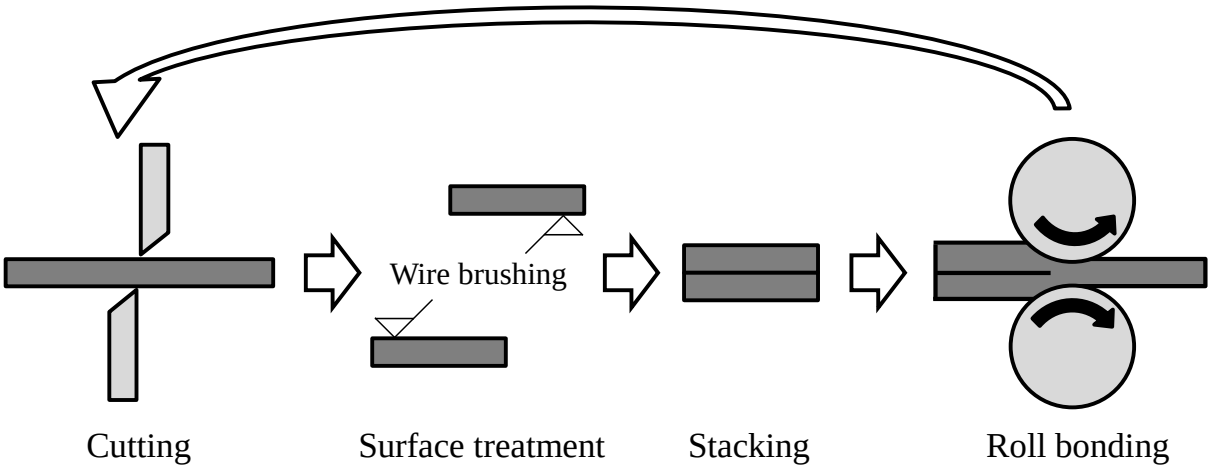


**Fig. 1-13 Schematic illustration of ARB method.**

# 1.5 Compression shearing method at room temperature (COSME-RT)

## 1.5.1 Overview of COSME-RT

Compression shearing method at room temperature (COSME-RT) is a novel powder molding method having both powder metallurgy and severe plastic deformation features [1-33]. Fig. 1-14 shows a schematic illustration of COSME-RT. First, feedstock powder is placed on the base plate at room temperature and in the atmosphere. Second, a moving plate is placed on the mixed powder, and a compression stress is applied to the powder and maintained during the forming process. Finally, a shearing strain is applied to the powder by displacing the moving plate parallel with the base plate, then a thin plate is solidified. COSME-RT can fabricate a thin metal plate material in one batch process.

According to the Hall–Petch relation [1-27, 1-28], a material with a finer crystalline structure has a higher mechanical strength. The metal powder material with finer crystalline structure than bulk materials is used as a feedstock and its small crystalline structure is retained during the forming process because no external heating is needed during COSME-RT process. Therefore, a material with high mechanical strength can be developed by COSME-RT.

For instance, the development of Aluminum (Al) [1-33, 1-34], Titanium (Ti) [1-35], Ti mesh [1-41], and magnetic materials [1-36, 1-37, 1-38, 1-39, 1-40] have been attempted. Fig. 1-15(a) and Fig. 1-15(b) show the cross-sectional backscatter SEM images of pure Al powder and pure Al sample formed by COSME-RT, respectively. In these SEM images, the crystal grains with different crystal orientations can be distinguished by a contrast difference thanks to the ion channeling. The Al powder originally had a crystalline structure with a particle size of 5.0 ~ 10 μm, and it became 0.5 ~ 1.0 μm in the sample formed by COSME-RT. Form this result, it was clarified that COSME-RT can fabricate a thin metal plate with fine crystalline structure without coarsening the original crystal grains of the feedstock powder particles.

As a method to consolidate the powder material by applying both compression stress and shearing strain like COSME-RT, there is the compression rotation shearing method [1-42]. Fig. 1-16 shows the schematic illustration of a compression rotation shearing system. A compressive stress is applied to the metal powder filled in the mold by inserting the tool from the top of the mold. By rotating the tool while maintaining the compressive stress, the powder is consolidated to a cylindrical metal piece. Although the compression rotation shearing method does not require the heat input from the outside, the material is heated by the friction heat between the powder particles because the material is continuously applied the larger strain than that of COSME-RT.

COSME-RT can fabricate not only pure metal material but also composite materials by using mixed powder consists of different materials. In the previous study, Horita et al. attempted the development of Ti/Al composite by using the mixed powder of pure Ti and Al [1-43, 1-47]. TiAl alloy has been expected as a next-generation material because of its excellent corrosion and heat resistances. It is needed to add other elements such as vanadium for stabilization of TiAl, but vanadium should be avoid because of its

toxicity. Therefore, Horita et al. attempted to fabricate the composite without alloying Ti and Al. Fig. 1-17 shows cross-sectional TEM image of Ti/Al composite formed by COSME-RT [1-47]. In this figure, the region with relatively lighter contrast is Al and that with darker contrast is Ti. There is no compound at the boundary of Ti and Al. From this work, it was clarified that COSME-RT can fabricate the composite material by coupling different kind of powder particles.

In addition, Fig. 1-18 shows cross-sectional SEM images of Ti/Al composites formed with various mixing time $M_T$ [1-47]. In this figure, the region with relatively lighter contrast is Ti and that with darker contrast is Al contrary to Fig. 1-17. Ti regions become finer when the mixing time increase. Therefore, COSME-RT can fabricate a composite material with controlling the microstructure of the material by changing its forming condition.

There are research reports of the developments of Cu and Zn composite and Cu-Zn alloy by using a compression rotation shearing method [1-44, 1-45]. When Cu and Zn powders were alternately divided into four layers and filled in the mold, Cu and Zn were separately and consecutively consolidated as shown in Fig. 1-19. There was no Cu-Zn alloy at the boundary between Cu and Zn. As this case, the compression rotation shearing method can fabricate a composite material with controlling the macrostructure of the material by changing filling condition of the feedstock powder. The similar results can be expected by using COSME-RT because the consolidation mechanisms of this method and COSME-RT is similar. In addition, when the mixed powder of Cu and Zn was used, even though the mixed powder had not reached at 737 K (the lowest temperature of β-phase formation obtained from the two-dimensional state diagram of Cu-Zn) Cu and Zn is alloyed as shown in Fig. 1-20. This result confirmed the alloying of different metal materials by a frictional force suggested by Sasada et al. [1-46], and also suggested the possibility of alloying by COSME-RT.

From these facts, it is suggested that COSME-RT is useful as a material molding method. However, there are some issues of COSME-RT toward practical use. For example, the material size formed by COSME-RT is around 20 × 20 $mm^2$ to 30 × 60 $mm^2$ and material thickness is around 0.20 to 0.30 mm. To be used as a structural material, the material formed by COSME-RT should be enlarged. In addition, the compression and shearing process is now automation but the powder filling process is manual, and it is needed to be automated for mass production. These issues is only technical ones and can be solved by making apparatus larger and developed additional system to fill the powder.

Third issue is more fundamental than others, that is, the consolidation mechanism of materials by COSME-RT. It is needed to clarify the mechanism for material design and reliability assurance of COSME-RT process. To clarify the consolidation mechanism, there are three major issues. First one is path to consolidation. There should be some stages of the bonding process of material powder particles such as deformation, crystal grain refinement, and bonding. The order of these stages was not considered in previous studies. Second one is threshold value of a physical quantity to proceed the process. How much stress, strain, or energy are needed to proceed the consolidation process is not clarified yet. Third one is the effect of material properties to consolidation process. If material of feedstock powder is different, consolidation process of material should be changed.

In this study, the path to consolidation is focused on as a first step of investigation of consolidation process. In the next section, the previous study about this issue and the unsolved problems are presented.

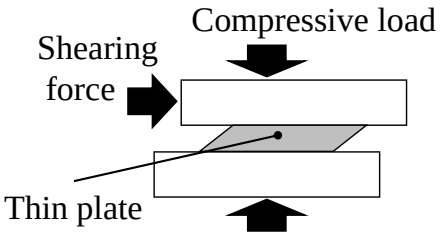


**Fig. 1-14 Schematic illustration of compression shearing method at room temperature [1-33].**

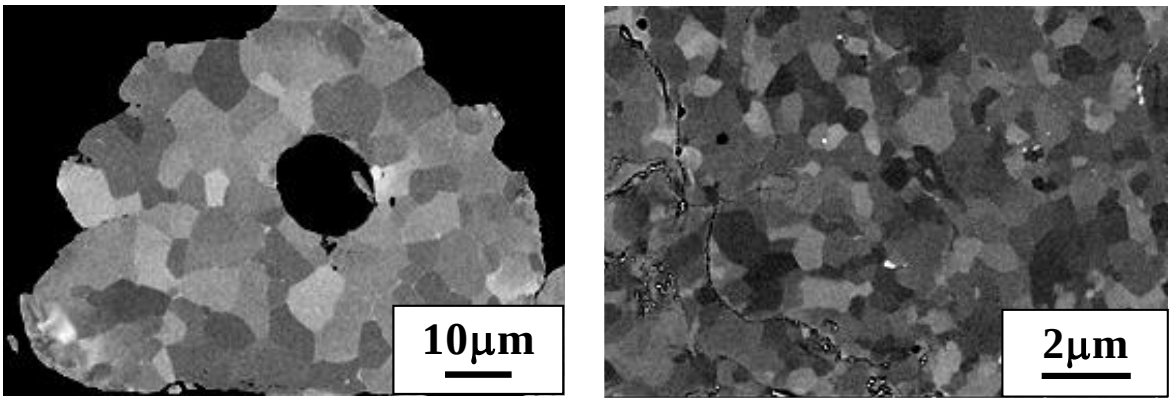


(a) Al powder. (b) Cross-section of Al sample.

**Fig. 1-15 Back scattering SEM images of pure Al feedstock powder and sample formed by COSME-RT [1-31].**

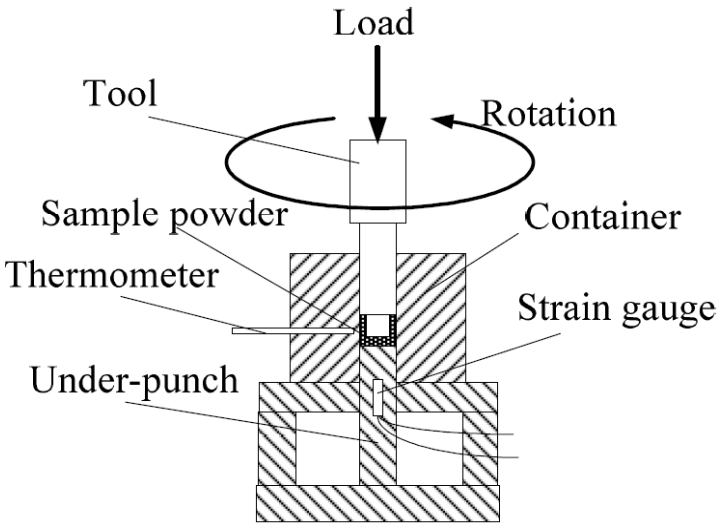


**Fig. 1-16 Schematic illustration of compression rotation shearing system at room temperature [1-39].**

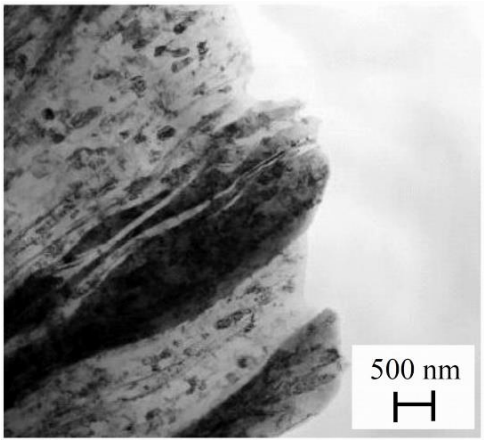


**Fig. 1-17 TEM cross-sectional image of Ti/Al sample formed by COSME-RT [1-47].**

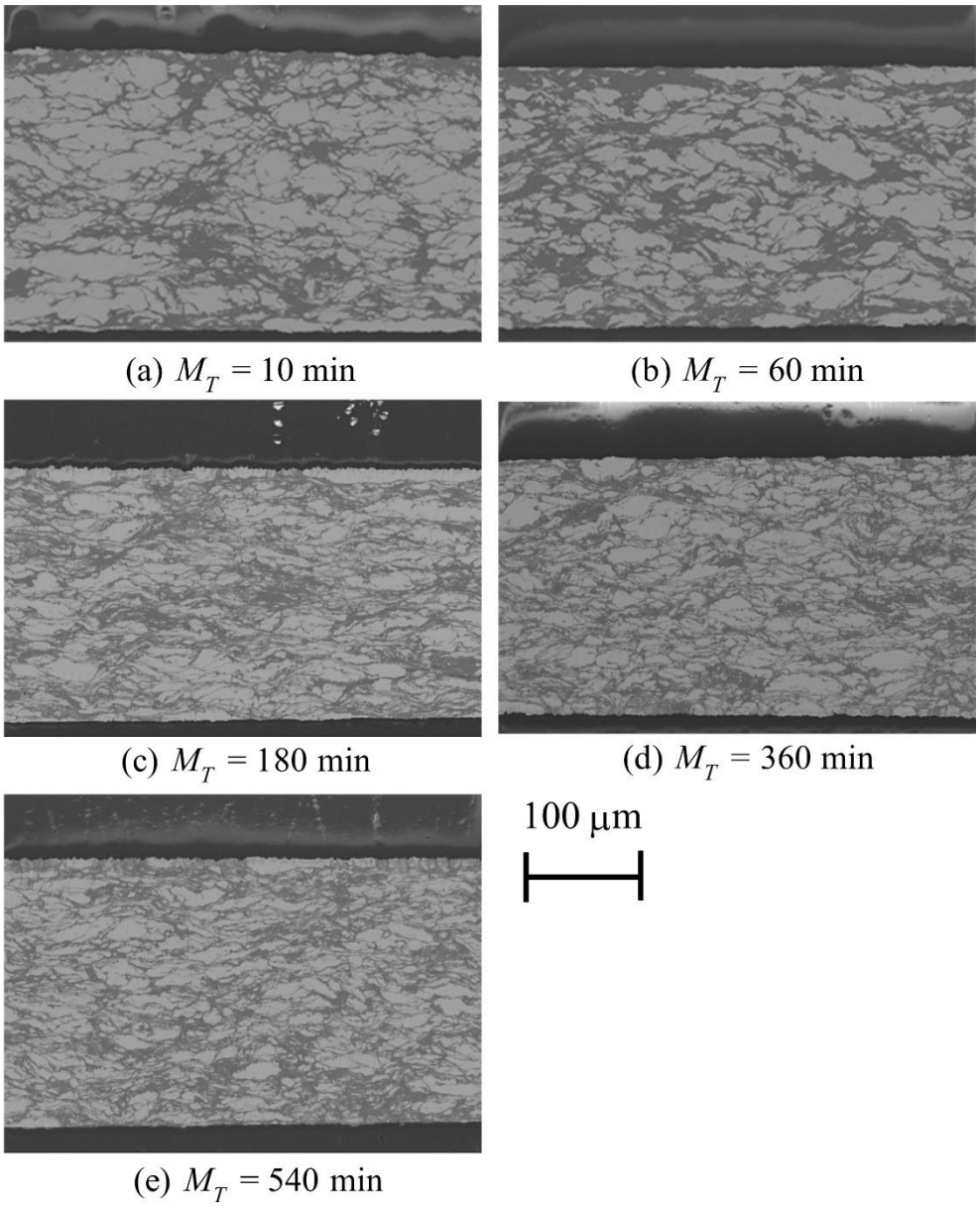


**Fig. 1-18 SEM images of cross-section of the Ti/Al samples formed by COSME-RT [1-47].**

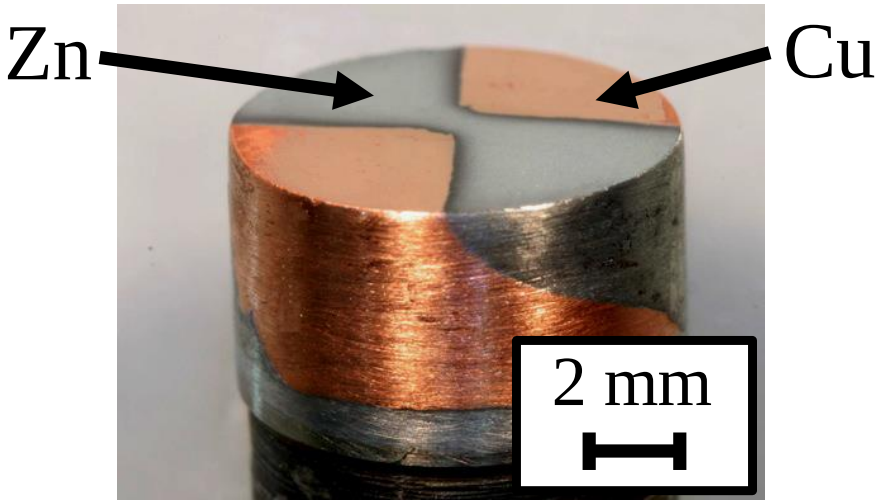


**Fig. 1-19 Overview image of four-layer Cu/Zn sample formed by compression rotating shearing method [1-45].**

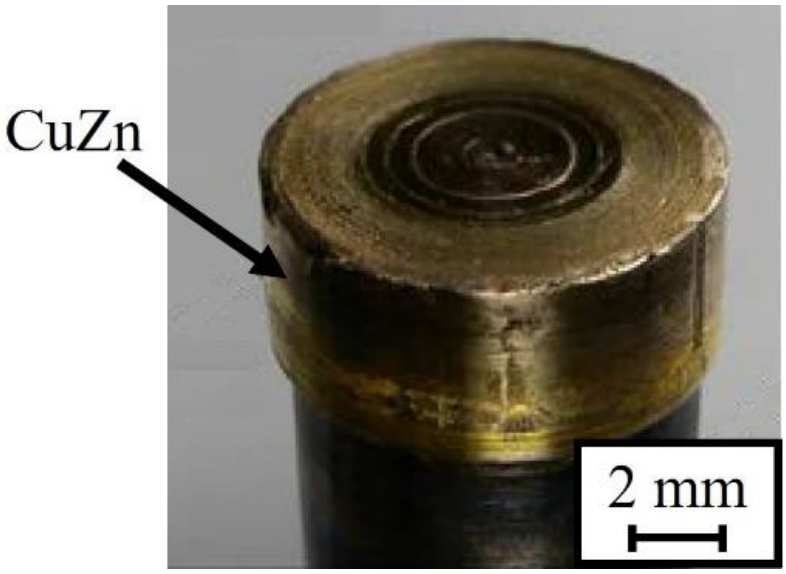


**Fig. 1-20 Overview image of CuZn alloy sample formed by compression rotating shearing method [1-45].**

### 1.5.2 Proposed consolidation mechanism by COSME-RT

In COSME-RT, it is considered that the two axes loads cause deformation of the powder particles and the native oxide films and contaminations around the particle are removed, and the powder particles are bonded each other. However, the detailed process of this interparticle bonding is not clarified yet, due to the difficulty in observing the microstructural changes in bonding condition of the powder particles.

Horita, et al. proposed the simple model of consolidation mechanism of pure Ti powder particles by COSME-RT [1-47]. Fig. 1-21 shows the schematic illustrations of the model of the consolidation mechanism of pure Ti powder by COSME-RT. The powder particles partly bonded by applying uniaxial compressive stress. The crystal grain partly becomes finer only by uniaxial compressive stress (Fig. 1-21(a)). By applying the shearing, the deformation, the bonding, and the crystal refinement of the powder particles are continuously happened. The powder particles deformed to fulfill the voids ((Fig. 1-21(b), (Fig. 1-21(c), (Fig. 1-21(d)). Finally, the fully dense material with fine crystalline structure was fabricated ((Fig. 1-21(e)). Horita, et al. explained that powder particles were connected by a diffusion bonding in the case of the Ti powder. In contrast, they explained that the oxide films around the powder particles were flaked by the friction between powder particles by applying the shearing in the case of the Al powder.

Although this model simply shows the bonding mechanism of the powder particles during the COSME-RT, it is not sufficient to explain the consolidation mechanism of powder particles. Horita et al. built this model based on only the structural observation of the uniaxial-compressed sample and the sample with bonded powder particles after applying shearing. Therefore, the path to the bonding of the powder particles was not observed yet. Especially the order of three processes, the deformation, the bonding, and the crystal grain refinement of the powder particles were not clarified yet. This is because it is difficult to control the applied shearing force.

As descried above, the powder particles appear to be bonded by the friction force between the particles due to the shearing applied. It means that the applied shearing force is one of important factors in the consolidation of materials by COSME-RT. However, in COSME-RT, the compressive stress, the shearing distance and the shearing rate can be controlled, and the applied shearing force is determined from these parameters and the material strength of the feedstock powder. Therefore, we could not control the shearing force and only we could is measurement of the resulting tangential force applied to the sample. From this reason, no previous study has attempted to control the shearing force. The measured tangential force usually increases with the shearing process proceed [1-47]. Nevertheless, the shearing distance cannot be controlled finely enough in the COSME-RT apparatus because of the technical reason.

Thus, it is necessary to find the way to control the applied shearing force and to visualize the bonding process of the powder particles to understand the consolidation mechanism of material by COSME-RT.

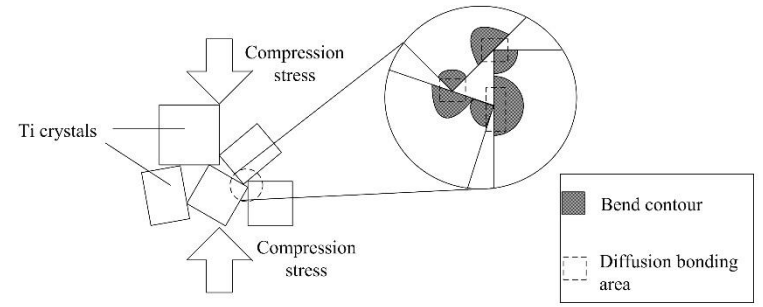


(a) Ti powders were loaded in compression (initial stage)

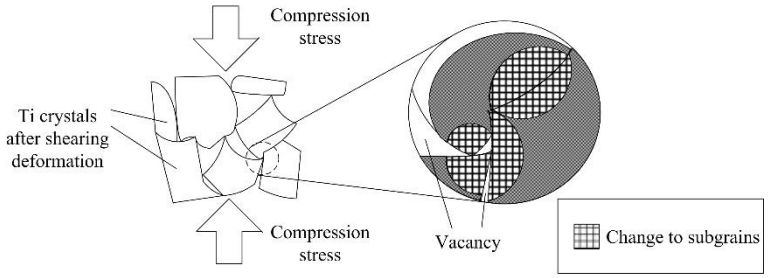


(b) Ti powders were loaded in compression (end stage)

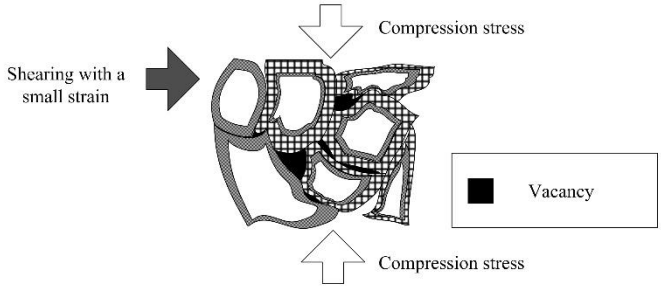


(c) Ti powders were loaded in compression and shearing ( initial stage )

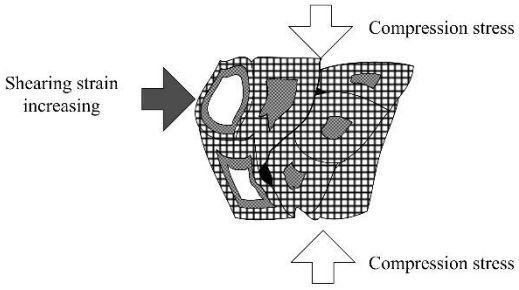


(d) Ti powders were loaded in compression and shearing
(strain increasing stage)

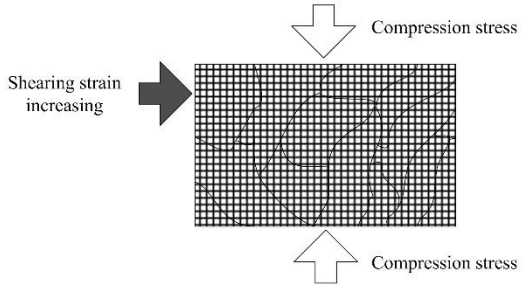


(e) Ti powders were loaded in compression and shearing
(end stage)

**Fig. 1-21 Model of consolidation mechanism of pure Ti powder by COSME-RT [1-44].**

## 1.6 Control of shearing force by using spherical contact

There are two main issues have to be solved for investigation of the bonding mechanism of powder particles by COSME-RT. Firstly, it is difficult to control the shearing force during COSME-RT process (as described previous section, 1.5.2). Second one is visualization. The COSME-RT process proceed in enclosed area between two steel plate, and the thickness of the sample is so thin (0.20 to 0.25 mm). Thus, in-situ observation of consolidation process is difficult.

To solve these problems, I propose the way to apply the compression shearing process to the powder particle not by a plane contact of steel plates but by a spherical contact of a ball.

Fig. 1-22 shows the schematic illustration of the stress distribution in the powder particles during the COSME-RT process. During the COSME-RT process, the stress applied to each powder particle homogeneously, so we can observe only an average bonding condition of the particles on a sample. Fig. 1-23 shows the schematic illustration of the stress distribution in the sliding spherical contact on the plane without friction. According to the Hertzian contact theory [1-48, 1-49], the applied stress along the depth direction ($\sigma_{zz}$) to the sample contacts with spherical material has distribution as shown in Fig. 1-23. The applied stress decreases with the depth from the sample surface. The bonding process of the powder particles appears to proceed by an applied stress. Therefore, there should be a distribution of bonding status of powder particles, and we can observe different bonding states of the particles on a sample. The frictional force is generated on the plane by sliding the spherical body, and any shearing stress that is not described in Fig. 1-23 expected to be applied simultaneously.

This experiment which applies a compression shearing process to the plane sample by pressing and displacing a spherical body is similar as a conventional friction test. Therefore, it appears to be possible to conduct this experiment by using a conventional tribometer. By changing the conditions of the friction experiment such as the normal load and the number of the sliding cycles, it is possible to prepare the samples having significantly different bonding conditions which cannot be clearly observed by the stress distribution in the depth direction.

Therefore, I propose a friction experiment using a ball as a counter material to clarify the mechanism of interparticle bonding during the compression shearing process. By this friction experiment, the path to bonding of the powder particles is clarified. Then, the intermediate process which couldn't investigated by the Horita's model will be complemented.

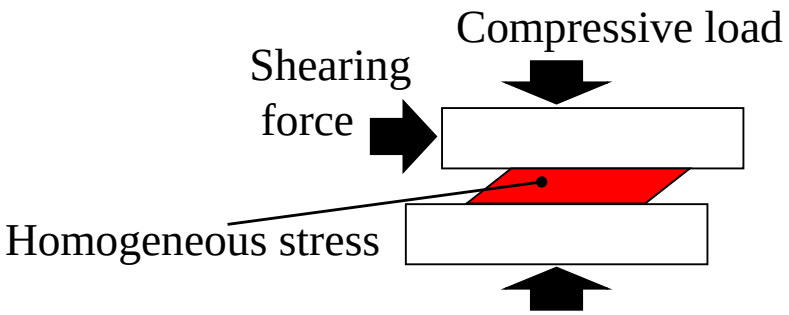


**Fig. 1-22 Stress applied to sample in COSME-RT.**

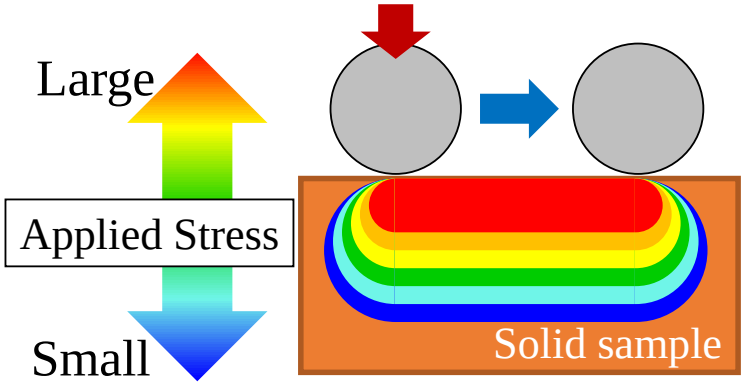


**Fig. 1-23 Stress distribution in spherical contact (without friction).**

## 1.7 Objective and Structure of Thesis

This literary chapter, the industrial background of materials and material molding methods were introduced. It was described that there are several requirements for materials and its molding methods, and COSME-RT appears to be one of the solutions to meet these requirements. The major problem of COSME-RT is that its detailed mechanism of consolidation process is not clarified yet.

The main objective of this study is clarification of COSME-RT process, that is, clarification of bonding mechanism of powder particles by applying two axes forces.

This thesis consists of six chapters as follow:

In chapter 1, the social and the industrial backgrounds of materials and its molding methods are introduced. There are several requirements for materials in an industrial use, and COSME-RT appears to be one of the solutions to meet these requirements. The objective of this thesis is proposed.

Chapter 2 is the chapter for experimental details. In this chapter, experimental and analytical methods are explained; such as a COSME-RT apparatus and a linear tribometer, analytical instruments, and raw materials used for experiments such as copper (Cu) powder.

In chapter 3, the way to suppress a shearing force applied to the powder particles by dispersing solid lubricant particles in the pure copper powder particles is explained to understand the effect of the shearing force on the consolidation process of copper by COSME-RT. Molybdenum disulfide ($MoS_2$) powder is used as a dispersed solid lubricant. The Cu/$MoS_2$ sample are formed under several shearing distances and their microstructures are observed. The microstructural change related to the reduction of the applied shearing force is discussed.

In chapter 4, a unidirectional friction experiment is performed to clarify the mechanism of interparticle bonding from a new point of view. A friction experiment which repeatedly makes spherical sliding contact on the uniaxial compressed Cu powder sample in the local area is used as a tool for visualizing timeline information of interparticle bonding during the compression shearing process. In

this experiment, the stress applied to the sample decreases from the surface to its inside. Bonding conditions of the powder particles change in the depth direction of the sample. The relation between the normal loads applied, the number of the sliding cycles, and the microstructural change of the powder particles is investigated by morphological and cross-sectional observations of the uniaxial compressed pure Cu powder samples after the friction experiments.

In chapter 5, the findings obtained from the previous experiments and the previous research results are took account and the consolidation mechanism of materials by COSME-RT is discussed.

In chapter 6, the summary of my research findings and the future perspectives of this study are stated. As the result of this study, the author succeed to obtain new knowledges about the consolidation process of Cu from powder to plate by COSME-RT, especially a new model of powder particle bonding by COSME-RT.

Firstly, in the next chapter, the experiments to achieve the objective is presented.

# References


(1-1) Tsuru, T., "Alloy Design and Mechanical Properties: First principles Calculations of Dislocation Core," Materia Japan, 56, 1, 2017, 5-13. (in Japanese)

(1-2) Kuniaki Umino, Nikkan Kogyo Shimbun, Know-It-All from today series Tokoton friendly metal processing, (2013), pp. 1 - 11. (in Japanese)

(1-3) Japan Society of Powder and Powder Metallurgy, Powder and Powder Metallurgy Book, Uchida Rokakuho, (2011), pp. 3 - 6. (in Japanese)

(1-4) R.M. German, Powder Metallurgy Science, Metal Powder Industry, (1994), pp. 2 - 6.

(1-5) T. Kimura, The Past, Present and Future of Powder Metallurgy, Journal of the Japan Society of Powder and Powder Metallurgy, 45, 9, (1996), pp. 827-832. (in Japanese)

(1-6) Japan Society of Powder and Powder Metallurgy, Powder and Powder Metallurgy Book, Uchida Rokakuho, (2011), pp. 262 - 277. (in Japanese)

(1-7) J. S. Benjamin, Dispersion Strengthened Superalloys by Mechanical Alloying, Metallurgical Transactions, 1, (1970), pp. 2943 - 2951.

(1-8) B. S. Murty, S. Ranganathan, Novel materials synthesis by mechanical alloying/milling, International Materials Reviews, 43, 3, (1998), pp. 101 - 141.

(1-9) USP3241956

(1-10) M. Tokita, Recent and Future Progress on Advanced Ceramics Sintering by Spark Plasma Sintering (SPS) Method, Journal of the Ceramic Society of Japan, 49, 2, (2014), pp. 91 - 96. (in Japanese)

(1-11) M. Suzuki, M. Moriyama, M. Nishimura, M. Hasegawa, Friction and wear of self-lubricating composites at temperatures to 450°C in vacuum, Wear, 162 - 164, (1993), pp. 471 - 479.

(1-12) H. Kato, M. Takama, Y. Iwai, K. Washida, Y. Sasaki, Wear and mechanical properties of sintered copper-tin composites containing graphite or molybdenum disulfide, Wear, 255, (2003), pp. 573-578.

(1-13) Y. Tsuya, From solid lubricant to solid lubrication, Journal of the Japan Society for Precision Engineering, 40, 2, (1974), pp. 191 - 197. (in Japanese)

(1-14) R. C. Dykhuizen, M. F. Smith, D. L. Gilmore, R. A. Neiser, X. Jiang, and S. Sampath, Impact of High Velocity Cold Spray Particles, Journal of Thermal Spray Technology, 8, 4, (1999), pp. 559 - 564.

(1-15) K. Ogawa, K. Ito, K. Ichimura, Y. Ichikawa, S. Ohno, and N. Onda, Characterization of Low-Pressure Cold-Sprayed Aluminum Coatings, Journal of Thermal Spray Technology, 17, 5-6, (2008), pp. 728 - 735.

(1-16) K. Sakaki, Promising Field in New Thermal Spray Technology, "Cold Spray", Journal of Japan Thermal Spray Society, 47, 3, (2010), pp. 113 - 119.

(1-17) R. S. Mishra, Z. Y. Ma, Friction stir welding and processing, Materials Science and Engineering R, 50, (2005), pp. 1 - 78.

(1-18) W.M. Thomas, E.D. Nicholas, J.C. Needham, M.G. Murch, P. Temple-smith, C.J. Dawes,

USP5460317.

(1-19) W.M. Thomas, E.D. Nicholas, J.C. Needham, M.G. Murch, P. Temple-smith, C.J. Dawes, G.B. Patent App., 9125978.8 (1991).

(1-20) Y. Morisada, H. Fuji, Nanocomposites Fabricated by FSP, Journal of Japan Welding Society, 76, 3, (2007), pp. 22 - 26. (in Japanese)

(1-21) Y. Morisada, H. Fujii, T. Nagaoka, M. Fukusumi, Effect of friction stir processing with SiC particles on microstructure and hardness of AZ31, Material Science and Engineering A, 433, (2006), pp. 50 - 54.

(1-22) D. A. Rigney, M. G. S. Naylor, and R. Divakar, Low energy dislocation structures caused by sliding and by particle impact, Material Science and Engineering, 81, (1986), pp. 409 - 425.

(1-23) D. A. Rigney, Transfer, mixing and associated chemical and mechanical processes during the sliding of ductile materials, Wear, 245, (2000), pp. 1 - 9.

(1-24) H. Miki, K. Ito, T. Sugawara, J. Fontaine, T. Takeno, M. Ruet, M. Belin, K. Adachi, Friction and Electrical Contact Resistance of Iridium-Containing DLC Coatings for Electrically Conductive Tribo-Elements, Tribology Online, 4, 3, (2009), pp. 60 - 65.

(1-25) R. Hombo, N. Kato, T. Nozu, N. Inayoshi, J. Fontaine, M. Belin, H. Miki, T. Takagi, T. Takeno, Relationship between electrical-tribological behavior and properties of sliding surfaces of copper containing diamond-like carbon nanocomposite coated plate and brass ball, 2014 IEEE 60th Holm Conference on Electrical Contacts, 12 - 15 Oct., (2014), New Orleans, Louisiana, USA.

(1-26) M. Goto, K. Ito, J. Fontaine, T. Takeno, H. Miki, T. Takagi, Formation Processes of Metal-Rich Tribofilm on the Counterface During Sliding Against Metal/Diamondlike-Carbon Nanocomposite Coatings, Tribology Online, 10, 5, (2015), pp. 306 - 313.

(1-27) E. O. Hall, The Deformation and Ageing of Mild Steel: III Discussion of Results, Proc. Phys. Soc., 64, (1951), pp. 747 - 753.

(1-28) N. J. Petch, The Cleavage Strength of Polycrystals, J. Iron Steel Inst., 174, (1953), pp. 25 - 28.

(1-29) V. M. Segal, Materilas processing by simple shear, Material Science and Engineering A, 197, (1995), pp. 157 - 164.

(1-30) Y. Saito, N. Tsuji, H. Utsunomiya, T. Sakai, R.G. Hong, Ultra-fine Grained Bulk Aluminum Produced by Accumulative Roll-bonding (ARB) Process, Scripta Materialia, 39, 9, (1998), pp. 1221 - 1227.

(1-31) T. Aida, N. Takatsuji, K. Matsuki, T. Sato, and S. Kamado, Mechanical properties of SiC particle-AZ31B magnesium alloy machined chips composites prepared by hot extrusion after ECAP, Journal of Japan Institute of Light Metals, 58, 3, (2008), pp. 104 -110. (in Japanese)

(1-32) S. Ohsaki, S. Kato, N. Tsuji, T. Ohkubo, K. Hono, Bulk mechanical alloying of Cu-Ag and Cu/Zr two-phase microstructures by accumulative roll-bonding process, Acta Materialia, 55, (2007), pp. 2885 - 2895.

(1-33) H. Takeishi, N. Nakayama, H. Miki, Consolidation with Grain Refinement by Compression Shearing Method under Room Temperature, Journal of the Society of Materials Science, 54, 3,

(2005), pp. 233- 238. (in Japanese)

(1-34) N. Nakayama, M. Horita, H. Miki, T. Miyazaki, H. Takeishi, Effects of Powder Size and Shape on Microstructure of Al Thin Plate Formed by Compression Shearing Method at Room Temperature, Journal of the Japan Society for Technology of Plasticity, 54, 625, (2013), pp. 191 - 195. (in Japanese)

(1-35) M. Horita, N. Nakayama, H. Miki, T. Miyazaki, H. Takeishi, Microstructure of Titanium Thin Plates Formed by Compression Shearing Method at Room Temperature, Journal of the Japan Society for Technology of Plasticity, 54, 625, (2013), pp. 186 - 190. (in Japanese)

(1-36) T. Saito, H. Takeishi, N. Nakayama, New method for the production of bulk amorphous materials of Nd-Fe-B alloys, J. Mater. Res., 20, 3, (2005), pp. 563 - 565.

(1-37) T. Saito, H. Takeishi, N. Nakayama, Production of amorphous bulk material of an $Nd_{15}Fe_{77}B_8$ magnetic alloy, J. Alloys and Compounds, 396, (2005), pp. 208 - 211.

(1-38) T. Saito, H. Takeishi, N. Nakayama, Production of Bulk Nanocomposite Magnets of An $Nd_4Fe_{77.5}B_{18.5}$ Alloy by Compression Shearing Method, IEEE Transactions on Magnetics, 41, 10, (2005), pp. 3781 - 3783.

(1-39) T. Saito, H. Sato, H. Takeishi, N. Nakayama, Anistropic Sm-Fe-N magnets produced by compression shearing method, Appl. Phys. Lett., 89, (2006), 162511.

(1-40) T. Saito, H. Takeishi, N. Nakayama, Consolidation of Nd-Fe-B melt-spun ribbon by compression shearing method, J. Appl. Phys., 101, (2007), 09K503.

(1-41) N. Nakayama, N. Izawa, M. Horita, N. Saito, H. Miki, H. Utsumi, H. Takeishi, Effect of Aspect Ratio on the bending property of Titanium Fiber Formed by the Compression Shearing Method at Room Temperature, J. JSEM, 13, (2013), pp. s1 26 - s1 30.

(1-42) N. Nakayama, S. Kato, H. Takeishi, H. Miki, Consolidation of Ti Powder by a Compression Rotation Shearing System at Room Temperature -Effect of pivot rotation speed on consolidation-, Advanced Materials Research, 409, (2012), pp. 3 -8.

(1-43) M. Horita, N. Nakayama, H. Miki, T. Miyazaki, and H. Takeishi, Effect of Ball-Milling Time on Tensile Properties of Ti/Al Thin Plate Formed by Compression Shearing Method at Room Temperature, 54, 625, (2013), pp. 181 - 185. (in Japanese)

(1-44) T. Sakuma, Fabrication of CuZn by Compression Shearing Method at Room Temperature, Master Thesis, Chiba Institute of Technology, Japan, (2014). (in Japanese)

(1-45) H. Miki, T. Sakuma, N. Nakayama, H. Takeishi, Alloying process of Cu-Zn based composite material prepared by compression rotation shearing method, Conference of the Japan Society of Mechanical Engineers 2013, S041015, (2013). (in Japanese)

(1-46) T. Sasada, S. Norose, T. Ozawa, and H. Mishina, Composition of Wear Particles in Metallic Friction -Formation of ε-phase alloy in Zn/Cu and Zn/Ag Rubbing-, Journal of Japan Society of Lubrication Engineers, 24, 7, (1979), pp. 447 - 453. (in Japanese)

(1-47) M. Horita, Doctor Thesis, Shinshu University, Japan, (2014). pp. 65 - 67.

(1-48) G. M. Hamilton, L. E. Goodman, The stress field created by a circular sliding contact, Journal of Applied Mechanics, (1996), pp. 371 - 376.

(1-49) K.L. Johnson, Contact Mechanics, Cambridge University Press, 1987.

# Chapter 2

# Experimental approaches for investigation of consolidation mechanism by COSME-RT

In this chapter, I will describe the detail of our experiments. To achieve the objective of this thesis presented in the previous chapter, two different experimental approaches were attempted.

First one is the control of consolidation process by dispersing $MoS_2$ into Cu matrix to investigate the effect of the applied shearing force on the consolidation process. Cu-based $MoS_2$-dispersed composite material fabricated from Cu/$MoS_2$ mixed powder by COSME-RT. The microstructure of the composite sample and pure Cu sample are investigated.

Second one is the friction experiment on the pure Cu sample to investigate the change of the bonding conditions of the powder particles. A liner sliding friction equipment was used in this study, and it was modified as a unidirectional friction apparatus. By applying a compressive stress and a shearing strain simultaneously to a uniaxial-compressed pure Cu sample by the friction experiment, like COSME-RT, I tried to trace the bonding path of the particles.

All samples fabricated by COSME-RT at Tohoku University, because COSME-RT apparatus is unique and there are only two apparatuses in the world (Both are in Japan. One is in Tohoku University and another one is in Shinshu University, Nagano). The material properties of the samples were analyzed by several methods. Especially about tribological property, the sample were investigated by using the tribometer with specific features at Laboratoire de Tribologie et Dynamique des Systèmes (LTDS), École Centrale de Lyon (ECL). Microstructural observations were carried out mainly at Tohoku University, but some observations were carried out at LTDS because it is not efficient to bring back the sample to Japan every time after the tribological analysis.

# 2.1 Materials

## 2.1.1 Feedstock powder

In this study, the metal material should be chosen as a feedstock powder. COSME-RT can consolidate several metal materials such as Al and Ti and it appears to be able to consolidate many kinds of metals. The feedstock should meet the following requirements. First one is soft material. If the material is hard like Ti, it will be difficult to observe the deformation of powder particles. Second one is tribological property. If friction coefficient of material is very high, the friction experiment cannot simulate the COSME-RT process because any abrasion wear and oxidation aren't happened during the COSME-RT process. From the previous study, Al seems to be good as a feedstock [2-7, 2-8, 2-9], but preliminary tribological experiments ware clarified that Al is not suitable for a feedstock because its tribological property is not sufficient. Pure Al sample was worn after the preliminary friction experiment while pure Cu sample was not worn. The oxide of Al, $Al_2O_3$ is much harder than pure Al and this oxide may cause wear of Al sample during the friction experiment. Therefore, pure Cu powder was chosen as a feedstock as a starting material in this study.

Powder shape is also one of important factors. Basically, there are two types of powder shape, spherical and non-spherical. Although the spherical powder appears to be suitable for the observation of the deformation of the powder particle, the uniaxial-compressed sample of the spherical powder is too brittle to withstand the high load friction experiment. The observation of the particle deformation of the non-spherical powder is harder than that of the spherical one, but the uniaxial-compressed sample of the non-spherical powder will keep its shape during the friction experiment because the uneven parts of the particles are physically intertwined. Actually, in the conventional powder metallurgy method, the non-spherical powder is used as a feedstock for this reason. From these reasons, non-spherical pure Cu powder was chosen as the feedstock.

Copper powder (99.9% purity, Fukuda Metal Foil & Powder Co., Ltd., Kyoto, Japan) was used as a feedstock. This powder was produced by the water atomize and average particle size was 35 μm. Cu powder particles have non-spherical shape as can be seen from Fig. 2-1.

## 2.1.2 Dispersant

As the lubricant to disperse in the matrix material, not a semi-solid or a liquid ones such as a lubricating oil or a grease that a flow loss during the forming process is feared, but a solid one appears to be suitable. There are four kinds of solid lubricants: (1) materials having layered structures such as a graphite and a molybdenum disulfide ($MoS_2$) and a tungsten disulfide ($WS_2$), (2) soft metals such as a silver (Ag) and lead (Pb), (3) soft materials such as polymers, and (4) carbon-based hard thin films such as a diamond like carbon (DLC).

It is difficult to coat Cu powder particles with carbon-based hard thin films homogeneously. The materials having layers structures usually show lower coefficient of friction than soft metals and polymers. In addition, $MoS_2$ is widely used as a dispersant into the oil or grease [(2-10)] and it is cheaper than $WS_2$. Therefore, $MoS_2$ was used as the dispersant in this study.

$MoS_2$ is used as a lubricant by mixing its powder with a grease or a lubricating oil which apply to sliding members because it is chemically stable. It is not dissolved in water, petroleum, lubricating oil, and most acids other than an aqua regia, a boiling hydrochloric acid, and a hydrofluoric acid [(2-11)].

In this study, $MoS_2$ powder (98.0% purity, Daitou Co., Ltd., Tokyo, Japan) was used as a dispersant. The average particle size of $MoS_2$ powder was 6.0 μm. Fig. 2-2 shows the SEM image of $MoS_2$ powder. $MoS_2$ has a layer structure at the molecular level, and it can be seen from Fig. 2-2 that the $MoS_2$ powder also has the layer structure. There are the particles with various sizes mixed from large particles larger than 10 μm to small particle as small as 1.0 μm. The $MoS_2$ powder particles are expected to disperse between the Cu powder particles homogeneously, because the $MoS_2$ powder particles are smaller than the Cu powder particles and there are the particles with various sizes.

Fig. 2-3 shows crystal structure of $MoS_2$ [(2-12)]. A $MoS_2$ molecule has a structure with laminated a layered structure with two S atoms sandwiching a single Mo atom. $MoS_2$ structure is broken like sliding even with a slight shearing force because the bonding force between the S atoms in the layer is smaller than that between the Mo and S atoms. It appears that the $MoS_2$ lubricatfion will not be lost even if it is finely dispersed because the lubrication are obtained by breaking the structure at the molecular level.

From the results of the preliminary experiment, it has been clarified that the formability by COSME-RT become worse when the oxide film of feedstock powder become thicker. The reason appears to be because the oxide film on the surface of the metal powder is fractures by biaxial force and the powder particles are bonded. Therefore, although powder exposed to the air and having oxide film can be consolidated to a thin plate by COSME-RT, it is better to store the feedstock powder in the environment preventing oxidation. Then, although Cu and $MoS_2$ powders are exposed to the air, it is stored at 20% or less relative humidity to prevent further oxidation of the powder.

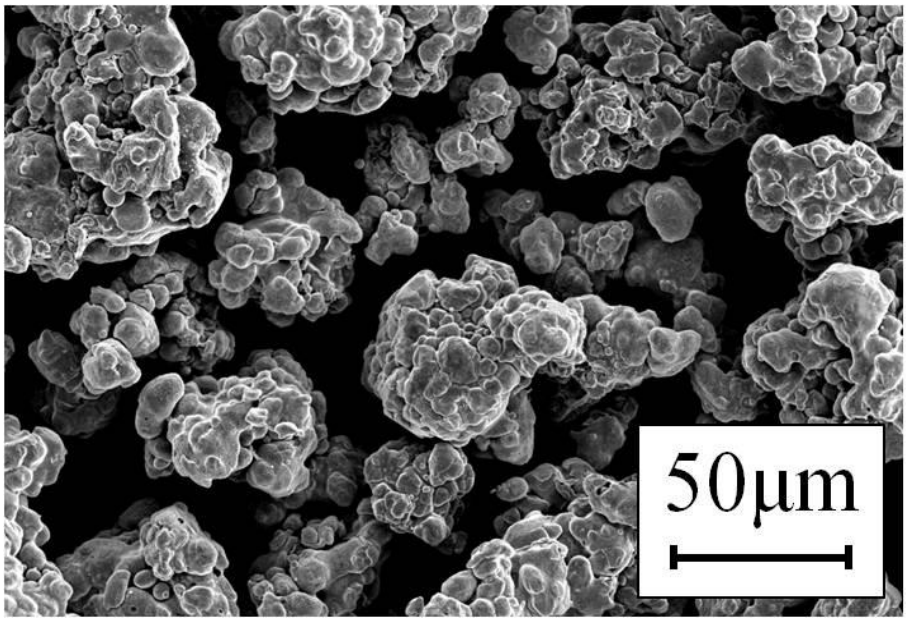


**Fig. 2-1 SEM image of pure Cu powder.**

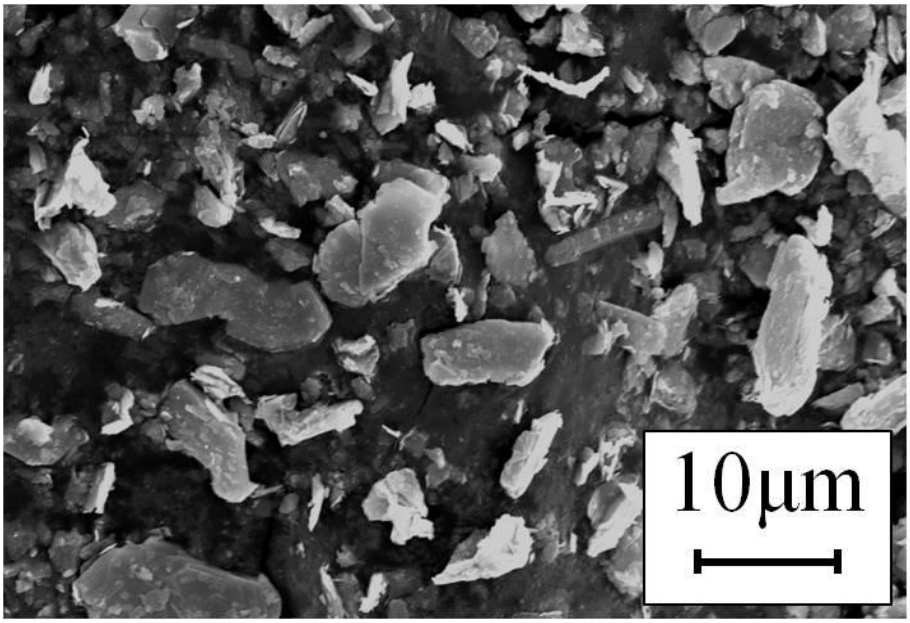


**Fig. 2-2 SEM images of $MoS_2$ powder.**

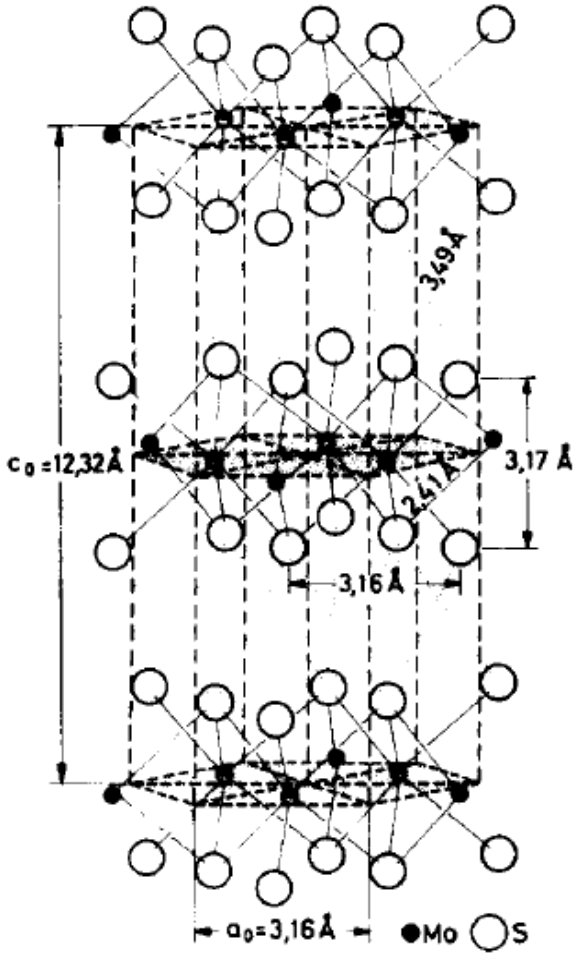


**Fig. 2-3 Crystal structure of molybdenum disulfide [2-12].**

## 2.2 Compression shearing method

Fig. 2-4 shows a schematic illustration of a compression shearing process [2-1]. The feedstock powder is placed between the base plate and the moving plate, and the compressive force $P_N$ is applied to the powder by elevating the compression stage. The compressive force $P_N$ is maintained during the forming process. Finally, the shearing force $P_S$ and the shearing strain are applied to the powder by displacing the moving plate parallel with the base plate at the constant rate, and a thin plate is formed.

The compression shearing apparatus (DRD-NNK-002, DIP Co., Ltd., Gunma, Japan) is used to form samples at Tohoku University. Fig. 2-5 shows a schematic illustration of compression shearing apparatus [2-2]. The moving plate is displaced by displacing the shearing rod. The compressive force $P_N$ and the shearing distance $L_S$ is measured by the load cell and the laser displacement sensor (OPTEX FA Co., Ltd., CD5-W150), respectively. As I described in the previous chapter, the shearing force $P_S$ cannot be measured and only the resulting tangential force can be measured. However, the shearing force is

applied to the sample during the COSME-RT process in the macroscopic view. Therefore, I define the shearing force as a measured tangential force. The shearing force $P_S$ is measured by the strain gauges on the shearing rod. These parameters are recorded in the personal computer through the A/D converter with amplifier (Kyowa Electronic Instruments Co., Ltd., PCD-320A and PCD-300B). Full bridge strain gauge circuit is adopted to remove the forces other than unidirectional shearing force. From the technical reason of this apparatus, maximum compressive force and shearing force can be applied to the sample is 500 kN and 250 kN, respectively. Maximum stroke of the shearing rod is 50 mm. The shearing strain $\gamma$ is determined from divide the shearing distance $L_S$ by the sample thickness $t_P$. Although the sample extends thinly by applying the shearing during the COSME-RT process, the initial thickness of the uniaxial compressed sample, $t_P$ = 0.25 mm was used for convenience. The shearing rate was programmed at 5.0 mm/min and target sizes of all samples were 20 × 20 × 0.25 $mm^3$. The amount of feedstock powder used for a fabrication of a sample is determined from the true density of the powder and the sample target size. For instance, when the fabrication of a pure Cu sample with 20 × 20 × 0.25 $mm^3$ target size, 0.89 g powder was used because the true density of pure Cu is 8.94 $g/cm^3$. The material of the base and moving plates are tool steel (SKD11). The geometry of the base plate and the moving plate are 165 × 50 × 52 $mm^3$, 120× 50 × 50 $mm^3$. The deformation of these plates during COSME-RT process can be neglected because the material of these plates is harder enough than feedstock powder. Both of these plates were mirror polished to arithmetic mean roughness $Ra$ = 0.04 μm.

Though the heat by friction is generating during the COSME-RT process, it has been clarified from the measurement by the type K (chromel–alumel) thermocouple that the temperature change falls within the range of the room temperature to several tens of degrees. Therefore, there is few effect by heating during the COSME-RT process.

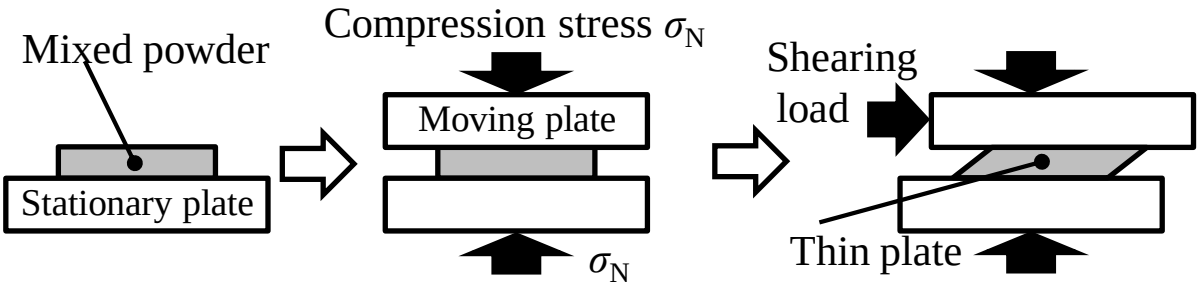


**Fig. 2-4 Schematic illustration of consolidation process by compression shearing method.**

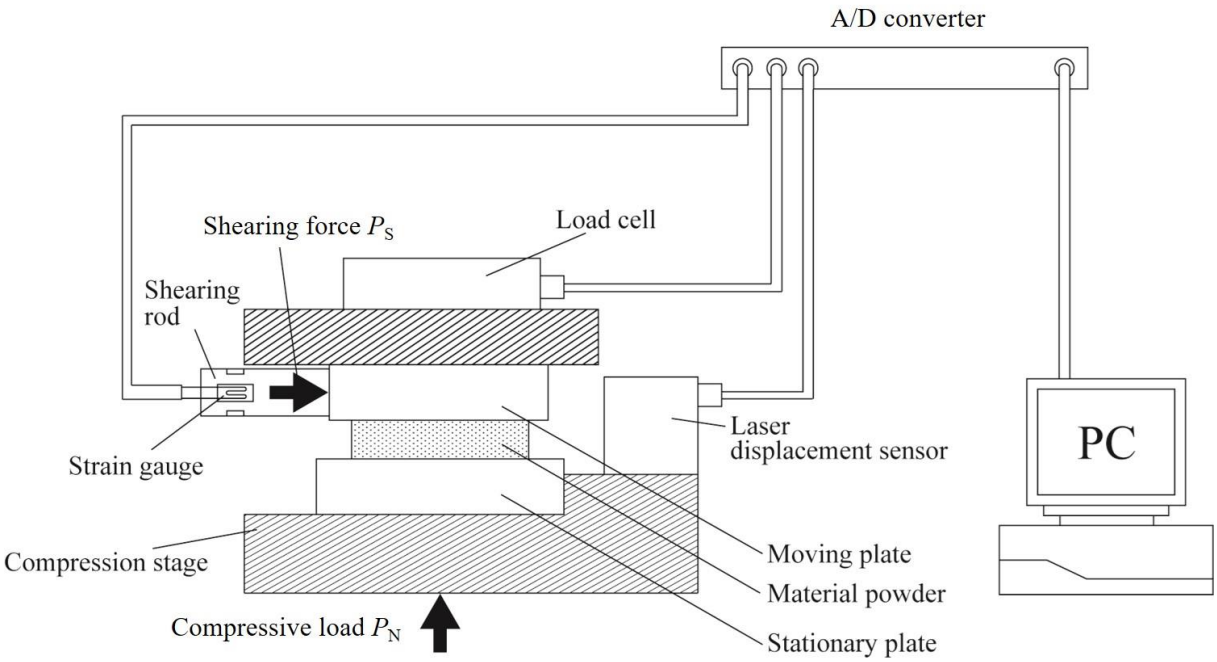


**Fig. 2-5 Schematic illustration of compression shearing apparatus (DRD-NNK-002).**

## 2.3 Sample preparation for electron microscopic observations

Samples for cross-sectional SIM observations were machined by using a FIB. However, other samples for cross-sectional observations were machined by a mechanical polishing because the machining by a FIB takes long time for large area processing.

In the mechanical polishing, firstly the sample was cut parallel with the shearing direction because the powder particles should be deformed in this direction (Fig. 2-6). Subsequently, the sample was mirror-polished by using a rotary polishing machine. Then the outer layer which was applied strain by mechanical polishing was shaved off by using an ion milling apparatus. Fig. 2-7 shows the overview image of the ion milling apparatus, PIPS Model 691 (Gatan Inc., Pleasanton, California, USA), at Tohoku University. This apparatus can polish a sample from both top and bottom sides, so it can machine thin plate sample for TEM observation.

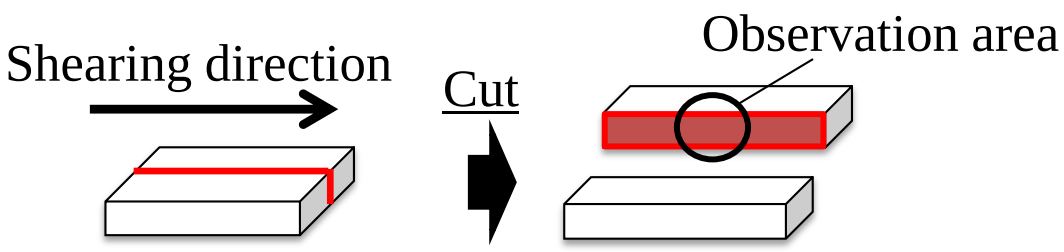


**Fig. 2-6 Schematic illustration of observed area of sample cross-section.**

**Fig. 2-7 Overview mage of ion milling apparatus, PIPS Model 691**

## 2.4 Scanning electron microscopy (SEM)

Scanning electron microscopy (SEM) detects various signals produced by interaction of the electron beam with the atoms of the sample. Fig. 2-8 shows the schematic illustration of interaction between an electron ray and a sample. These signals contain information about the composition and topography of the sample.

Secondary electron is one of most common signals produced at SEM. The number of the emitted secondary electrons changes depends on sample surface topography. For instance, the amount of the emitted secondary electrons becomes larger when the electron beam is made incident from an oblique direction than when the electron beam is perpendicularly made incident on the sample.

Characteristic X-ray has information about the composition of the sample. The compositions of the samples are analyzed qualitatively or quantitatively by measuring the number and energy of the characteristic X-rays. This analysis is called as an energy dispersive X-ray spectrometry (EDS).

I used different SEM apparatuses because of two reasons. I have stayed both LTDS and Tohoku University to do different experiments, and sometimes SEM observation was needed to proceed another experiments. It is not efficient to send some samples to another laboratory and observe by same SEM. For efficient work, I used different SEM at different laboratory. Second reason is some options attached

SEMs. I used different SEMs depending on the analysis what should be done. I used three SEMs. Most I used one is JSM-6510 (JEOL ltd., Tokyo, Japan) because it is owned by my laboratory and a time management of this SEM is easiest among three. Fig. 2-9 shows the overview image of JSM-6510 [2-3]. This SEM has an EDS equipment (Thermo Scientific™ UltraDry EDS Detector, Thermo Fisher Scientific Inc., Waltham, Massachusetts, USA). For an electron backscatter pattern (EBSP) analysis, I use JSM-7100F (JEOL ltd., Tokyo, Japan) because JSM-6510 has no EBSP equipment. Fig. 2-10 shows the overview image of JSM-6510. When I at ECL, I used MIRA3 (TESCAN, Brno, Czech Republic) [2-4]. Fig. 2-11 shows the overview image of MIRA3. It was mainly used for the observation of the sample fracture surface.

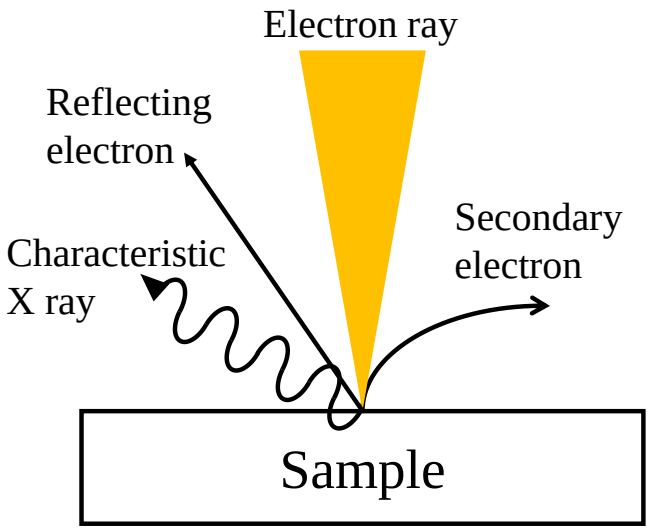


**Fig. 2-8 Schematic illustration of interaction between electron ray and sample.**


**Fig. 2-9 Overview image of SEM, JSM-6510.**

**Fig. 2-10 Overview image of SEM, JSM-7100F [2-3].**


**Fig. 2-11 Overview image of SEM, MIRA3 [2-4].**

## 2.5 Focused ion beam (FIB)

Focused ion beam (FIB) is an extremely thinly focused ion beam as the name suggests, and FIB apparatus can do micromachining, deposition, surface observation by irradiating the ion beam to the sample surface.

It is possible to perform the micromachining a sample by irradiating the focused ion beam and removing atoms on the sample surface. Based on this feature, the sample preparation for the cross-sectional observation and the sample thinning for TEM observation are performed by using FIB apparatus.

In addition, a certain kind of material can be deposited on the sample surface by irradiation the focused ion beam while blowing a gas containing atoms of that material on the sample surface. This feature is used for the deposition of the protective film on the sample surface at the preparation of the thin film sample and is used for the wiring of the semiconductor device.

FIB can be used for the topography imaging of the samples by detecting the secondary electrons or the secondary ions emitted from the sample when the focused ion beam is irradiated like SEM. The image obtained by FIB observation is called as the scanning ion microscopy (SIM) image. The secondary electrons are emitted only from the topmost surface layer of the sample surface because the ion penetration depth into the sample is shallower than that of electrons. Therefore, the information on the region closer to the sample surface than the SEM observation can be obtained by the SIM observation. In SIM images, the composition contrast and crystal orientation contrast appear more strongly than SEM images because the secondary yield of the ion beam is higher than the electron beam. In contrast, the resolution of the SIM image is lower than that of the SEM image because the beam diameter of the ion beam is larger than that of electron beam.

In this study, Helios NanoLab$^{TM}$ 600i (FEI Company, Hillsboro, Oregon, USA) at Tohoku University was used for micro-size processing and SIM observation. Fig. 2-12 shows the overview image of Helios NanoLab$^{TM}$ 600i [2-5]. This apparatus is using a gallium (Ga) ion source. To protect the sample from the damage by Ga ion beam, a 200 nm carbon protective layer was deposited on the sample surface by using the carbon evaporation apparatus and a 2.0 μm Pt protective layer was deposited on the carbon layer before the machining by FIB. The acceleration voltage was programmed at 30 kV, and the irradiation current was adjusted to perform the machining, deposition, and observation. The sample cross-section was processed as shown in Fig. 2-13. The sample was excavated like steps and cross-section was observed from an angle because it is difficult to observe the cross-section vertically.

**Fig. 2-12 Overview image of FIB apparatus, Helios NanoLab™ 600i [2-5].**

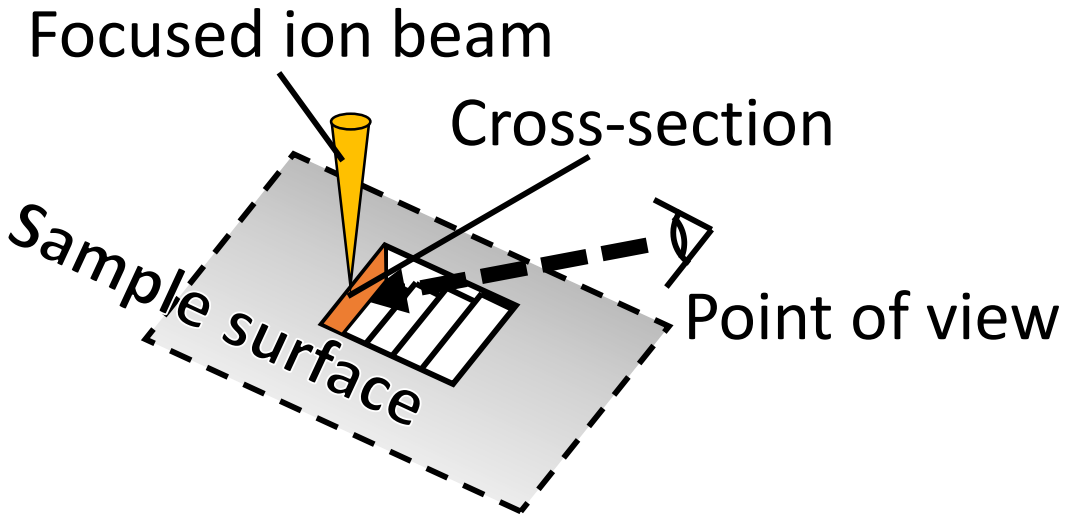


**Fig. 2-13 Schematic illustration of sample processing and observation by FIB.**

## 2.6 Transmission electron microscopy (TEM)

Transmission electron microscopy (TEM) uses an electron to obtain an image beam like SEM but the beam is transmitted through a sample. Fig. 2-14 shows the schematic illustration of TEM. The accelerated electron beam from several tens to several hundreds of kV is irradiated to the thinned sample (~100 nm thickness), and the transmitted electrons are magnified and observed with a magnetic lens. In addition, the structure of the sample can be observed from the interference image resulting from a diffraction of electrons in the sample utilizing the wave nature of electrons.

In this study, HF-2000 (Hitachi High-Technologies Corporation., Tokyo, Japan) was used. Fig. 2-15 shows the overview image of HF-2000 [2-3]. All TEM observations were carried out at Tohoku University.

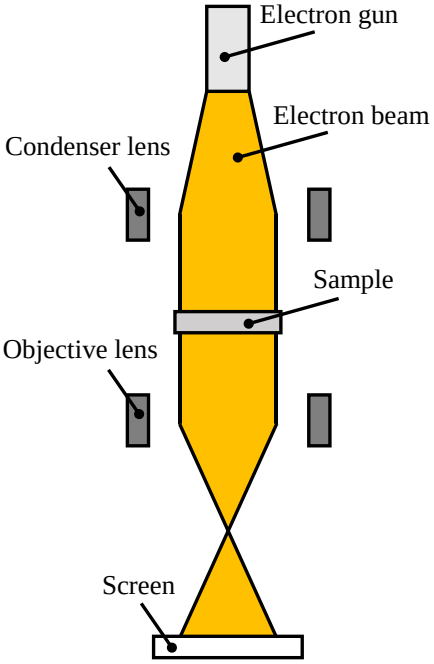


**Fig. 2-14 Schematic illustration of TEM.**

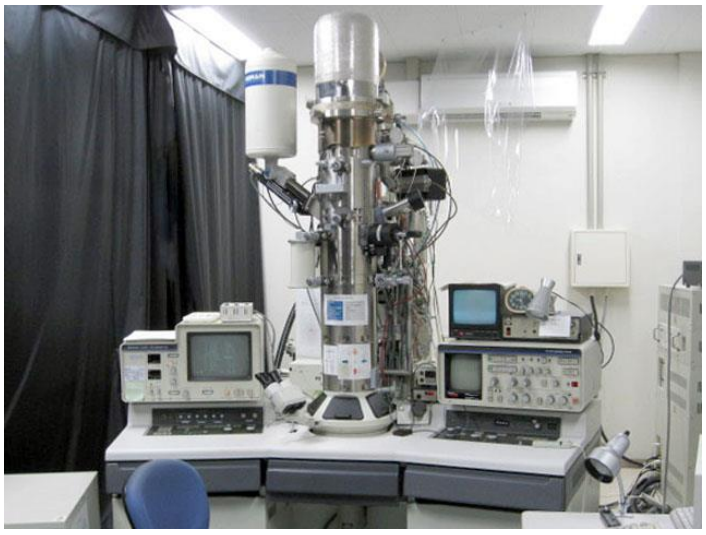

**Fig. 2-15 Overview image of TEM, HF-2000 [2-3].**

## 2.7 X-ray diffraction (XRD)

X-ray diffraction (XRD) is a phenomenon that X-ray irradiated to the crystal lattice is scattered from electrons and these scattered X-ray show the diffraction pattern. The technique which use the XRD to determine a molecular structure of a crystal is called as X-ray crystallography or just as XRD.

In this study, X-ray diffraction was used to investigate whether any compounds are generated during the COSME-RT process or not. In conventional powder metallurgical techniques, heating process is needed and sometimes material properties are deteriorated by generating compounds. Even no compound should be generated during COSME-RT because whole process is carried out at room temperature, this investigation is important to consider the effect of compound during the COSME-RT process.

In addition, X-ray diffraction was used for the texture analysis of the sample because the metal materials applied huge strain often exhibit the texture.

Fig. 2-16 shows the overview image of an X-ray diffractometer (D8 Discover, Bruker, Billerica, Massachusetts, USA) which was used in this study [2-6]. All XRD investigations were carried out at Tohoku University.


**Fig. 2-16 Overview image of X-ray diffractometer (D8 Discover).**

## 2.8 Friction test

### 2.8.1 Overview of friction test

Friction test is originally to investigate the friction and the wear phenomena between materials. Generally in friction test, a set of samples are slide under constant load and rate, and the coefficient of friction and the wear property of sample are investigated by measuring the frictional force and the wear amount, respectively. The tribological properties of the samples under specific environments can be investigated by the friction test with the controlled atmosphere. For instance, the tribological properties of materials used in outer space are investigated under high vacuum condition with the apparatus inside the vacuum chamber. By adding lubricants such as oils or greases on the contact surface, the lubricating properties of the lubricants can be investigated.

The friction test is classified by the shape of the samples such as ball, pin and disc, but it is also roughly classified as a rotation friction test and a linear friction test by how to slide the sample. Fig. 2-17 shows the schematic illustrations of the typical friction tests. In both friction tests, one of two samples is placed on a stage, and a normal load is applied to the samples through the counter material. Then, the samples slide by movement of the stage. The friction force applied to the sample is measured by sensors on the stage or jig which fixed the counter material. The friction coefficient of the sample is calculated by dividing the friction force by the normal load.

In the rotation friction test, although both samples are always sliding in the same direction, the direction of applied friction force is circumferential (Fig. 2-17(a)). Hence, it is difficult to cut the sample along the sliding direction and observe the microstructural change of the sample in the depth direction.

In contrast, in the linear friction test, the sliding direction changes because of the reciprocating movement of the sample as shown in Fig. 2-17(b). Thus, the sample is applied a round trip friction from the counter material. However, the microstructural observation of the sample is easier than that of the rotation friction test because the direction of applied friction force is linear.

Therefore, both methods have advantage and withdraw, and the modified way is required. The linear friction test was chosen in this study as a base of a new method. The reciprocating linear friction test was modified to the unidirectional sequence to achieve the objective of this study. I introduce this friction sequence, termed as the unidirectional friction experiment, in the next section.

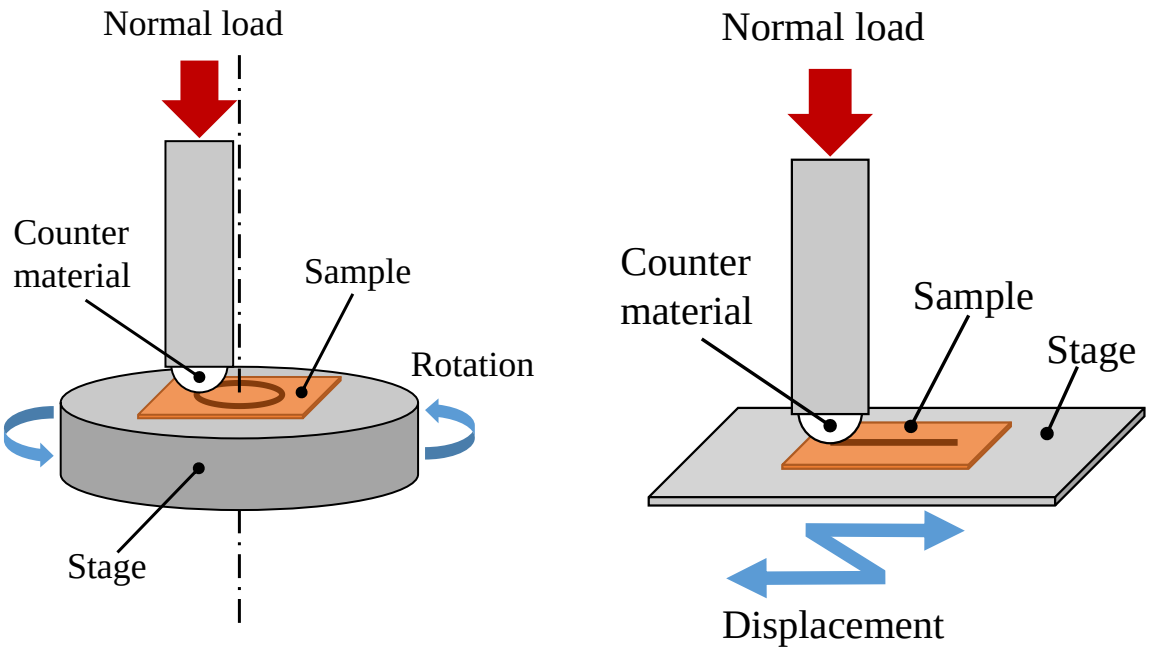


(a) Rotation type tribometer (b) Linear tribometer

**Fig. 2-17 Schematic illustrations of friction tests.**

## 2.8.2 Unidirectional friction experiment

Fig. 2-18 shows a schematic illustration of the unidirectional friction experiment by a linear tribometer. The following four steps are defined as one cycle, and the shearing strain was accumulated by the sample through repetition of this cycle. (1) The ball is placed on a uniaxially compressed sample and a normal force is applied to the sample through the ball. (2) A tangential force is applied to the ball while maintaining the applied normal force. Then, the ball was sliding on the sample surface and a tangential force was applied to the sample. (3) Pull off the ball from the sample. (4) The ball is moved to the initial position of the first step.

During the COSME-RT process, the tangential force applied to each powder particle homogenously, such that we could observed only the average bonding condition of all the particles on a sample. In contrast, the applied stress from the spherical contact has a certain distribution according to Hertzian contact theory.

Fig. 2-19 shows the overview image of the linear tribometer used for unidirectional friction experiment in this study. This tribometer is built by LTDS, and it can conduct friction test with lubricant. The maximum normal load can be applied is 100 N. This tribometer is usually used for reciprocating friction test, but the Lab View program for this tribometer was modified for unidirectional friction sequence.

Pure metal powder was compressed under the uniaxial normal stress of 1000 MPa in order to get uniaxial-compressed samples with the target size of 20 × 20 × 0.25 $cm^3$. The samples were formed by using a COSME-RT apparatus. The conditions of the friction experiments were set to correspond with the forming conditions of the pure Cu plate by COSME-RT [12] to interpret its process. There is no oxidation and wear during the COSME-RT process because powder particles are placed between two steel plates and whole process is carried out in this enclosed area. To avoid the oxidation of the sliding surface, all the experiments were carried out with 5.0 l/min nitrogen blowing around the contact surface (Fig. 2-20). In addition, a $ZrO_2$ ball of half-inch diameter was chosen as a counter material to avoid the wear of the sliding surface because it shows better tribological behavior with Cu than that of a bearing steel SUJ2 (AISI52100) ball from the preliminary experiments. The amplitude and the sliding velocity were set to be 10 mm and 5.0 mm/min, respectively. The normal load *P* was programmed to 4.0 N and 27 N, which correspond to the theoretical maximum Hertzian contact pressure of 500 MPa and 1000 MPa, respectively. The number of the sliding cycles *N* was changed from 100 to 200. All the friction experiments were carried out at room temperature.

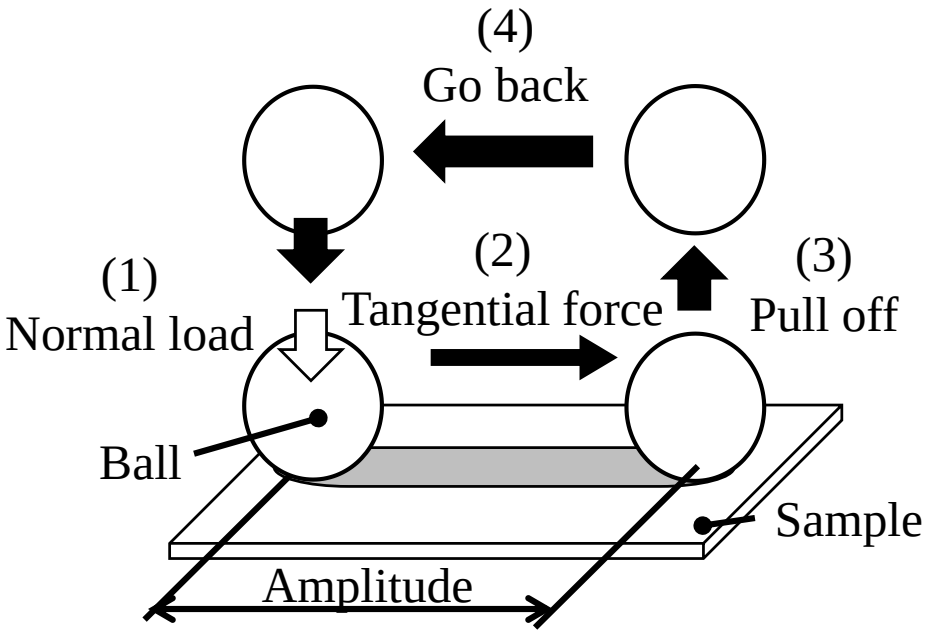


**Fig. 2-18 Schematic illustration of unidirectional friction experiment.**

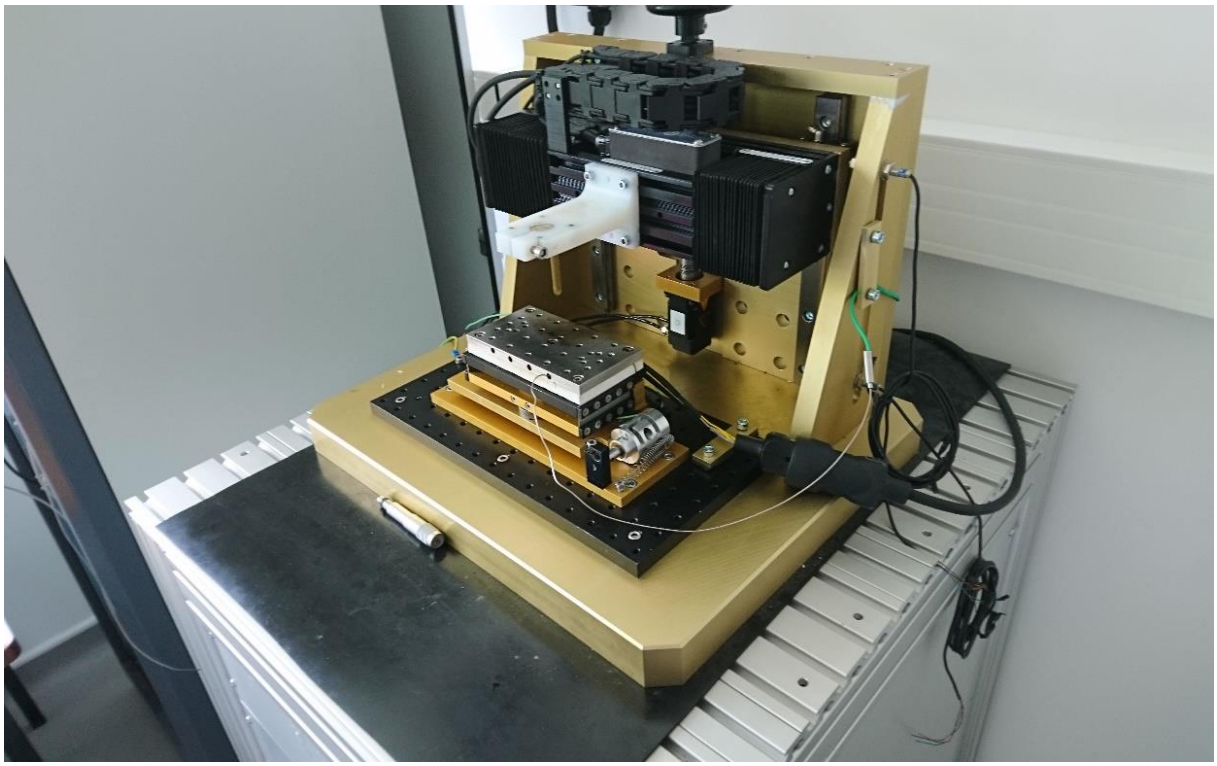

**Fig. 2-19 Overview image of linear tribometer.**

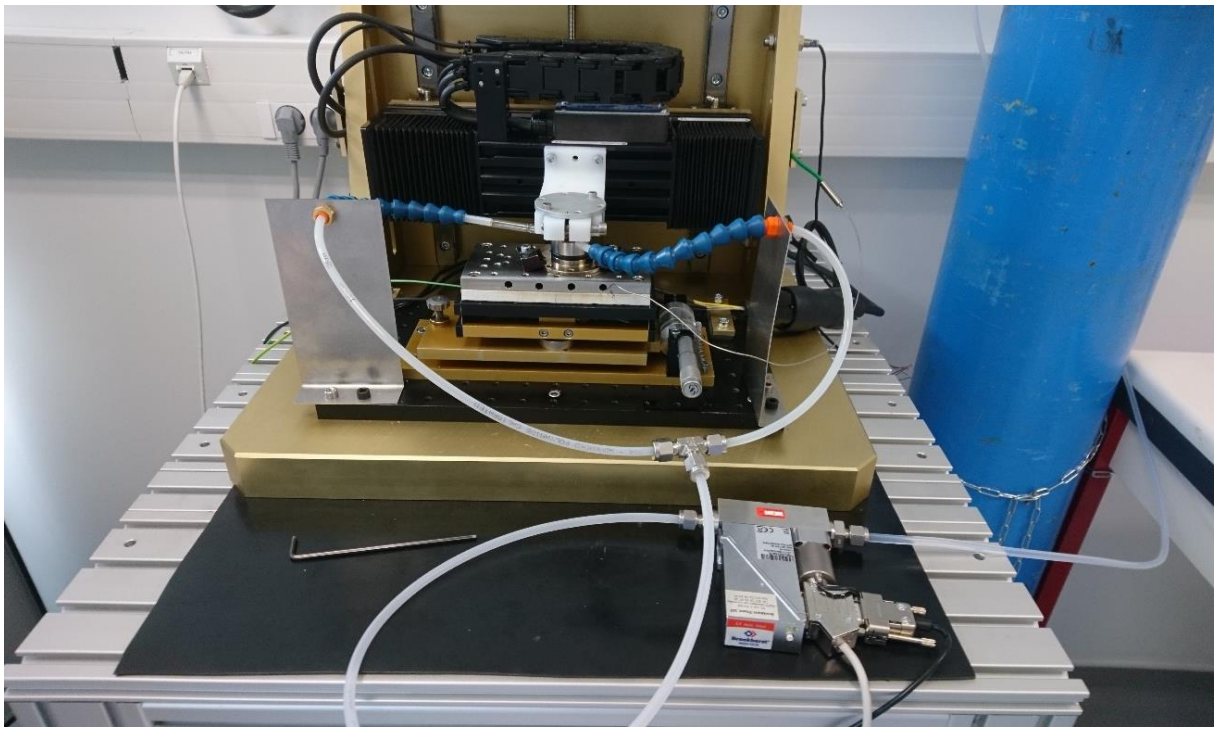

**Fig. 2-20 Overview of linear tribometer with nitrogen flow system.**

# References

(2-1) H. Takeishi, N. Nakayama, H. Miki, Consolidation with Grain Refinement by Compression Shearing Method under Room Temperature, Journal of the Society of Materials Science, 54, 3, (2005), pp. 233 - 238. (in Japanese)

(2-2) S. Takeda, H. Miki, H. Takeishi, T. Takagi, Cu-Based $MoS_2$-Dispersed Composite Material Formed by the Compression Shearing Method at Room Temperature, Tribology Online, 12, 2, (2017), pp. 29 - 36.

(2-3) Technical Division, School of Engineering, Tohoku University, (2018), [online] http://www.tech.eng.tohoku.ac.jp/sosiki/goudou/b01/b01.html (2018/January/10 access), (in Japanese).

(2-4) MIRA3 | TESCAN, (2018), [online] https://www.tescan.com/en-us/technology/sem/mira3 (2018/January/10 access).

(2-5) Material Solutions Center, Tohoku University, (2018), [online] http://www.masc.tohoku.ac.jp/shared/f.html (2018/January/10 access), (in Japanese).

(2-6) D8 DISCOVER Family - X-ray Powder Diffractometer, DAVINCI.DESIGN - X-ray Diffraction and Scattering | AXZ Bruker | Bruker, (2018), [online] https://www.bruker.com/products/x-ray-diffraction-and-elemental-analysis/x-ray-diffraction/d8-discover-family.html (2018/January/10 access).

(2-7) N. Nakayama, M. Horita, H. Miki, T. Miyazaki, H. Takeishi, Effects of Powder Size and Shape on Microstructure of Al Thin Plate Formed by Compression Shearing Method at Room Temperature, Journal of the Japan Society for Technology of Plasticity, 54, 625, (2013), pp. 191 - 195. (in Japanese)

(2-8) M. Horita, N. Nakayama, H. Miki, T. Miyazaki, H. Takeishi, Microstructure of Titanium Thin Plates Formed by Compression Shearing Method at Room Temperature, Journal of the Japan Society for Technology of Plasticity, 54, 625, (2013), pp. 186 - 190. (in Japanese)

(2-9) M. Horita, Doctor Thesis, Shinshu University, Japan, (2014). pp. 65 - 67.

(2-10) E. W. Roberts, Thin solid lubricant films in space, Tribol. Inter., 23, 2, (1990), pp. 95 - 104.

(2-11) E. Takeuchi, Lubrication of Molybdenum Disulfide ($MoS_2$) (1), The Journal of the Metal Finishing Society, 11, 1, (1960), pp. 30 – 35.

(2-12) R. Holinski, J. Gänsheimer, A Study of the Lubricating Mechanism of Molybdenum Disulfide, Wear, 19, (1972), pp. 329 – 342.

# Chapter 3

# Effect of the Shearing Force on the Consolidation Process

In the previous chapters, I mentioned the importance of understanding and controlling the consolidation process of material formed by COSME-RT.

From the hypothesis that the powder particles are bonded by the friction due to application of the shearing force in the COSME-RT process, the shearing force applied to the powder particles is considered to be one of the important factors for the bonding of the powder particles. Thus, in this study, I attempt to control the shearing force to understand and control the consolidation process of material formed by COSME-RT.

In this chapter, the effect of the applied shearing force on the consolidation process of the powder particles by controlling the shearing force will be clarified.

In the previous study, the development of a Cu-based $MoS_2$-dispersed composite was attempted and the composite exhibited a low friction coefficient and a high material strength [3-1]. Microstructural studies of the Cu/$MoS_2$ sample indicated that the bonding and crystalline grain refinement of Cu powder particles of Cu/$MoS_2$ were incomplete compared with the pure Cu sample. This result suggested that shearing forces that were applied to the Cu powder particle were dissipated because of the lubricity by $MoS_2$ particles between the Cu powder particles. Therefore, the COSME-RT process can be controlled by dispersing solid lubricant into the matrix material, which might decreases the applied shearing force.

The main objective of this chapter was to understand the effect of the solid lubricant $MoS_2$ on the consolidation process. We used a Cu/$MoS_2$ composite to perform a new approach to control material consolidation by COSME-RT. Cu/$MoS_2$ samples were formed under several shearing distances and the microstructures of the samples were observed. The microstructural change related to the decrease in applied shearing force is discussed.

# 3.1 Material and forming conditions

## 3.1.1 Mixed powder

The mortar was used for the mixing of pure Cu and $MoS_2$ powders. These powders were mixed for 10 minutes in the air atmosphere. A mixed powder with a $MoS_2$ concentration $r$ = 5.0 vol.% was prepared. The $r$ = 5.0 vol.% sample showed the lowest coefficient of friction and a high mechanical strength, according to our previous study [3-1]. Although a pure Cu powder particle originally has some pores inside and is not a fully-dense material, these pores are expected to be crushed by compressed and sheared, and then a sample become a dense material. A true density was used for calculation of the mixing ratio of powders, and 8.94 g/cm$^3$ and 4.96 g/cm$^3$ were used as the true densities of Cu and $MoS_2$, respectively. The mixed powder was prepared in several batches by 1.0 cm$^3$ because it is difficult to mix a large amount of mixed powder at once by using a mortar. 0.10 cm$^3$ mixed powder is used for one sample because the target size of the sample is 20 × 20 × 0.25 mm$^3$. Hence, it is possible to prepare the mixed powder enough amount to produce ten samples by one mixing. The amounts of Cu and $MoS_2$ powders used for one mixing are 8.49 g and 0.248 g, respectively.

If $MoS_2$ is not homogeneously dispersed in the matrix material, an unevenness of a suppression of the shearing force by $MoS_2$ may be caused and the effect by dispersing $MoS_2$ may not be sufficiently obtained. Therefore, the dispersion of $MoS_2$ in the mixed powder should be confirmed preliminary by using an EDS.

Fig. 3-1 shows the SEM image and EDS mapping image of the mixed powder. The colored regions on the mapping images are Mo. In the previous study on the composite materials by COMSE-RT, a three axes ball milling machine or a uniaxial ball milling machine were used for the powder mixing to disperse the $MoS_2$ powder particles homogeneously in the Cu powder particles. From Fig. 3-1, the $MoS_2$ powder particles were homogeneously dispersed. Therefore, it is possible to sufficiently disperse the $MoS_2$ powder particles in the Cu powder particles even by mixing with a mortar.

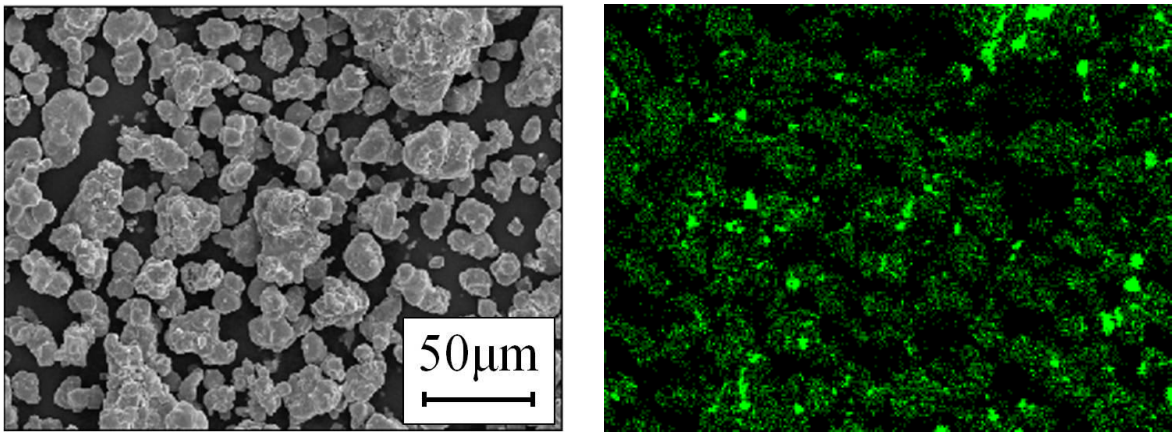


(a) SEM image (b) Mo Lα

**Fig. 3-1 (a) SEM image and (b) mapping image of Mo of Cu/$MoS_2$ mixed powder.**

### 3.1.2 Forming conditions of samples by COSME-RT

Fig. 3-2 shows a simplified schematic illustration of COSME-RT process [3-2]. The compressive force $P_N$ was 500 kN, which corresponds to a compressive stress $\sigma_N$ = 1250 MPa, and the shear rate was 5.0 mm/min. The samples were formed with several shearing distances $L_S$ = 0, 0.25, 0.50, 2.5, and 5.0 mm. The sample that was formed without applying a shearing strain ($L_S$ = 0 mm) was termed the "uniaxial compressed sample". All samples were fabricated at room temperature under ambient atmosphere. Pure Cu samples were fabricated with same conditions as Cu/$MoS_2$ for comparison.

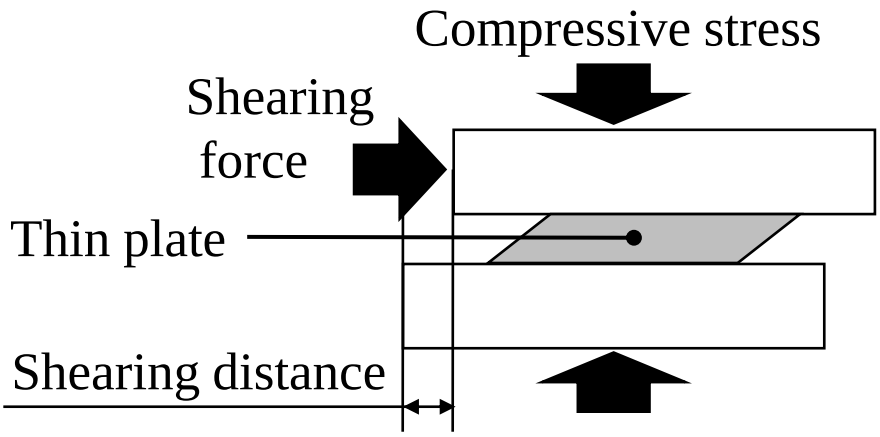


**Fig. 3-2 Simplified schematic illustration of COSME-RT process.**

## 3.2 Microstructural change of sample

### 3.2.1 Overview observation

Firstly, overviews of samples were observed to investigate the formability of the samples. Fig. 3-3shows $r$ = 0 vol.% and Fig. 3-4 shows $r$ = 5.0 vol.% samples. Each sample has a metallic luster and was consolidated in one piece of thin plate, but these outer edges doesn't have a metallic luster and appeared to be not consolidated. Compared with pure Cu sample, $r$ = 5.0 vol.% sample became darker color because a color of dispersed $MoS_2$ is darker than Cu and has no metallic luster.

These samples were consolidated into a thin plate with similar size as the target size, but the pure Cu sample was deformed along the shearing direction with increasing the shearing distance. Particularly, the part with metallic luster gradually expanded. The length of deformation appears to be similar as the shearing distance. In contrast, the size of Cu/$MoS_2$ samples didn't change even the shearing distance changed. The thicknesses of these samples were around 0.23 mm.

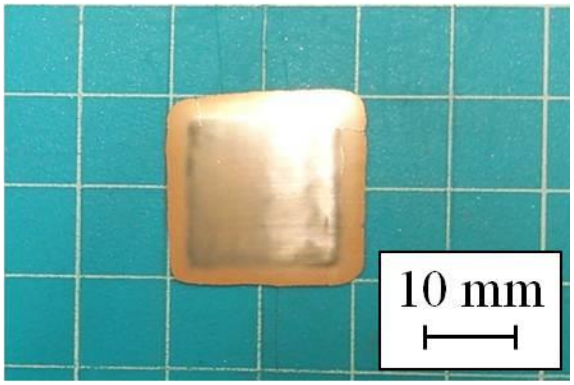


(a) $r$ = 0 vol.%, $L_S$ = 0 mm

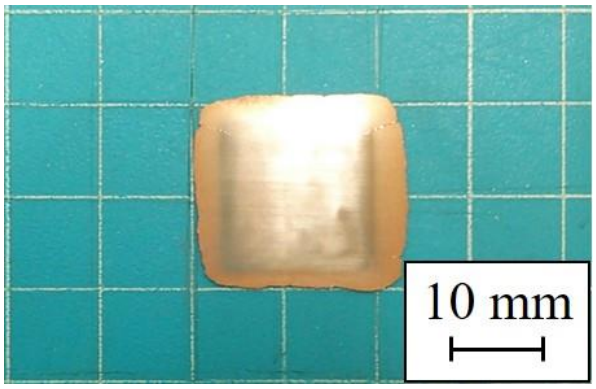


(b) $r$ = 0 vol.%, $L_S$ = 0.25 mm

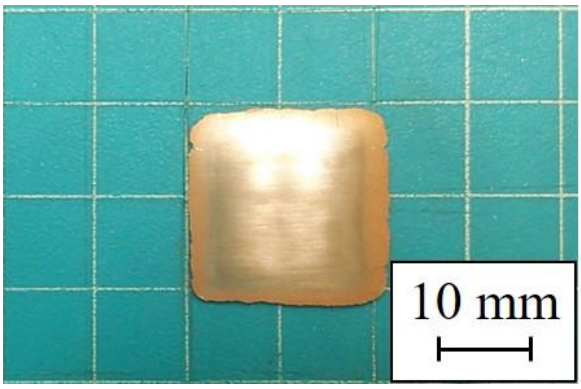


(c) $r$ = 0 vol.%, $L_S$ = 0.50 mm

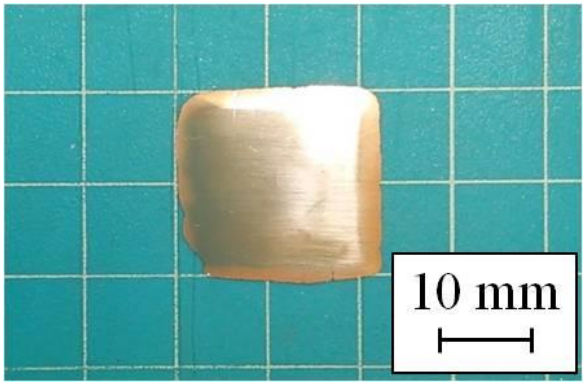


(d) $r$ = 0 vol.%, $L_S$ = 2.5 mm

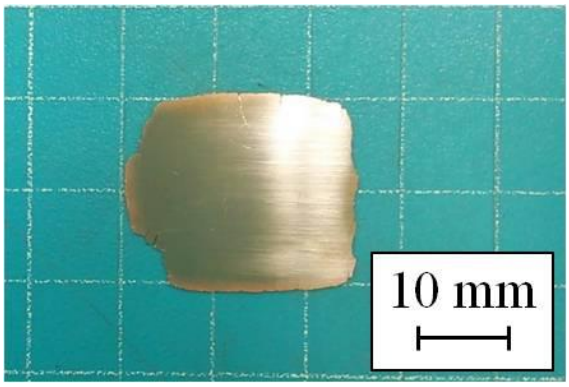


(e) $r$ = 0 vol.%, $L_S$ = 5.0 mm

**Fig. 3-3 Overviews of pure Cu samples formed by COSME-RT with various shearing distances.**

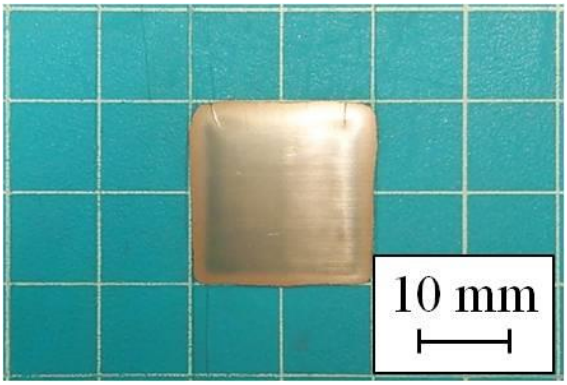


(a) $r$ = 5.0 vol.%, $L_S$ = 0 mm

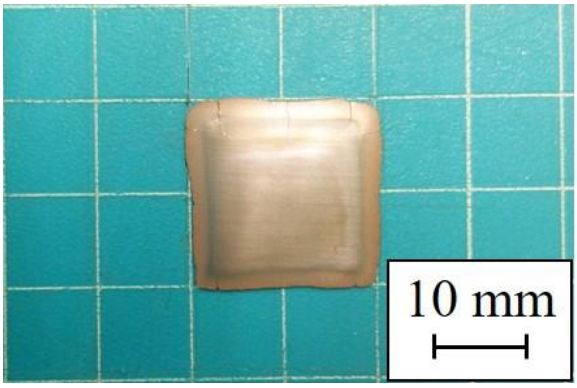


(b) $r$ = 5.0 vol.%, $L_S$ = 0.25 mm

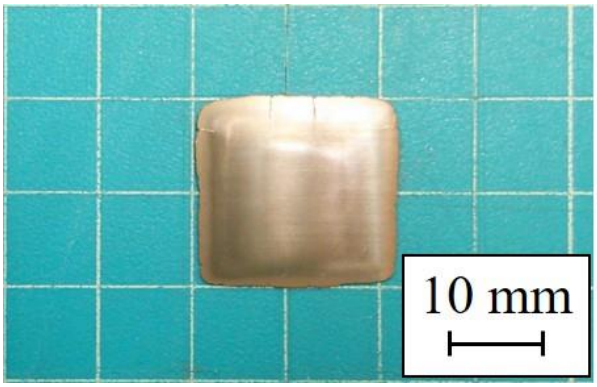


(c) $r$ = 5.0 vol.%, $L_S$ = 0.50 mm

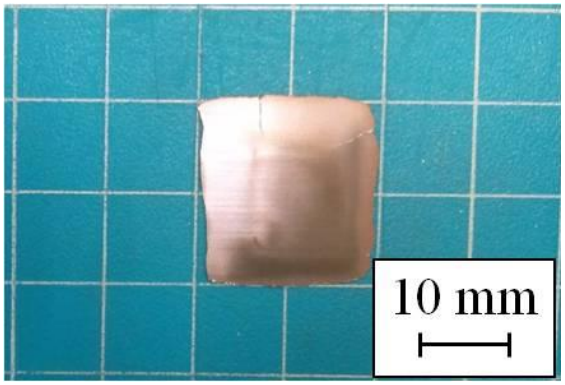


(d) $r$ = 5.0 vol.%, $L_S$ = 2.5 mm

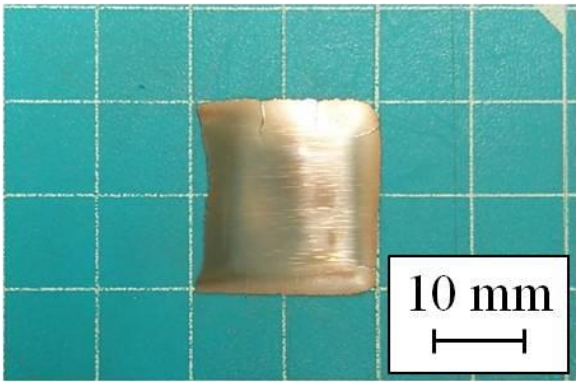


(e) $r$ = 5.0 vol.%, $L_S$ = 5.0 mm

**Fig. 3-4 Overviews of Cu/$MoS_2$ samples formed by COSME-RT with various shearing distances.**

### 3.2.2 Optical microscope observation of sample surface

Fig. 3-5 and Fig. 3-6 shows the optical microscope images of the top and bottom surfaces of the Cu/$MoS_2$ sample that were formed at various shearing distances $L_S$. The darkest dots must be voids. When $L_S$ = 0 mm, the morphology of the both sides are similar and these have many voids. The morphology of the top surfaces did not change with an increase in $L_S$. In contrast, a significant change was observed on the bottom surfaces when $L_S$ was increased: the morphology of the bottom surface was similar to the top surface until $L_S$ = 0.25 mm, but when $L_S$ = 0.50 mm or more, deformed gray dots were observed along the shearing direction. For comparison, Fig. 3-7 shows optical microscope images of the surface of a pure Cu sample that was formed at $L_S$ = 5.0 mm. The morphology of both sides of the pure Cu sample were the same. A difference exists between the forming processes of the pure Cu sample and the Cu/$MoS_2$ composite sample.

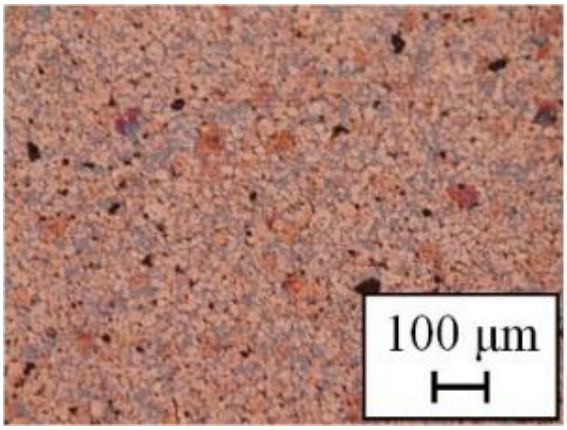


(a) $L_S$ = 0 mm, Top

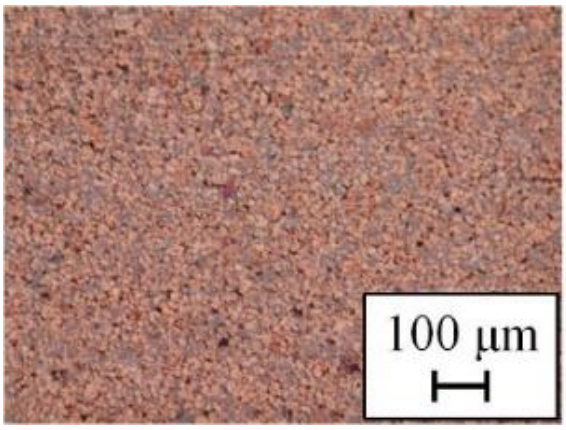


(b) $L_S$ = 0 mm, Bottom

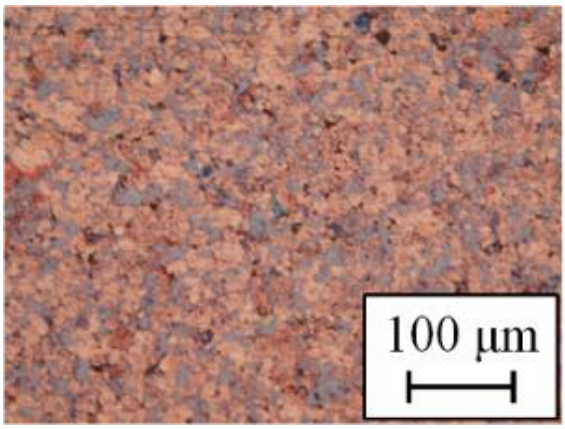


(c) $L_S$ = 0.25 mm, Top

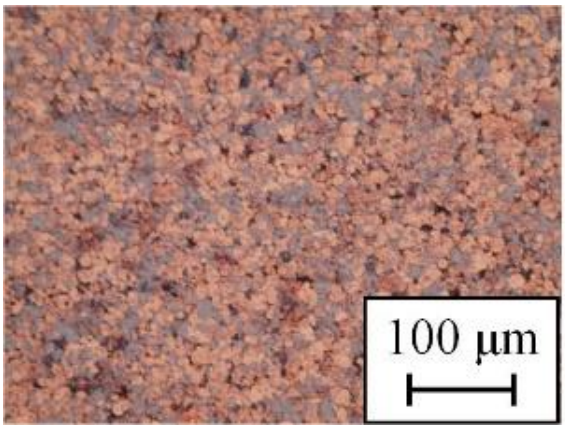


(d) $L_S$ = 0.25 mm, Bottom

**Fig. 3-5 Optical microscope images of Cu/$MoS_2$ sample surfaces ($L_S$ = 0, 0.25 mm).**

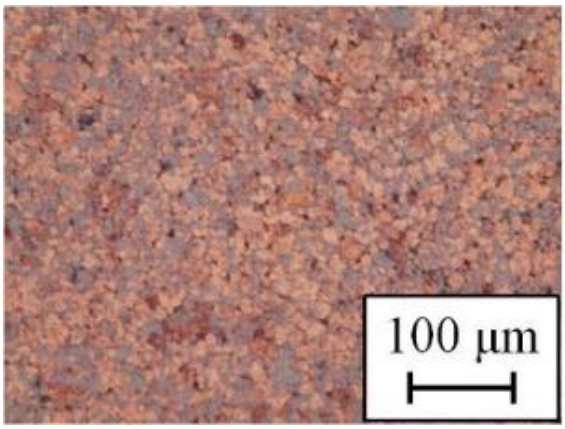


(e) $L_S$ = 0.50 mm, Top

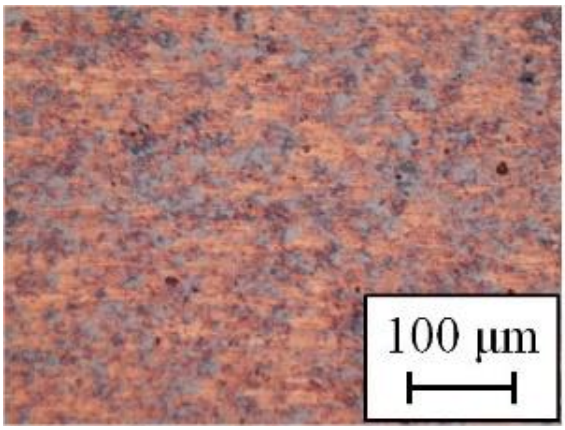


(f) $L_S$ = 0.50 mm, Bottom

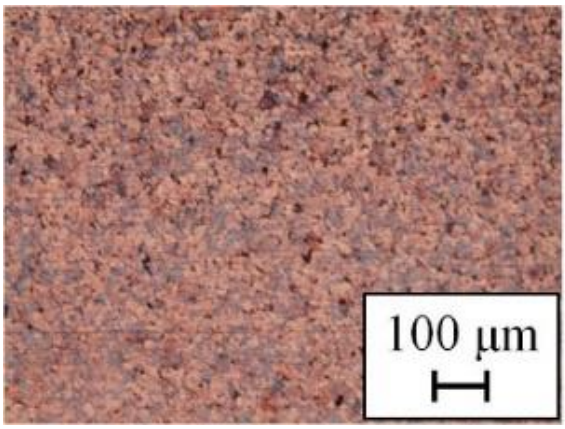


(g) $L_S$ = 2.5 mm, Top

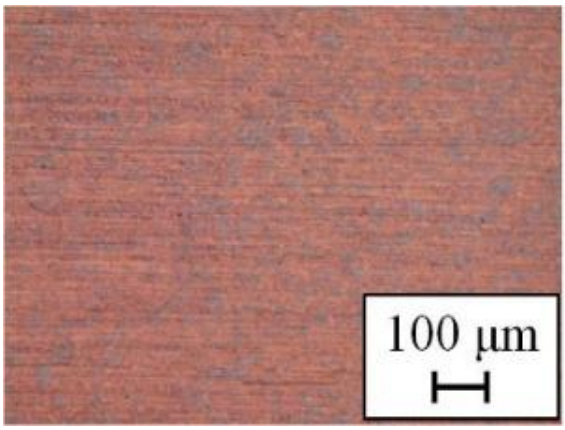


(h) $L_S$ = 2.5 mm, Bottom

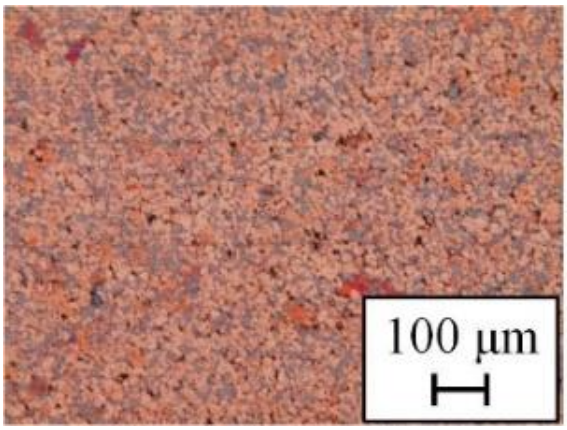


(i) $L_S$ = 5.0 mm, Top

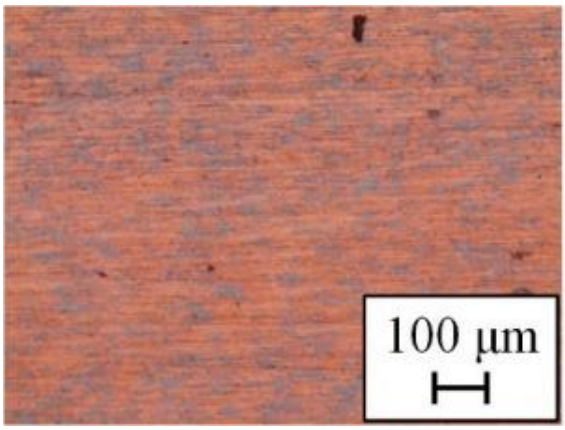


(j) $L_S$ = 5.0 mm, Bottom

**Fig. 3-6 Optical microscope images of Cu/$MoS_2$ sample surfaces ($L_S$ = 0.50, 2.5, 5.0 mm).**

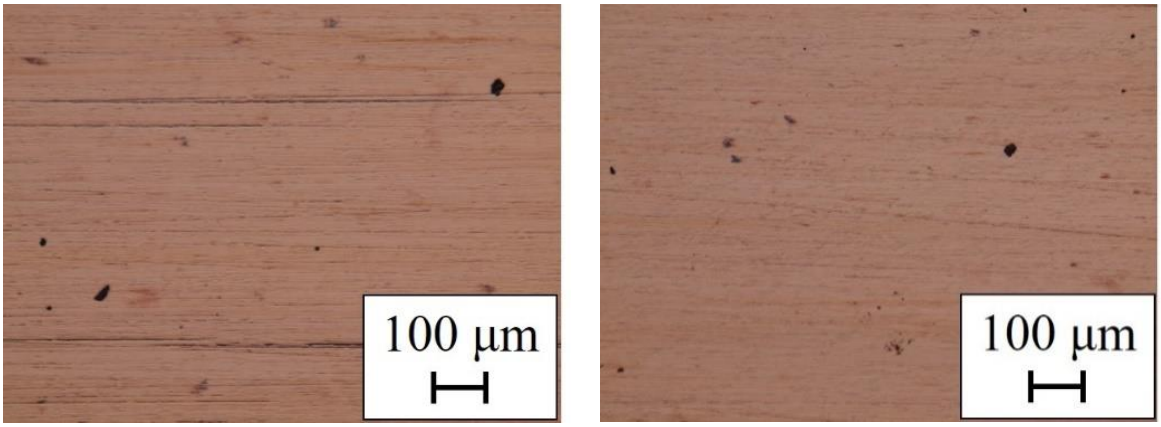


(a) $L_S$ = 5.0 mm, Top (b) $L_S$ = 5.0 mm, Bottom

**Fig. 3-7 Optical microscope images of pure Cu sample surfaces.**

### 3.2.3 SEM observation and EDS analysis of sample surface

To investigate the microstructural evolution of the Cu/$MoS_2$ samples, SEM observations and EDS analyses were carried out. Fig. 3-8 shows the SEM images and EDS mapping images of Mo Lα at the sample surfaces when $L_S$ = 0.50 mm. The colored regions on the mapping images are Mo. The 10–20-μm aggregates of $MoS_2$ were dispersed homogeneously on the top surface. While those on the bottom surface deformed along the shearing direction. The bottom surface appears to be deformed by applying shearing stress, whereas the top surface maintains its initial structure. Therefore, the Cu/$MoS_2$ sample appeared to slip on the bottom surface during the COSME-RT process.

These results also suggest that the gray dots on Fig. 3-4 appear to be $MoS_2$ aggregates.

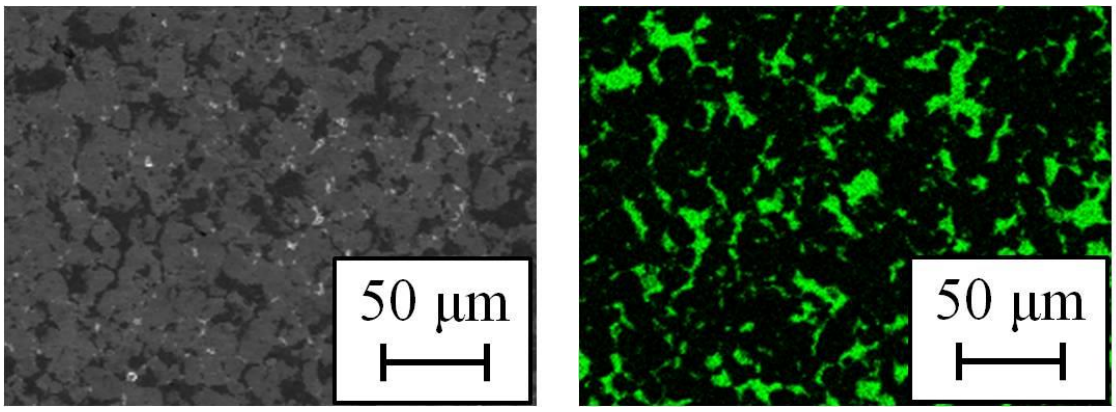


SEM image　　Mo

(a) Top surface

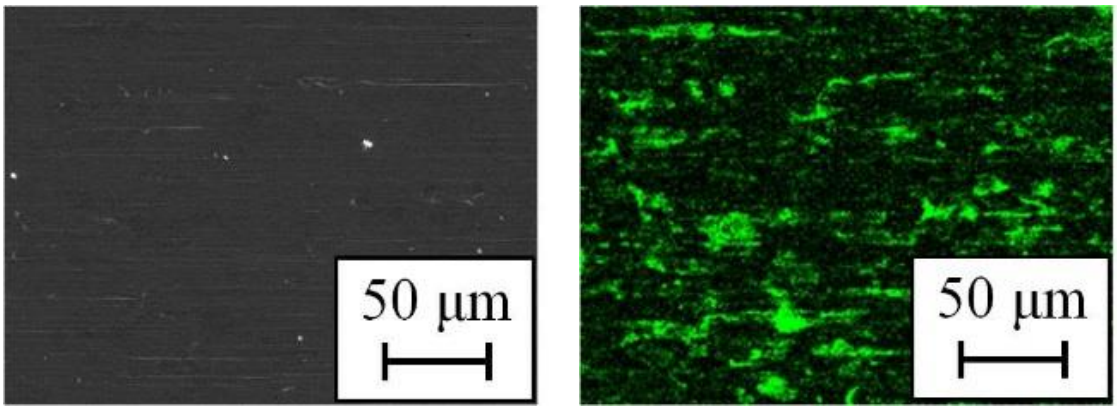


SEM image　　Mo

(b) Bottom surface

**Fig. 3-8 SEM images and EDS mapping images of Mo on both sides of Cu/$MoS_2$ sample ($L_S$ = 5.0 mm)**

### 3.2.4 XRD analysis

The sample surface was analyzed by XRD to investigate whether the crystalline structure changed before and after COSME-RT process. Fig. 3-9 shows the X-ray diffraction pattern of $r$ = 5.0 vol.% sample. The peaks other than Cu and $MoS_2$ such as $MoO_3$ or $CuMo_2S_3$ which are produced by oxidation or chemical reaction was not confirmed. Therefore, $MoS_2$ is expected to exhibit its lubrication without being deteriorated.

It has been clarified that Al having face-centered cubic structure like Cu is textured by COSME-RT process [3-3], and the structural anisotropy of Cu/$MoS_2$ is expected to be occurred by texturing of Cu. However, Cu/$MoS_2$ sample doesn't show the preferred orientation of Cu clearly. While Cu doesn't appear to make clear texture structure, $MoS_2$ shows a strong peak intensity on the (0 0 2) plane which is a slip plane. This difference in the peak intensity appears to be caused by applying a shearing strain during the forming process. It means that $MoS_2$ appears to be textured because it was shear fractured by applying shearing.

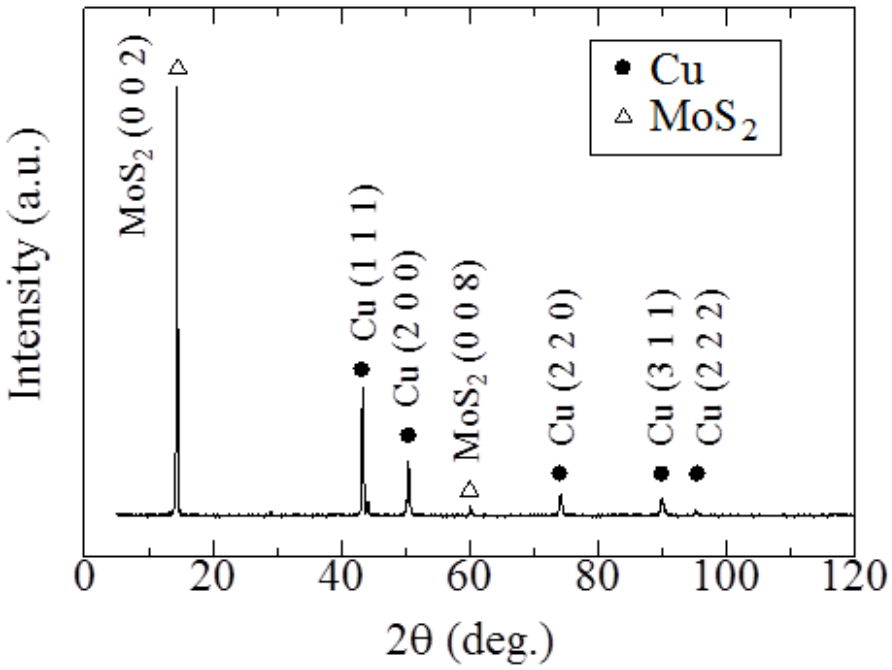


**Fig. 3-9 X-ray diffraction pattern of $r$ = 5.0 vol.% Cu/$MoS_2$ sample formed by COSME-RT.**

## 3.2.5 Observation of cross-sectional structures

### 3.2.5.1 EBSP analysis

Firstly, the change of the crystal grain size of the Cu was investigated by using EBSP.

Fig. 3-10(a) shows the unique grain map of cross-section of Cu of $r$ = 0 vol.% sample and

Fig. 3-10(b) shows that of $r$ = 5.0 vol.% sample. In this grain map, crystal grain boundaries are defined with reference to a deviation angle between adjoining Cu particles of 15° or more. When calculating the average crystal grain sizes of Cu of the samples based on this definition, that of $r$ = 0 vol.% sample was 1.0 μm, whereas that of $r$ = 5.0 vol.% sample was much larger, 5.2 μm. From this result, it appears that $MoS_2$ particles existing between the Cu powder particles inhibit crystal grain refinement of Cu.

Subsequently, the texture structures of the sample were investigated. The inverse pole figure maps of Cu of cross-section of the samples with $r$ = 0 and 5.0 vol.% are shown in Fig. 3-11(a) and Fig. 3-11(b), respectively. The crystal anisotropies of samples due to the preferred orientation of Cu appears to be relatively small even if it existed. However, the shape anisotropy exist in the material structure in the shearing direction and the thickness direction because the crystal grains of pure Cu sample ($r$ = 0 vol.%) have elongated shapes. In contrast, it was clarified that Cu doesn't make textured structure even if there was no lubrication of $MoS_2$.

To investigate the crystal anisotropies of pure Cu sample in detail, the EBSP analysis was performed in the relatively large area than that of Fig. 3-11(a). Fig. 3-12 shows the inverse pole figure maps of Cu of cross-section of the pure Cu sample. In fact, the crystal anisotropies also cannot be observed clearly from this figure. Therefore, the degree of the preferred orientation was investigated by measurement of pole figures. The {001} and {111} pole figures of the area of Fig. 3-12 are shown in Fig. 3-13. From the intensity distribution map, it was suggested that the surface of the pure Cu sample was parallel to the (100) plane. In addition, the shearing direction was parallel to the [011] axis.

From these result, it was clarified that the pure Cu sample showed crystal anisotropies and the Cu/$MoS_2$ sample didn't show that. The reason of this difference appears to be the dissipation of the applied shearing force and strain to the sample by $MoS_2$ lubrication.

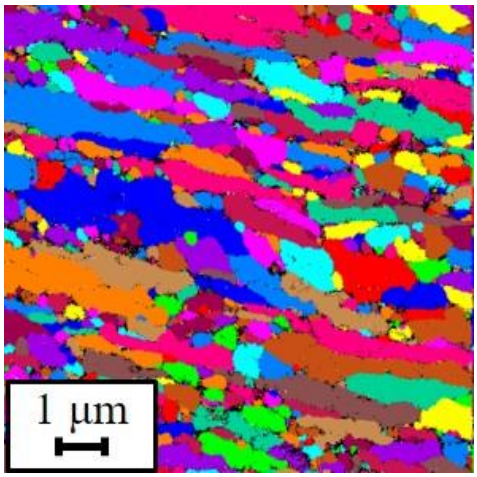


(a) $r$ = 0 vol.%

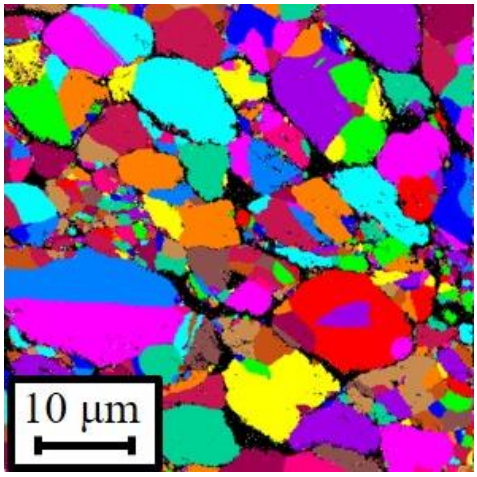


(b) $r$ = 5.0 vol.%

Fig. 3-10 Unique grain map of Cu of cross-section of the samples.

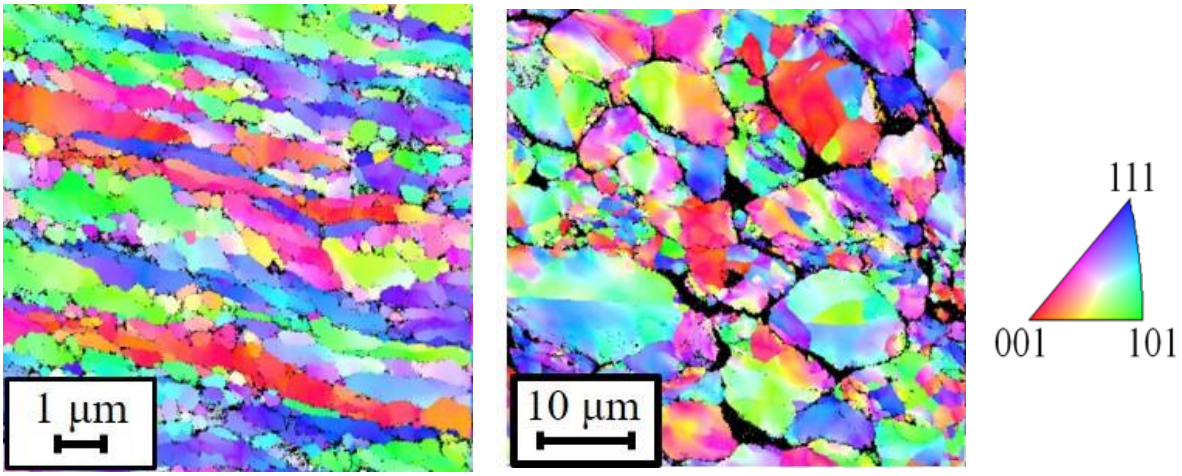


(a) $r$ = 0 vol.% (b) $r$ = 5.0 vol.%

**Fig. 3-11 Inverse pole figure maps of Cu of cross-section of the samples.**

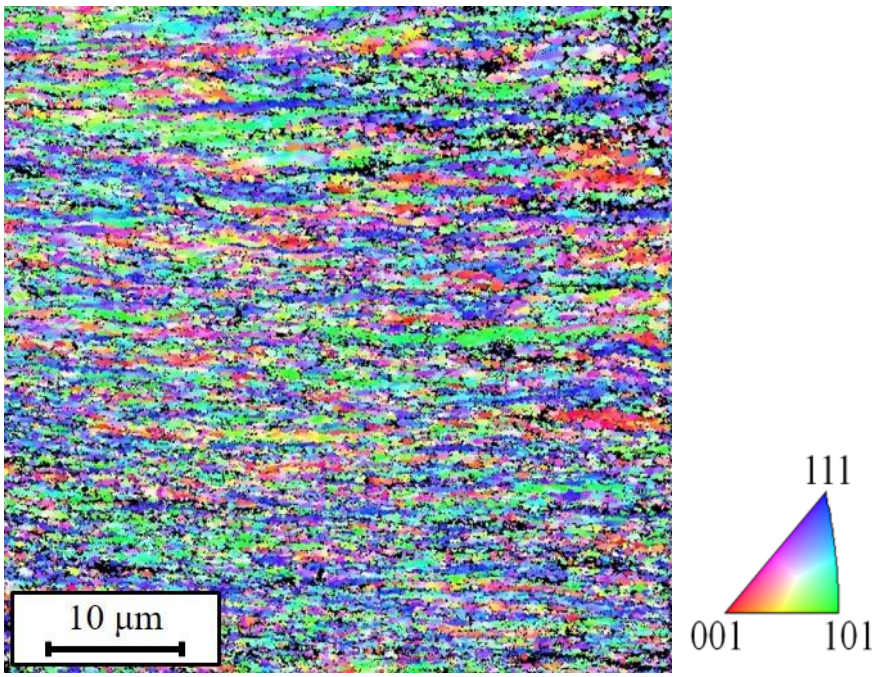


**Fig. 3-12 Inverse pole figure maps of Cu of cross-section of pure Cu sample.**

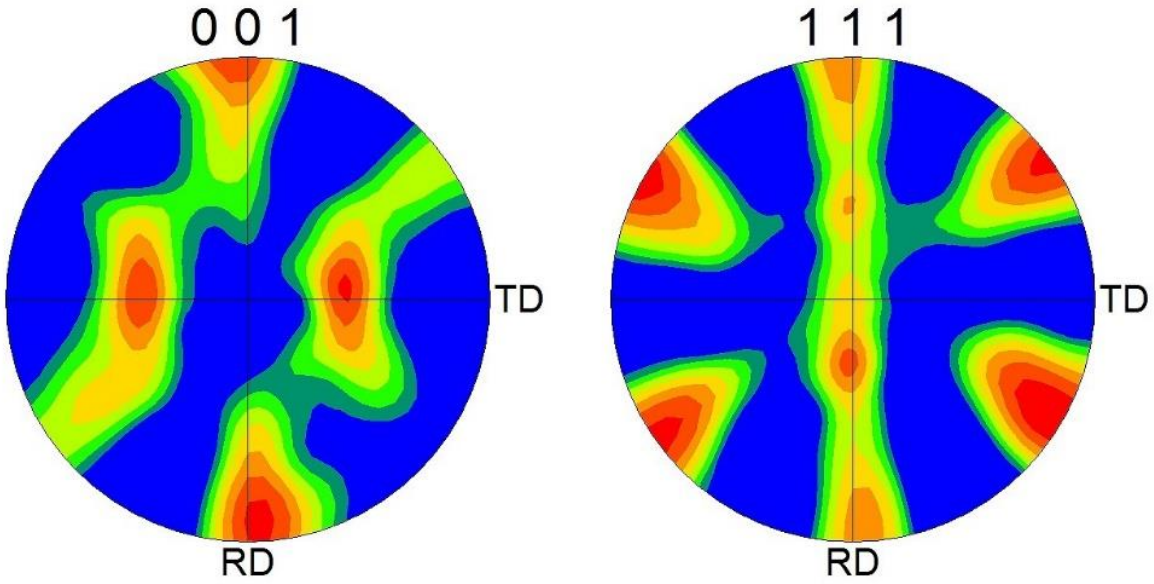


**Fig. 3-13 Pole figure of Cu of cross-section of pure Cu sample.**

### 3.2.6 TEM observation

How $MoS_2$ particles exists in the sample is observed in detail by TEM. The cross-sectional observations of both the pure Cu sample with no $MoS_2$ ($r$ = 0 vol.%) and Cu/$MoS_2$ sample with 5.0 vol.% $MoS_2$ were carried out to investigate the bonding state between Cu and $MoS_2$, and that between Cu and Cu.

First, the bonding state between Cu particles in the pure Cu sample was investigated. Fig. 3-14 shows a typical TEM cross-sectional image of $r$ = 0 vol.% sample. The crystal grain around the center of this image is finer than that of at the outer edge. An enlarged image of center part of Fig. 3-14 having a fine crystalline structure is shown in Fig. 3-15. In the central part of Fig. 3-15, from the upper left to the lower right, an oxide layer which may covered the material powder particle can be confirmed. This part is the original contact interface of powder particles. This oxide layer became thinner from the upper left to the lower right, and it can be observed that the oxide layer partly disappeared and the Cu particles were partly bonded. The oxide layer may be dispersed into the Cu matrix. The crystal grains have and elongated shape along this oxide layer and are refined to submicron size. From these results, it was clarified that the Cu powder particles were well bonded each other. It was also found that crystal grains of Cu in the vicinity of the contact interface of the particles are refined by applying shearing strain.

Subsequently, the bonding conditions of Cu and $MoS_2$ in the Cu/$MoS_2$ sample were observed. Fig. 3-16 shows TEM image of the cross-section of $r$ = 5.0 vol.% sample. There is a region traversing the central part. The layer structure of $MoS_2$ cannot be clearly confirmed because the Ar ion beam causes the damage in the structure of $MoS_2$ during the thinning process for TEM observation by using the ion milling machine. However, an EDS analysis indicated that this region appears to be $MoS_2$. The strains applied to powder particles during COSME-RT process were dissipated by fracture of $MoS_2$ between Cu particles, and the crystal refinement of Cu appeared to be suppressed.

The bonding condition of Cu and Cu in the Cu/$MoS_2$ sample were observed. Fig. 3-17 shows TEM image of the cross-section of $r$ = 5.0 vol.% sample around the boundary of Cu powder particles. It was confirmed that there was an oxide layer similar to Fig. 3-15 and the particles were partly bonded. From there results, it was suggested that the Cu powder particles were bonded each other at the place where $MoS_2$ doth not exist.

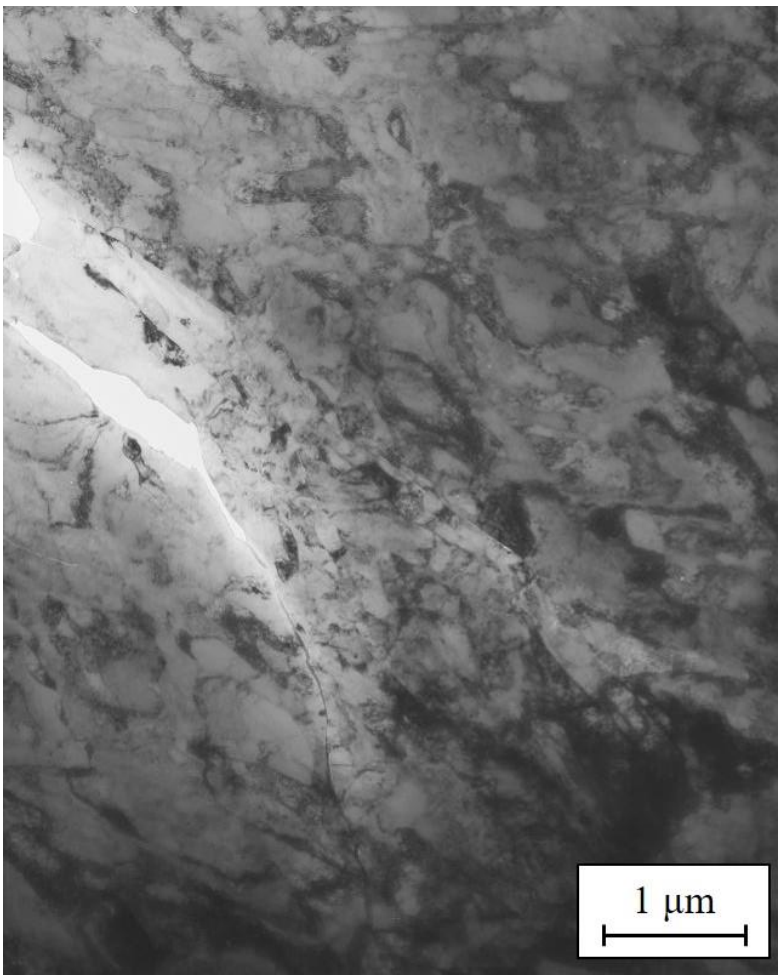


**Fig. 3-14 TEM image of cross-section of *r* = 0 vol.% sample.**

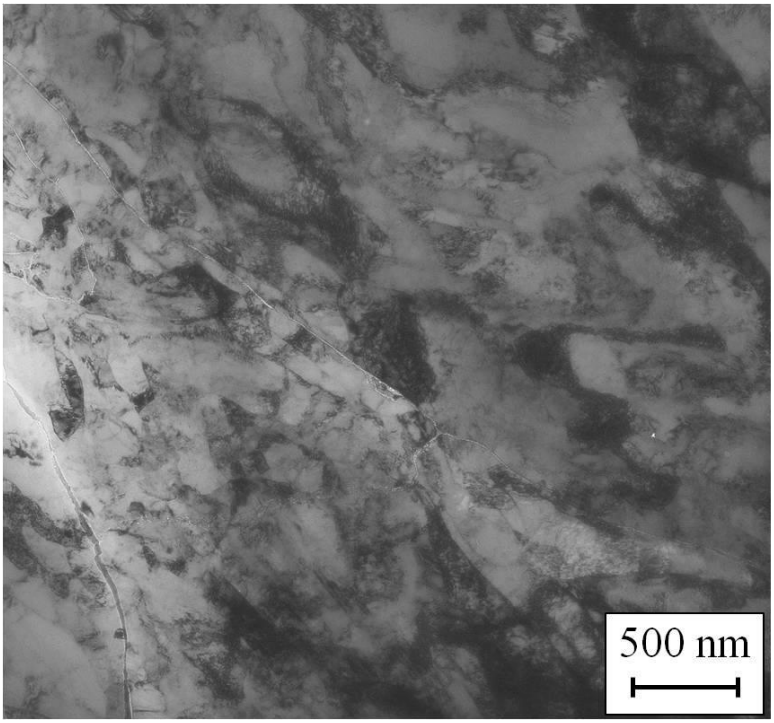


**Fig. 3-15 TEM image of cross-section of *r* = 0 vol.% sample (Enlarged image of Fig. 3-14).**

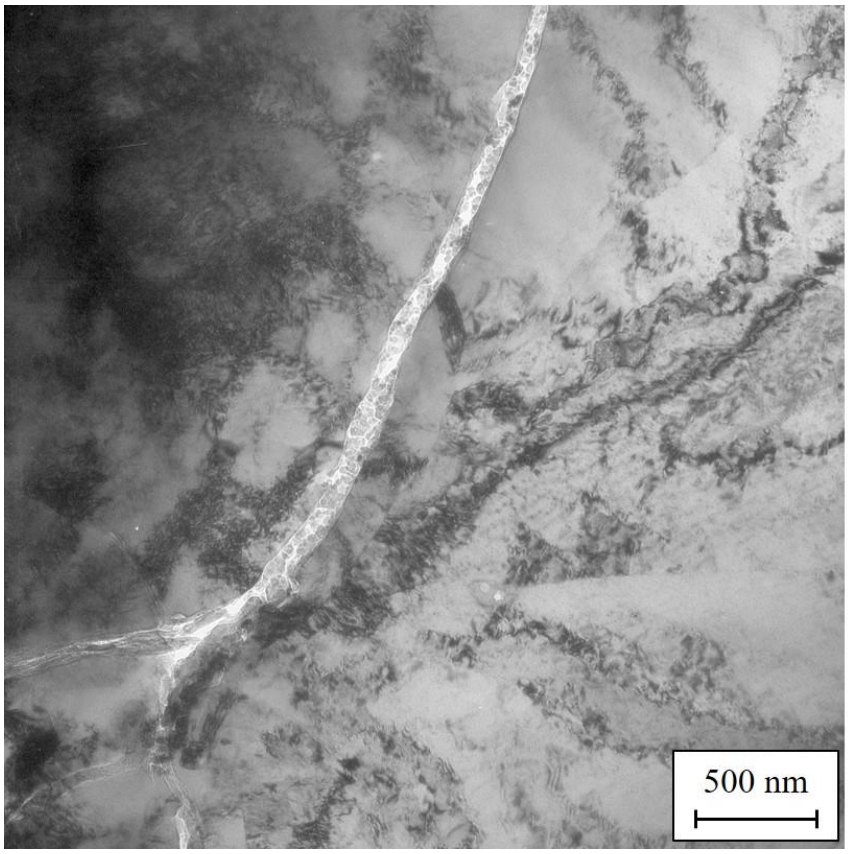


**Fig. 3-16 TEM image of cross-section of *r* = 5.0 vol.% sample(Cu and $MoS_2$).**

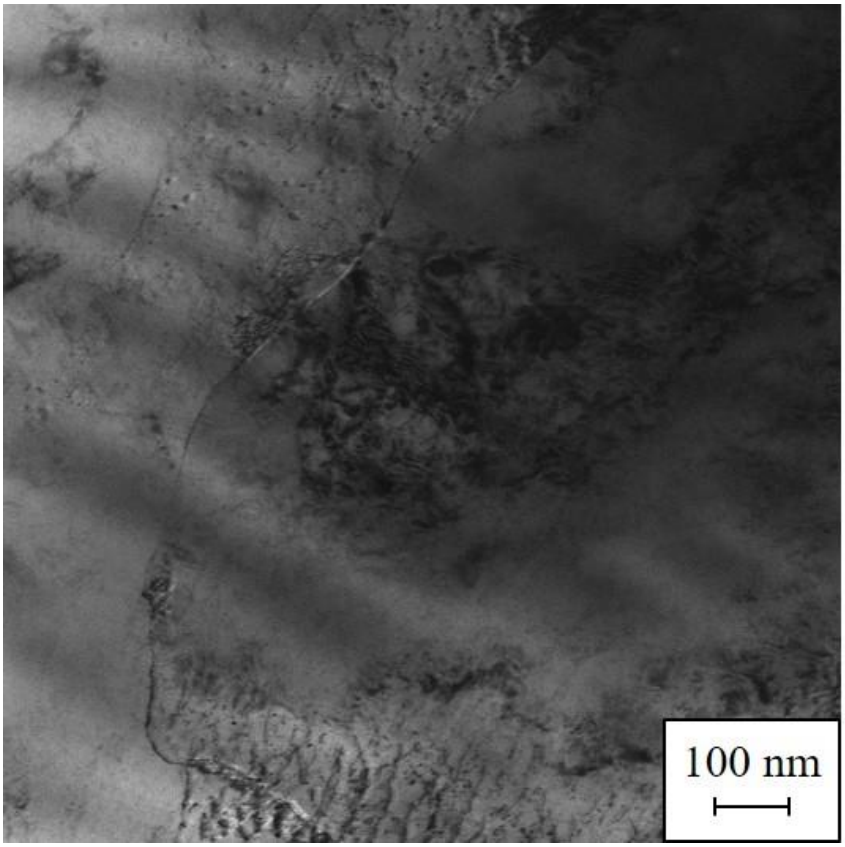


**Fig. 3-17 TEM image of cross-section of *r* = 5.0 vol.% sample (Cu and Cu)**

### 3.2.7 SIM observation

SIM observation of the sample cross-section was carried out to clarify the microstructural change of the powder particles with changing the shearing distance. Fig. 3-18 shows the SIM cross-sectional images of the pure Cu samples that were formed under different shearing distances from their top surface to a 20-μm depth. No noticeable difference resulted between the top and bottom microstructures for the pure Cu sample. In the SIM images, the crystal orientation of the Cu grain is represented as the change in contrast variation. Cu grain size of the sample was detected by observing this contrast. In the pure Cu samples, the Cu powder particles and their crystal grains were deformed along the shearing direction. They appeared to be flowing with an increasing shearing distance $L_S$, as shown in Fig. 3-18 (a) and Fig. 3-18 (b). The grain sizes around the boundaries of the powder particles were finer than in other regions. These fine grain regions widened when the shearing distance increased. At the longest shearing distance $L_S$ = 5.0 mm, this grain refinement extended to the entire sample. This grain refinement process corresponds to the model of the COSME-RT process as proposed by Dr. M. Horita [3-3].

Fig. 3-19 and Fig. 3-20 show the SIM cross-sectional images of Cu/$MoS_2$ samples near the top and bottom surfaces, respectively. The dark regions correspond to $MoS_2$ grains. The Cu grain size of the Cu/MoS2 and pure Cu samples were almost the same when $L_S$ = 0 mm, regardless of their position, near the top or bottom surface, as shown in Fig. 3-18 (a), Fig. 3-19 (a) and Fig. 3-20 (a). The shapes and grain sizes of the Cu powder particles of the Cu/$MoS_2$ sample near the top surface did not change with an increase in shearing distance as shown in Fig. 3-19. This result well agrees with the morphological observations.

In contrast, the Cu powder particles near the bottom surface of the sample were deformed with an increasing shearing distance, as shown in Fig. 3-20 (a) and Fig. 3-20 (b). In a region at around1.0 μm thickness from the bottom surface, the Cu powder particles were deformed along the shearing direction and were partly bonded. In this region, the grain sizes of the Cu powder particles were 1.0–2.0 μm, which is finer than the grain size of the uniaxial compressed sample, but not as fine as a fully dense pure Cu sample (Fig. 3-18 (c)). Fig. 3-20 (b) and Fig. 3-20 (c) show that the crystal grains in a region up to a depth of 5.0 μm from the bottom surface were deformed slightly and refined along the shearing direction, like a plastic flow.

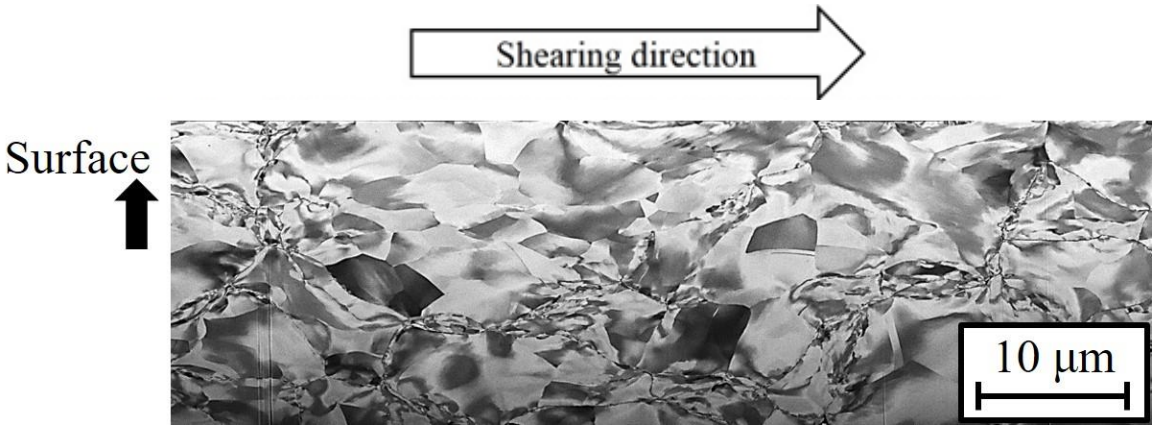


(b) $L_S$ = 0 mm

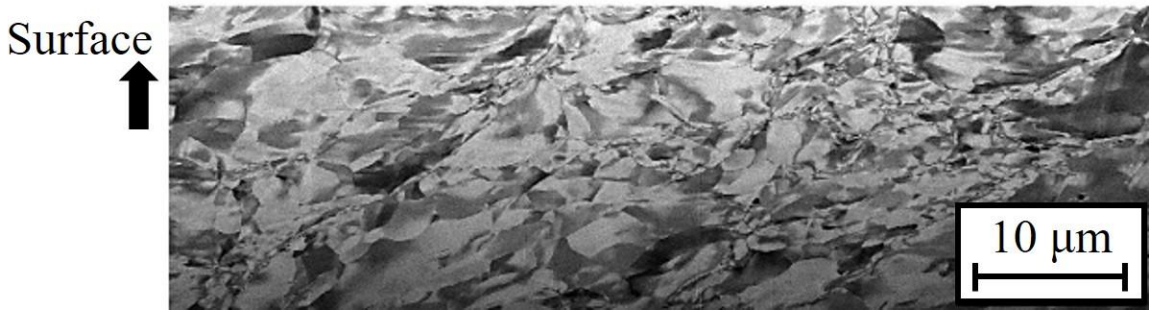


(b) $L_S$ = 0.50 mm


(c) $L_S$ = 5.0 mm

**Fig. 3-18 SIM images of cross-section of pure Cu samples (Top surface).**

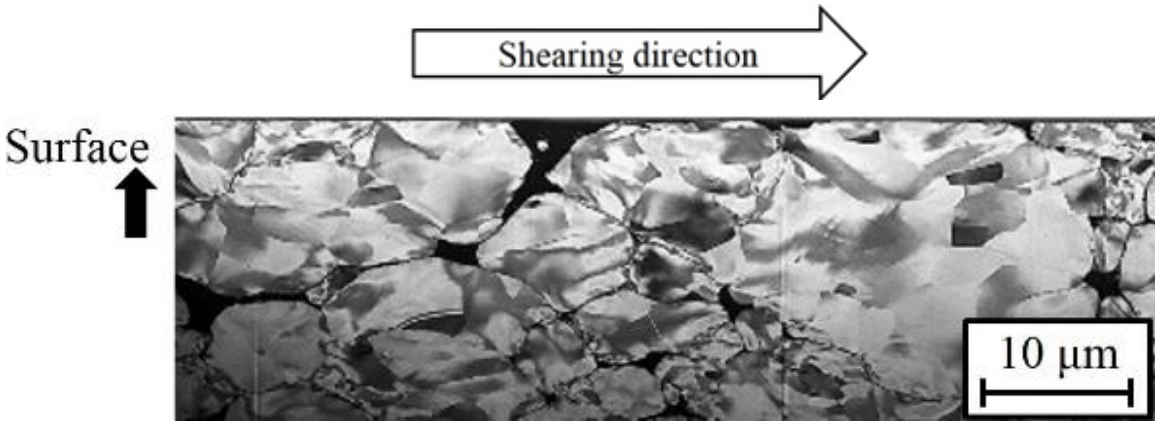


(a) $L_S$ = 0 mm

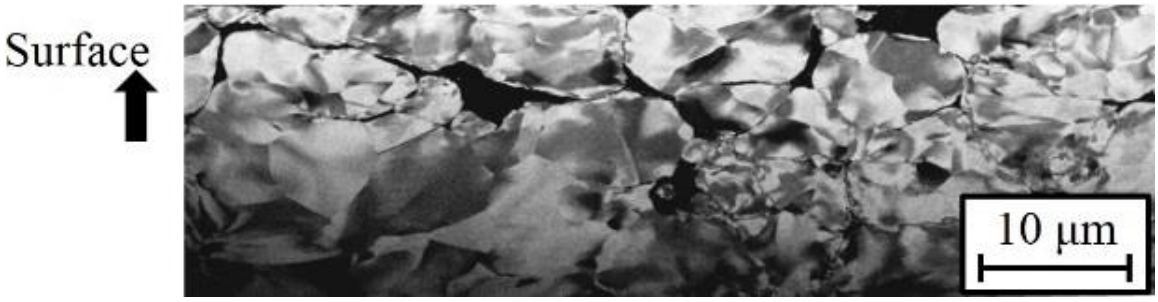


(b) $L_S$ = 0.5 mm


(c) $L_S$ = 5.0 mm

**Fig. 3-19 SIM image of cross-section of Cu/$MoS_2$ samples (Top surface).**

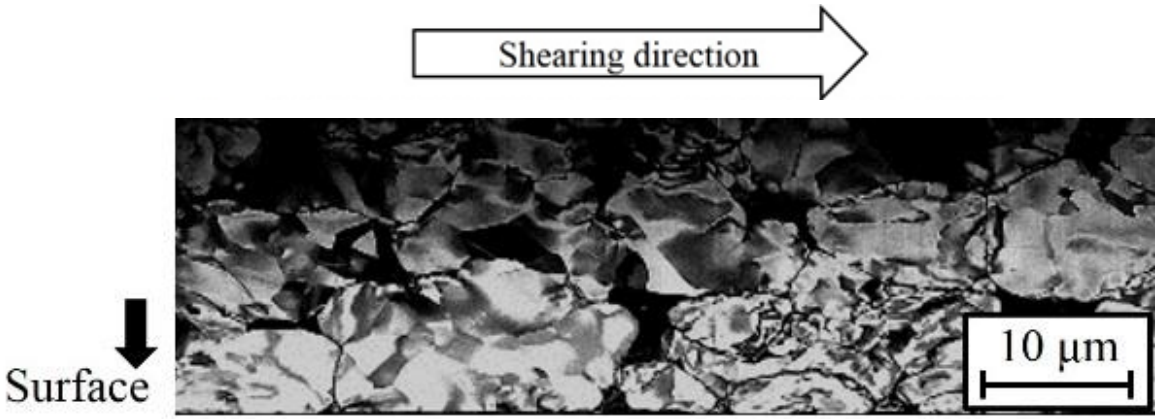


(a) $L_S$ = 0 mm

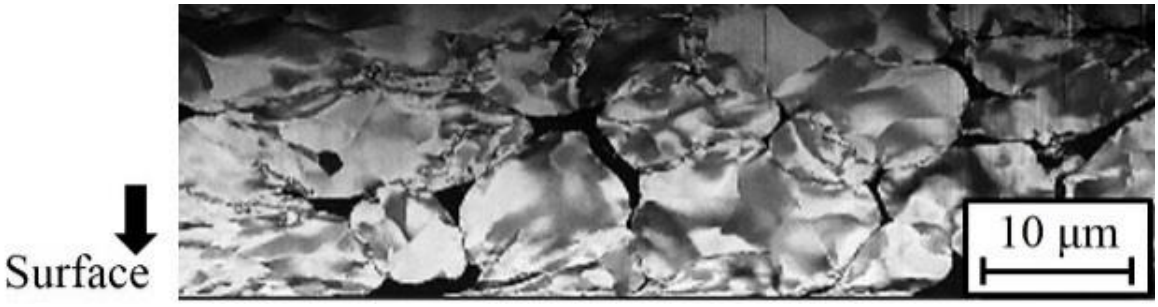


(b) $L_S$ = 0.50 mm


(c) $L_S$ = 5.0 mm

**Fig. 3-20 SIM images of cross-section of Cu/$MoS_2$ samples (Bottom surface).**

## 3.3 Shearing force change during COSME-RT processes

From the previous observations, it appears that the Cu grains experienced the different stresses which depended on $MoS_2$ inclusions and the applied shearing strain. Fig. 3-21 shows the evolution of shearing force $P_S$ as a function of shearing distance $L_S$ during COSME-RT for pure Cu and Cu/$MoS_2$ composite samples. The initial shearing force $P_S$ was the same value of 40 kN for both samples.

The $P_S$ of pure Cu increased significantly to 65 kN, whereas $L_S$ increased from 0 to 0.10 mm. Subsequently, $P_S$ increased monotonically when the shearing distance $L_S$ was increased, and finally reached ~100 kN, for $L_S$ = 5.0 mm. This tendency of $P_S$ is consistent with previous observations of the pure Ti and Al process [3-3]. It appears that the material strength of the pure Cu sample increased because of the bonding and refinement of their crystalline structure, and it lead to an increase of the shearing force needed to displace the moving plate. The pure Cu sample was solidified as a material with a sub-micrometer crystalline structure by applying a 5.0-mm shearing distance and a 100-kN shearing force.

For Cu/$MoS_2$, the $P_S$ decreased significantly, whereas $L_S$ increased from 0 to 0.50 mm. It decreased moderately after $L_S$ = 0.50 mm and became constant at 26 kN after $L_S$ = 1.0 mm. From structural observations, the reason for this reduction in shearing force appears to be a slip between the Cu/$MoS_2$ sample and the base plate because of the lubricity of $MoS_2$ as shown in Fig. 3-22. The friction coefficient of the Cu/$MoS_2$ sample is around 0.05 if it is calculated by dividing the shearing force by the compressive force. This value is similar as that of the bottom surface of the Cu/$MoS_2$ sample (about 0.07) measured at the same testing conditions of the previous study [3-1] except in the nitrogen atmosphere. The sliding surface was not exposed much to air during COSME-RT process and this value appears to be reasonable. The internal structure of the Cu/$MoS_2$ sample appears to be interrupted midway during the consolidation process, because of the reduction in shearing force. This result suggests that a high shearing force is required to obtain a fully dense material by using COSME-RT. In contrast, particle bonding and grain refinement occur only on the sample surface where sliding which affects the inside of the sample gradually with the progress of shearing occurs.

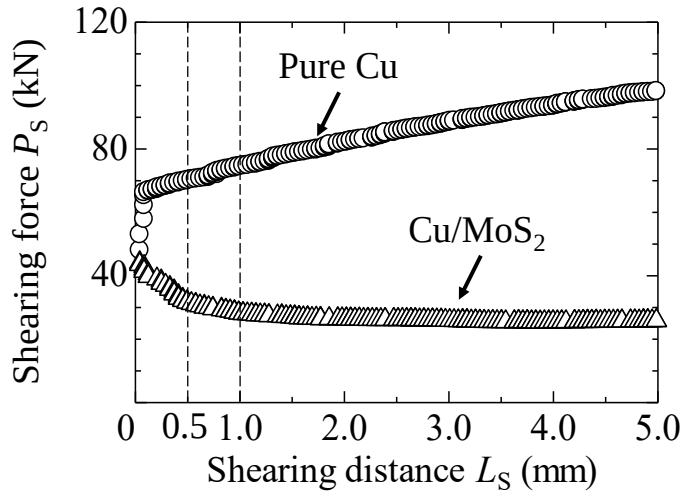


**Fig. 3-21 Evolution of the shearing force as a function of the shearing distance.**

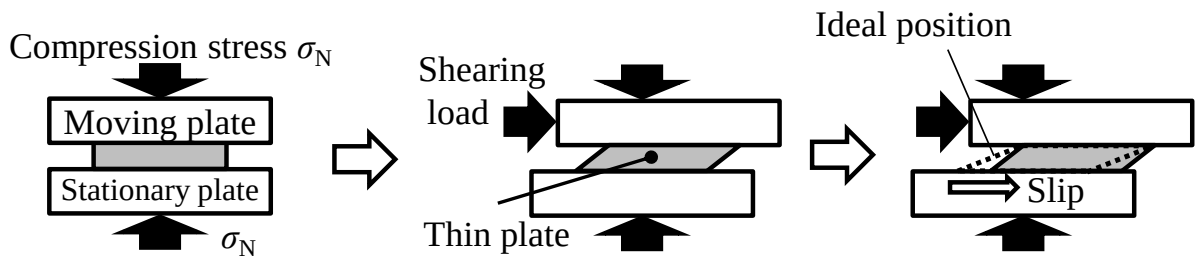


**Fig. 3-22 Schematic illustration of sample slip during consolidation process of Cu/$MoS_2$ by compression shearing method.**

## 3.4 Conclusions

Cu/$MoS_2$ samples were formed under several shearing distances and their microstructures were observed. The microstructural change related to the decrease in applied shearing force was discussed. The results obtained are as follows.

1) Dispersed $MoS_2$ lubricant suppress the progress of the consolidation of Cu powder particles by dissipating the applied shearing stress during COSME-RT.
2) Particle bonding and grain refinement occur only on the sample surface by a slip between the sample and the steel plate. The shearing force affected part gradually extended to the inside of the sample when the shearing distance increased.

By dispersing $MoS_2$ into pure Cu material, the applied shearing force was reduced significantly, and I succeeded to introduce the flexibility on the consolidation process. The applied shearing force appears to be one of the important factors to promote metal consolidation by COSME-RT. In contrast, the shearing distance is less effective on the consolidation process by the slip between the Cu/$MoS_2$ sample and the steel plate. Nevertheless, there was a slight change in sample structure of the surface layer when the shearing distance increased. Therefore, it appears to be important to clarify whether the shearing force and the shearing distance have a greater effect on the bonding process of the particles.

# References

(3-1) S. Takeda, H. Miki, H. Takeishi, T. Takagi, Cu-Based $MoS_2$-Dispersed Composite Material Formed by the Compression Shearing Method at Room Temperature, Tribology Online, 12, 2, (2017), pp. 29 - 36

(3-2) H. Miki, N. Nakayama, H. Takeishi, Dynamic Molding of Powder Particles at Room Temperature, Materials Science Forum, Vols. 706-709, (2012), pp. 1955 - 1960.

(3-3) M. Horita, Doctor Thesis, Shinshu University, Japan, (2014). pp. 65 - 67.

# Chapter 4

# Effect of the Stress Distribution on the Consolidation Process

By the experiments presented in the previous chapter, it was clarified that the applied shearing force appears to be one of the important factors to proceed metal consolidation by COSME-RT. In addition, although the shearing distance appeared to be less effective on the consolidation process in contrast, there was a slight change of the surface layer structure when the shearing distance increased.

For the next step, I would like to clarify the detail of the bonding process of powder particles and the threshold shearing force to proceed the process.

In this chapter, a tribometer is used as a tool for the clarification of the mechanism of interparticle bonding during the compression shearing process. In the friction experiment, compressive stress, shearing force, and shearing distance could be controlled by changing the applied normal load and the number of the sliding cycles.

I performed a linear unidirectional friction experiment on uniaxial-compressed (1000 MPa) pure Cu sample. The relation between the normal loads applied, the number of sliding cycles, and the microstructural change of the powder particles is investigated by morphological and cross-sectional observations of the samples after the friction experiments. Based on the question of whether the shear force and the shear distance have a significant effect on the bonding process of the particles, which emerged from the results of the previous chapter, we first focus on the number of sliding cycles.

## 4.1 Forming conditions of pure Cu samples

Pure Cu uniaxial-compressed powder samples were prepared by using COSME-RT apparatus, same as that formed samples in the Chapter 3. The compressive force $P_N$ was 400 kN, which corresponds to a compressive stress $\sigma_N$ = 1000 MPa was applied to the sample without displacing the moving plate. Approximately 0.89 g pure Cu powder was used to fabricate one sample because a target size of a sample was 20 × 20 × 0.25 $mm^3$ and the true density of pure Cu is 8.94 $g/cm^3$.

## 4.2 Effect of the number of cycles on the uniaxial compressed pure Cu sample

### 4.2.1 Coefficient of friction (100 and 200 cycles friction experiments)

Fig. 4-1 shows the relationship between the sliding distance and the coefficient of friction of the pure Cu uniaxial compressed samples with normal load $P$ = 4.0 N, (a) the number of cycles $N$ = 100 and (b) $N$ = 200. The coefficient of friction of all samples were stable at 0.2-0.3 regardless the shearing distance and the number of cycles. This result suggested that the shearing force constantly applied to the sample during the friction experiment.

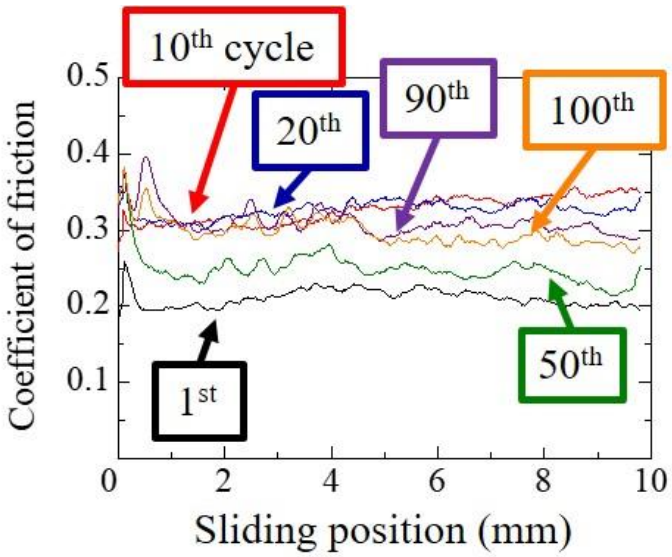


(a) $P$ = 4.0 N, $N$ = 100

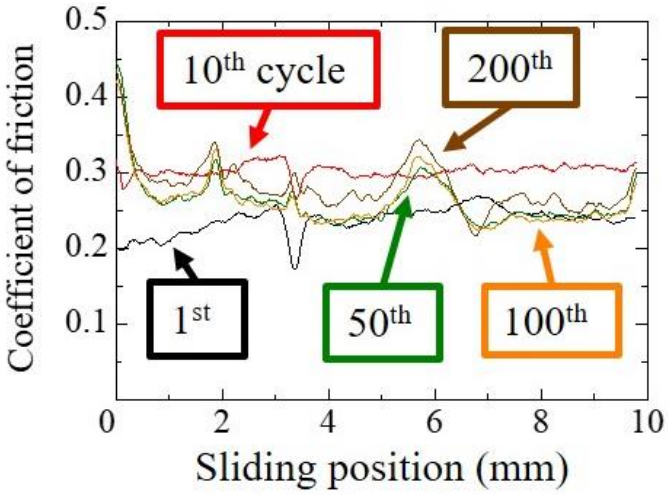


(b) $P$ = 4.0 N, $N$ = 200

**Fig. 4-1 Relationship between sliding position and coefficient of friction of pure Cu samples.**

### 4.2.2 Optical micrograph of sample surface (100 and 200 cycles friction experiments)

Fig. 4-2 shows the optical micrographs of the sample surfaces before and after the friction experiments. There were many voids (dark spots) on the sample surface before the friction experiment, but voids disappeared after the friction experiment. Powder particles were deformed and bonded each other by the sliding of the counter ball ($ZrO_2$) during the friction experiment. Even the number of the sliding cycles increased, there were few oxidation and almost no wear on the sample even after the friction experiment. The widths of the wear tracks are almost same and these are corresponded with Hertzian contact diameter calculated, 100 μm.

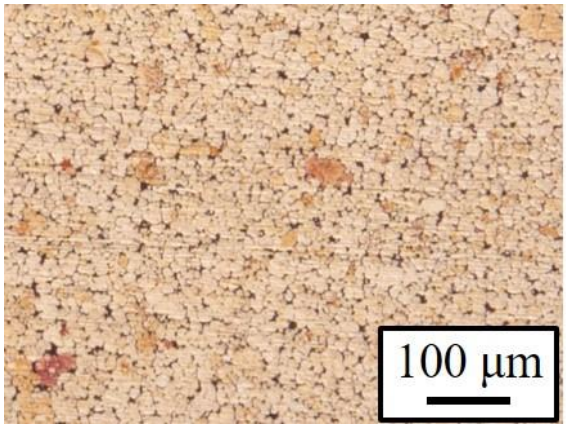


(a) Before friction experiment

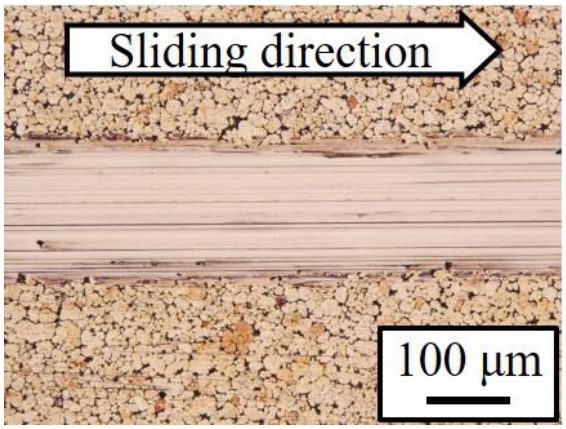


(b) $P$ = 4.0 N, $N$ = 100

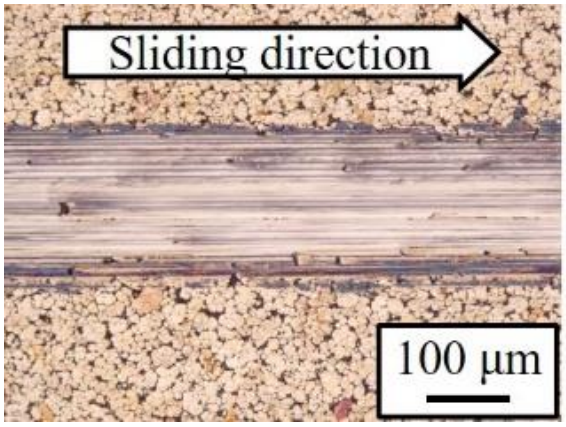


(c) $P$ = 4.0 N, $N$ = 200

**Fig. 4-2 Optical micrographs of the pure Cu sample surfaces before (a) and after (b), (c), and (d) friction experiments.**

### 4.2.3 SEM images of fracture surfaces of sample wear tracks (100 and 200 cycles friction experiments)

Fig. 4-3 shows the SEM images of the fracture surfaces of the samples after the friction experiments. In all the samples, the powder particles deformed along the sliding direction. In the case of the normal load $P$ = 4.0 N and the number of sliding cycles $N$ = 100, the powder particles appears to be deformed in the region from the surface to the 1.0 μm depth. The powder particles appears to be bonded in this region because any boundaries of the powder particles could not be observed in this region. The thickness of this region did not change even though the number of the sliding cycles $N$ increased from 100 to 200, as shown in Fig. 4-3 (a) and Fig. 4-3 (b).

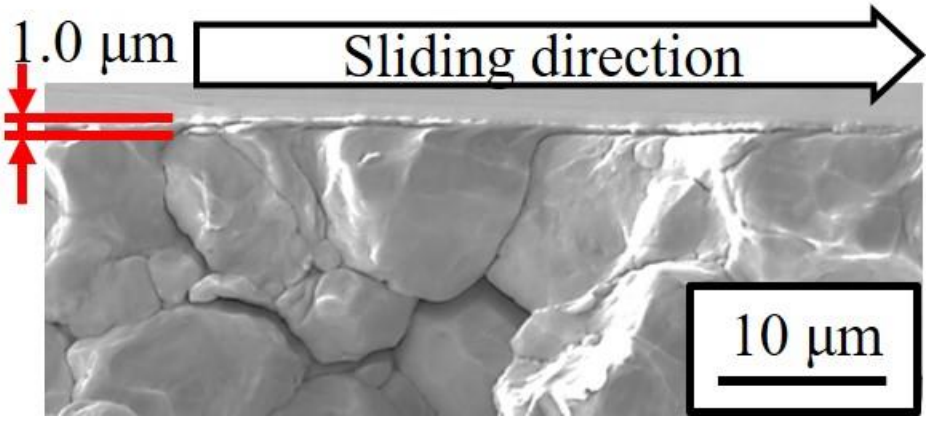


(a) $P$ = 4.0 N, $N$ = 100

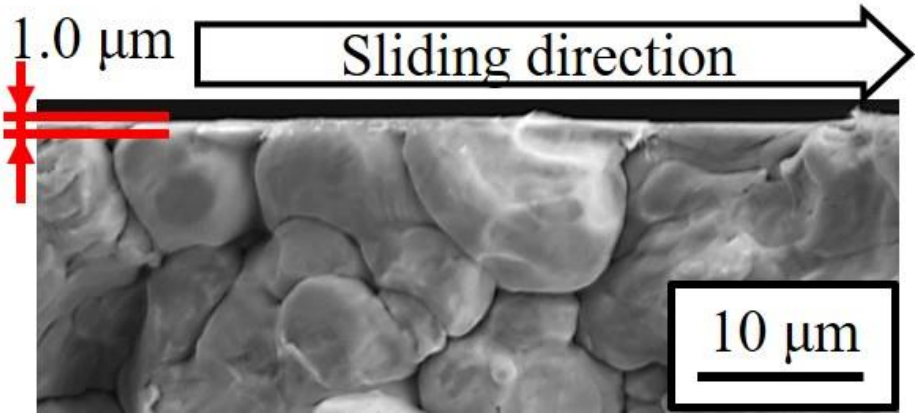


(b) $P$ = 4.0 N, $N$ = 200

**Fig. 4-3 SEM images of pure Cu sample fracture surfaces after friction experiments.**

### 4.2.4 Cross-sectional SIM images of sample wear tracks (100 and 200 cycles friction experiments)

Fig. 4-4 shows the cross-sectional SIM images of the sample after the friction experiments with normal load $P$ = 4.0 N, (a) the number of cycles $N$ = 100 and (b) $N$ = 200. On both samples, there are two zones in the sample cross-section, the zone which the powder particle deform and the zone which the particle does not deform. These zones are defined as the deformed zone and the non-deformed zone. In the deformed area, the powder particles and these crystal grains were deformed along the sliding direction. There are two layer structures having different microstructures in deformed zone. From the surface, these regions were individually termed; sub-micro size crystalline region, and micro size crystalline region. The sub-micro size crystalline region and the micro size crystalline region are those having sub-micro and micro size crystalline structure as these names suggest. The deformed zone consists of only sub-micro and micro size crystalline regions.

Fig. 4-5 shows the enlarged image of Fig. 4-4. The boundaries of the powder particles were disappeared in the micro size crystalline region. Therefore, the powder particles appears to be bonded in the micro size crystalline region.

The average thicknesses of the regions of the samples except the non-deformed zone are listed in Table 4-1. The average thickness of these regions didn't change even the number of sliding cycles $N$ increased. This result suggested that the range of applied stress was constant even the number of sliding cycles changed.

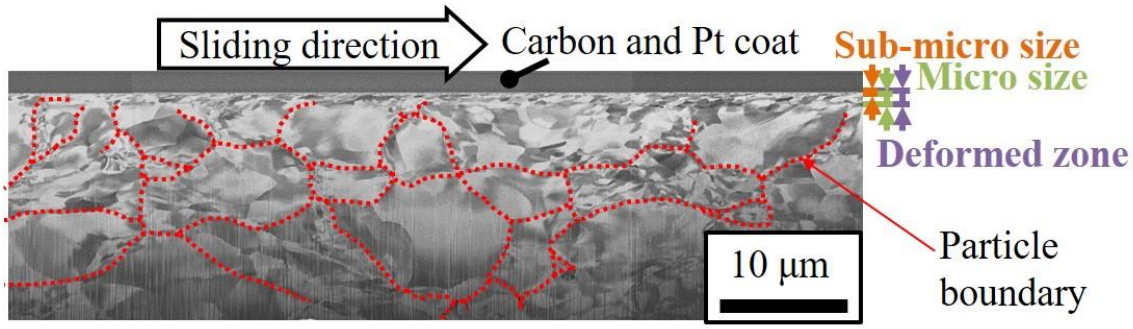


(a) $P$ = 4.0 N, $N$ = 100

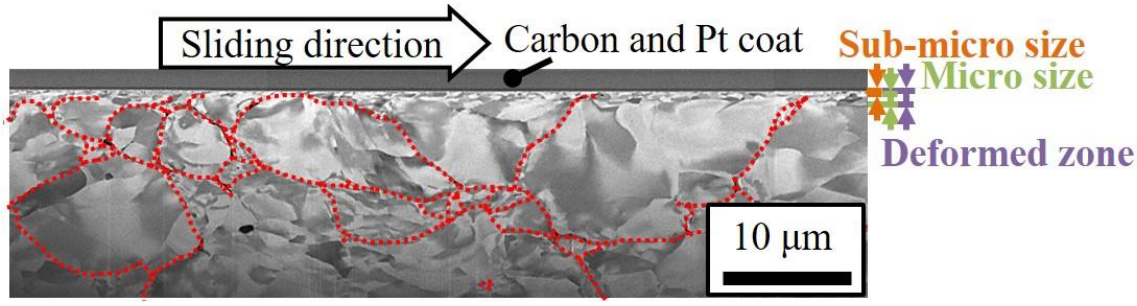


(b) $P$ = 4.0 N, $N$ = 200

**Fig. 4-4 SIM images of pure Cu sample cross-sections after 100 and 200 cycles friction experiments.**

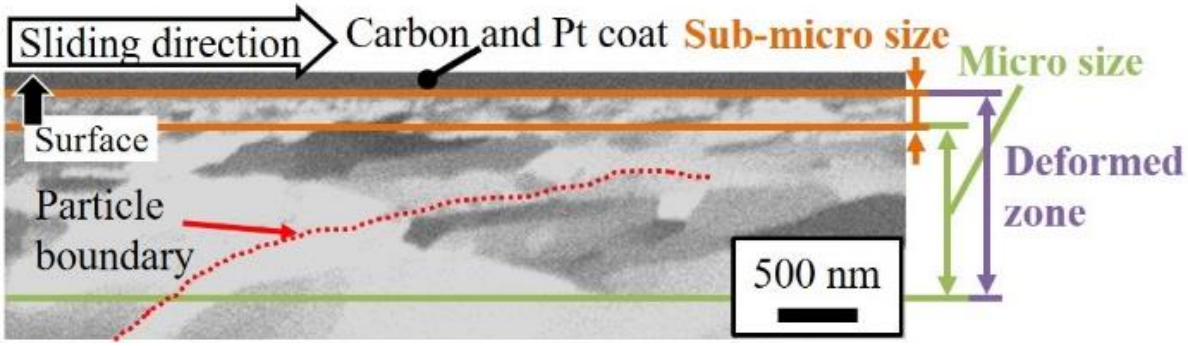


(a) $P$ = 4.0 N, $N$ = 100

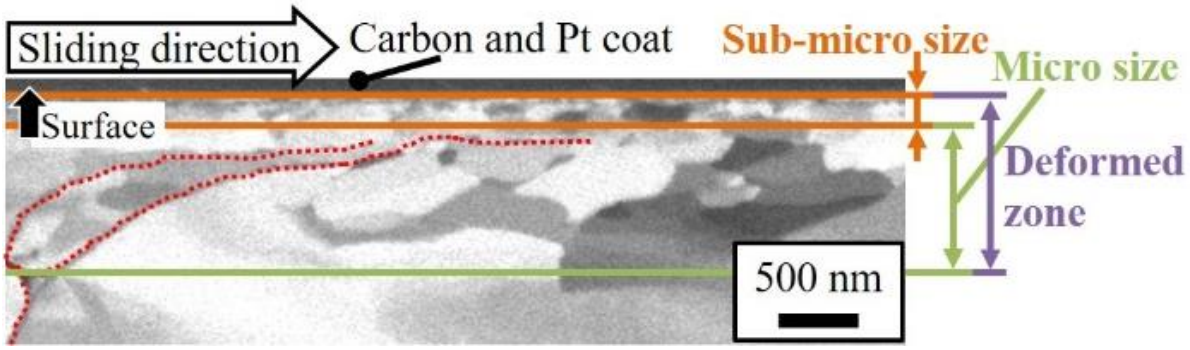


(b) $P$ = 4.0 N, $N$ = 200

**Fig. 4-5 SIM images of pure Cu sample cross-sections after 100 and 200 cycles friction experiments (Enlarged image of Fig. 4-4).**

**Table 4-1 Average thicknesses of three regions of pure Cu samples after 100 and 200 cycles friction experiments.**

| $P$ (N), $N$ (-) | 4.0, 100 | 4.0, 200 |
|---|---|---|
| Deformed zone (μm) | 1.3 | 1.1 |
| Micro size crystalline region (μm) | 1.1 | 0.9 |
| Sub-micron crystalline region (μm) | 0.2 | 0.2 |

## 4.3 Effect of the normal load on the uniaxial compressed pure Cu sample

### 4.3.1 Coefficient of friction (Friction experiments with different normal loads)

Fig. 4-6 shows the relationship between the sliding distance and the coefficient of friction of the pure Cu samples during the friction experiment with the normal load $P$ = 27, 40, 60 N. When the normal load $P$ = 40 and 60 N, the unidirectional compressed samples were fractured after 100 cycles friction experiments. However, it was suggested that the range of applied stress was constant even the number of sliding cycles changed thanks for the previous experimental results. Therefore, the sample after 10 cycles friction experiments with the normal load $P$ = 40 and 60 N were investigated instead of that of after 100 cycles friction experiments.

The coefficient of friction of the samples were stable at 0.2-0.3 when $P$ = 27 N and $N$ = 100. When $P$ = 40 N, the coefficient of friction of the sample increased with number of cycles from $N$ = 1 to 5, then it became stable at 0.53. When $P$ = 60 N, the coefficient of friction of the sample were stable at 0.53. These results suggest that the tangential force was constantly applied to the sample during the friction experiment for each condition, but the friction behaviors changed when the normal load increased. The reason of this increase is investigated by morphological observations in the next section.

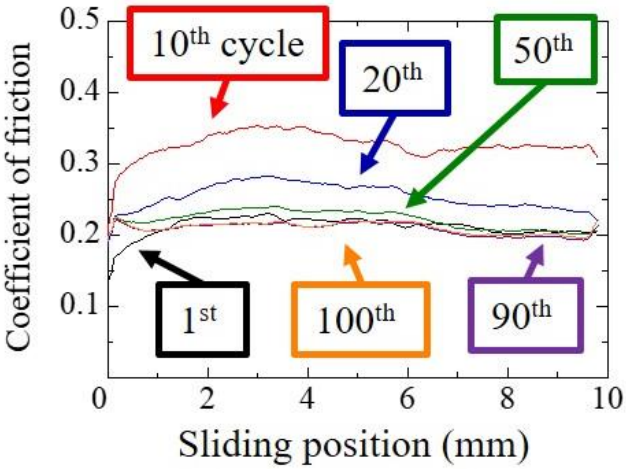


(a) $P$ = 27 N, $N$ = 100

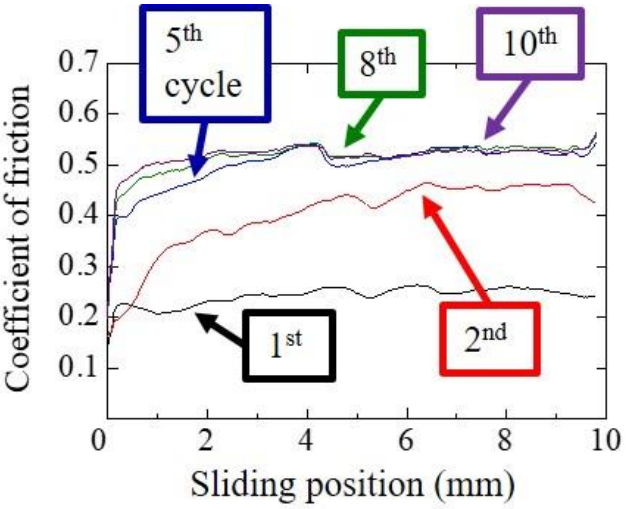


(b) $P$ = 40 N, $N$ = 10

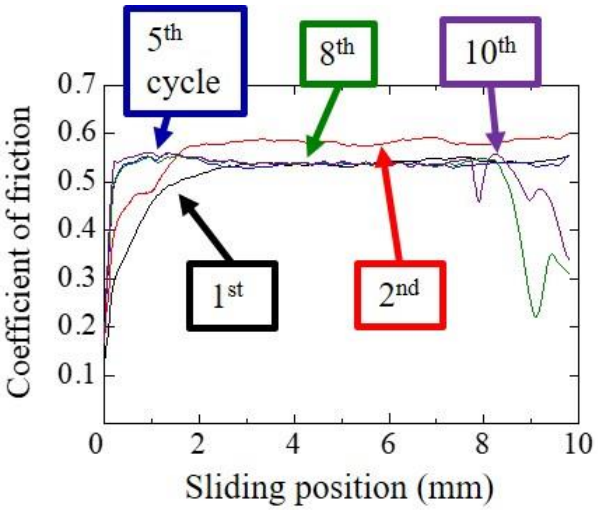


(c) $P$ = 60 N, $N$ = 10

**Fig. 4-6 Relation between sliding position and coefficient of friction of pure Cu samples during friction experiments with various normal loads and number of sliding cycles.**

### 4.3.2 Optical micrograph of sample surface (Friction experiments with different normal loads)

Fig. 4-7 shows the optical micrographs of the pure Cu sample surfaces after the friction experiments. The voids on the sample surface before the friction experiment (Fig. 4-2(a)) disappeared after the friction experiment as in case with $P$ = 4.0 N. The Hertzian contact area increased when the normal load $P$ increased, and the width of the wear track also enlarged. When $P$ = 40 and 60 N shown in Fig. 4-7(b) and Fig. 4-7(c), some gray dots appeared on the wear track. By EDS analysis, it was clarified that these dots has higher contents of O elements than other regions. Therefore, it appears that these dots are Cu oxide, and the coefficient of friction of the sample increased by this oxide when $P$ = 40 and 60 N. This result suggested that the friction experiment might be affected by external factor, that mean those conditions are not accurately simulate the COSME-RT process. Thus the larger shearing strain should be applied to the sample and it is expected that we can observe the change of the bonding condition of powder particles in the much deeper region.

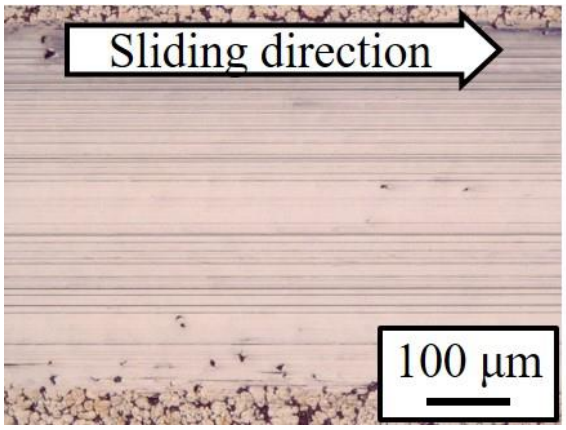


(a) $P$ = 27 N, $N$ = 100

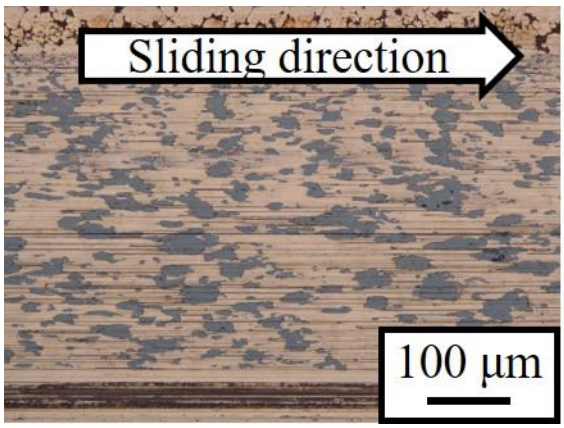


(b) $P$ = 40 N, $N$ = 10

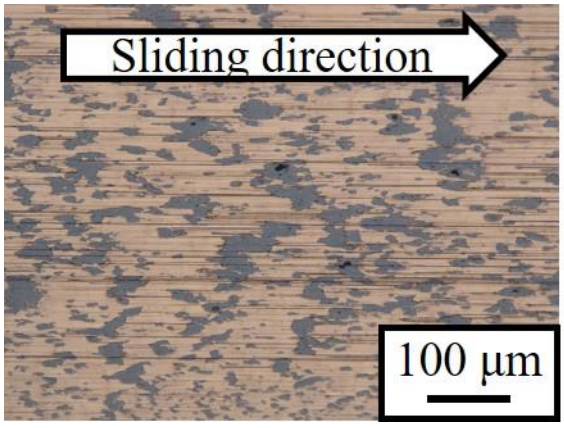


(c) $P$ = 60 N, $N$ = 10

**Fig. 4-7 Optical micrographs of pure Cu sample surfaces before and after friction experiments with different normal loads *P*.**

### 4.3.3 SEM images of fracture surface of the wear track (Friction experiment with different normal load)

Fig. 4-8 shows the SEM images of the fracture surfaces along the wear track of the sample after the friction experiment. When the normal load *P* increased from 27 N to 60 N, the thickness of the region where the powder particles were deformed increased from about 4.0 μm to 19 μm. This result suggested that the normal load was more effective for the deformation of the powder particles than the number of cycles. The average particle size of the pure Cu powder is around 38 μm as described in 2.1.1, but the particles were compressed and its particles thickness became thinner to around 15 μm. Therefore, when *P* = 60 N, the deformed region became larger than the average diameter of one compressed powder particle. This result means the shearing force was applied to deeper region exceeding one particle.

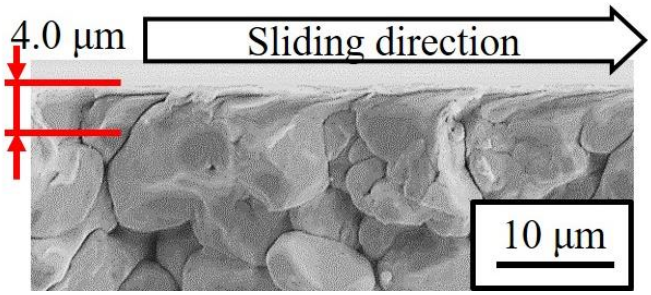


(a) *P* = 27 N, *N* = 100

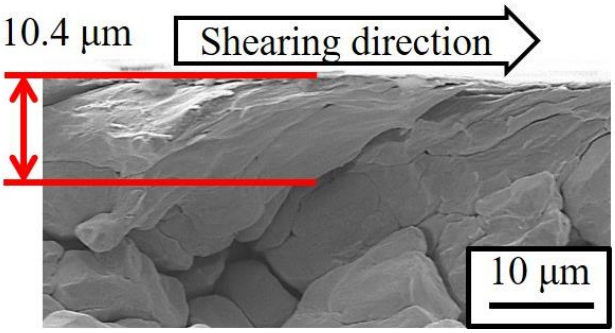


(b) *P* = 40 N, *N* = 10

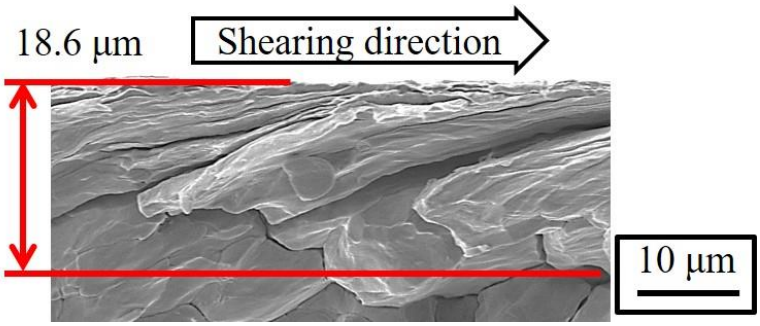


(c) *P* = 60 N, *N* = 10

**Fig. 4-8 SEM images of pure Cu sample fracture surfaces after friction experiments with different normal loads.**

### 4.3.4 Cross-sectional SIM images of the wear track (Friction experiment with different normal load)

Fig. 4-9 shows the cross-sectional SIM images of the sample after the friction experiments with the normal load $P$ = 27, 40, and 60 N. There were layer regions with different microstructures in the depth direction as in the case of relatively small normal load $P$ = 4.0 N (Fig. 4-4). The deformed zone enlarged when the normal load increased. This result corresponded with that of the fracture surface observations (Fig. 4-8).

When the normal load $P$ = 4.0 N, the deformed zone consists of only sub-micro and micro size crystalline regions (Fig. 4-4). In contrast, when the normal load $P$ = 27, 40, 60 N, there is the region with crystalline structure not so refined as micro or sub micro size. This result suggested that the powder particle was partly deformed while maintaining relatively larger grain size than micro-size crystalline region when the normal load $P$ = 27, 40, 60 N.

Fig. 4-10 shows the enlarged image of Fig. 4-9. As when the normal load $P$ was 4 N (Fig. 4-5), the boundaries of the powder particles were disappeared in the micro size crystalline region even the normal load $P$ increased. From these results, it was suggested that the powder particles were bonded at the micro size crystalline region after the friction experiment regardless how large the normal load was applied.

Table 4-2 shows the average thicknesses of the regions of the samples except the non-deformed zone. The average thicknesses of the deformed zone and the micro size crystalline region enlarged when the normal load $P$ increased. That of the sub-micro size crystalline region enlarged when the normal load $P$ increased from 27 to 40 N, and didn't change when the $P$ increased from 40 to 60 N.

Fig. 4-11 shows the relation between the normal load and the average thicknesses of the regions of the samples except the non-deformed zone. This graph was drawn from the results of Table 4-1 and Table 4-2. The thickness of the regions increased when the normal load $P$ increased from 4.0 to 27 N. Thus, the thickness of the regions appeared to be increase when the normal load $P$ increased regardless the increase of the coefficient of friction by oxidation of the sample.

From these results, it was clarified that the range of applied stress enlarged with increasing the normal load while it was constant even the number of sliding cycles changed.

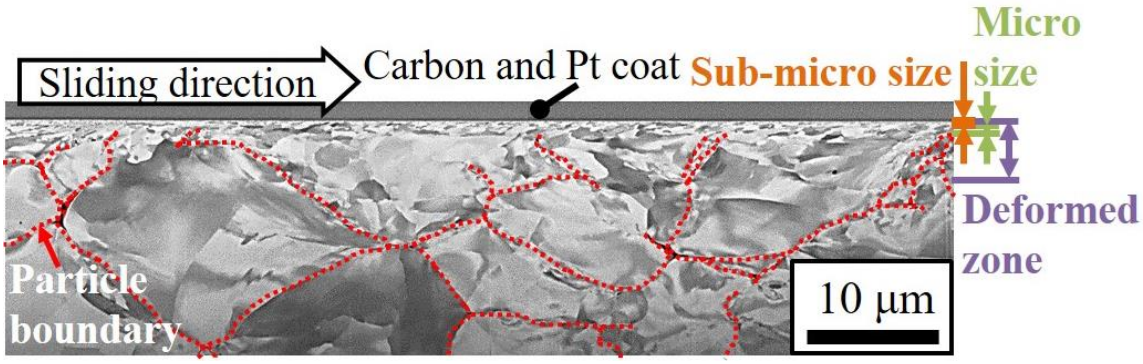


(a) $P$ = 27 N, $N$ = 100

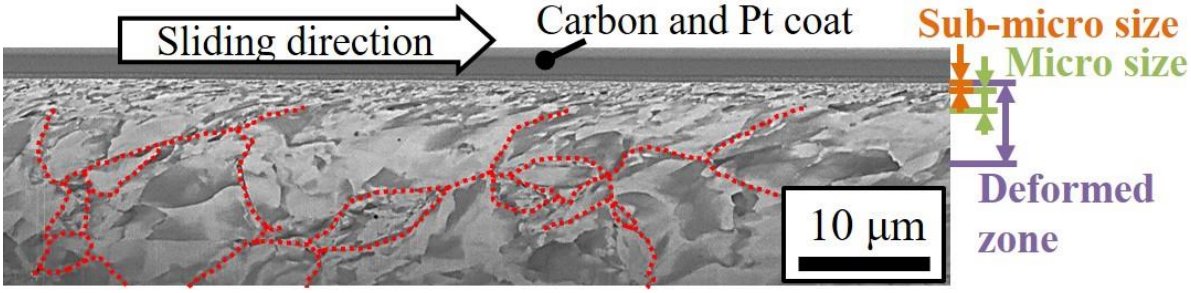


(b) $P$ = 40 N, $N$ = 10

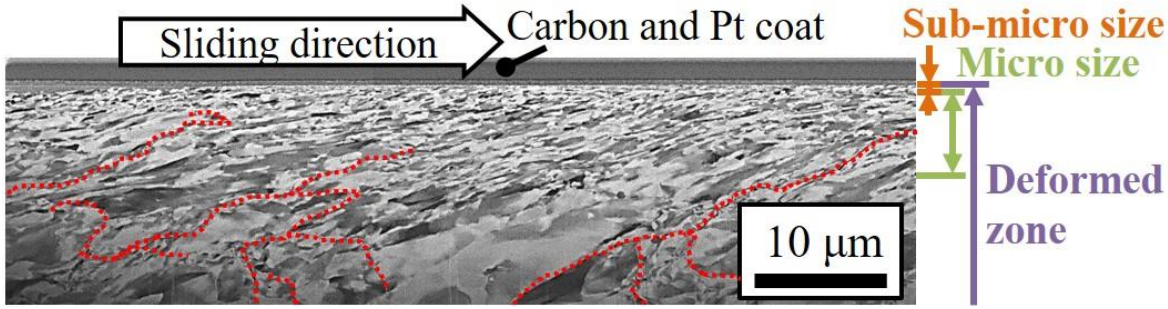


(c) $P$ = 60 N, $N$ = 10

**Fig. 4-9 SIM images of pure Cu sample cross-sections after friction experiments with $P$ = 27, 40, 60 N.**

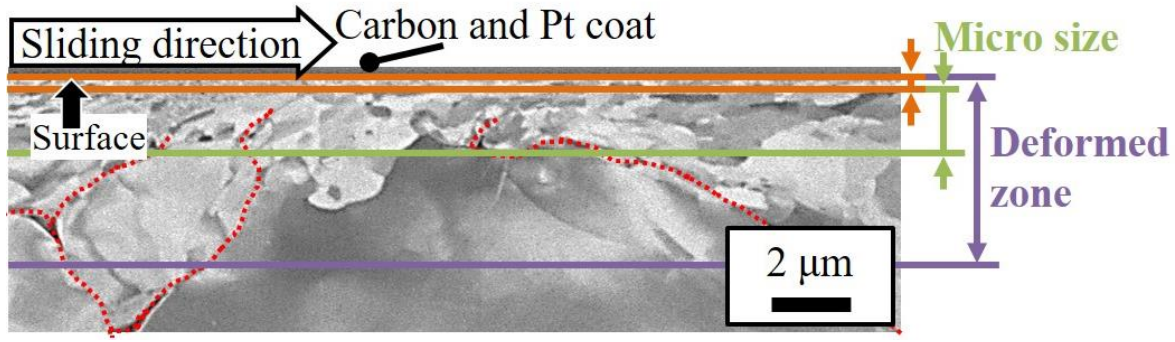


(a) $P$ = 27 N, $N$ = 100

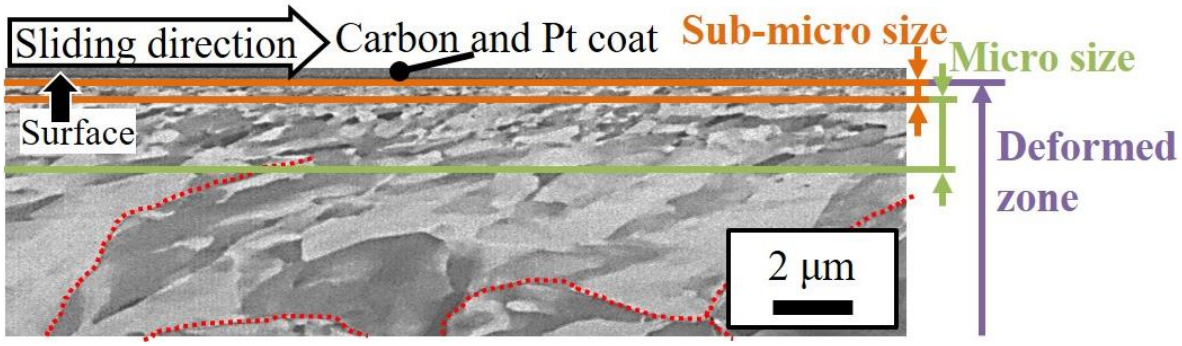


(b) $P$ = 40 N, $N$ = 10

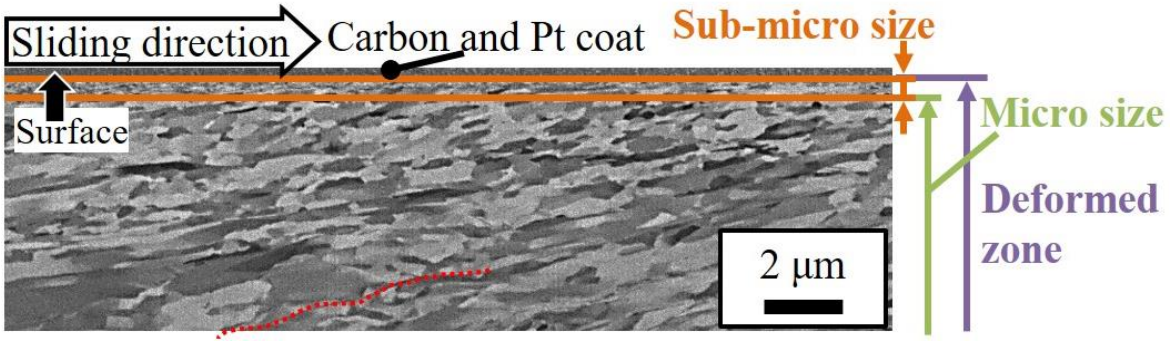


(c) $P$ = 60 N, $N$ = 10

**Fig. 4-10 SIM images of pure Cu sample cross-sections after friction experiments with $P$ = 27, 40, 60 N. (Enlarged image of Fig. 4-9)**

**Table 4-2 Average thicknesses of three regions of pure Cu samples after friction experiments with different normal loads.**

| *P* (N), *N* (-) | 27, 100 | 40, 10 | 60, 10 |
|---|---|---|---|
| Deformed zone (μm) | 4.5 | 6.3 | (19) |
| Micro size crystalline region (μm) | 1.6 | 1.7 | 6.3 |
| Sub-micron crystalline region (μm) | 0.3 | 0.4 | 0.7 |

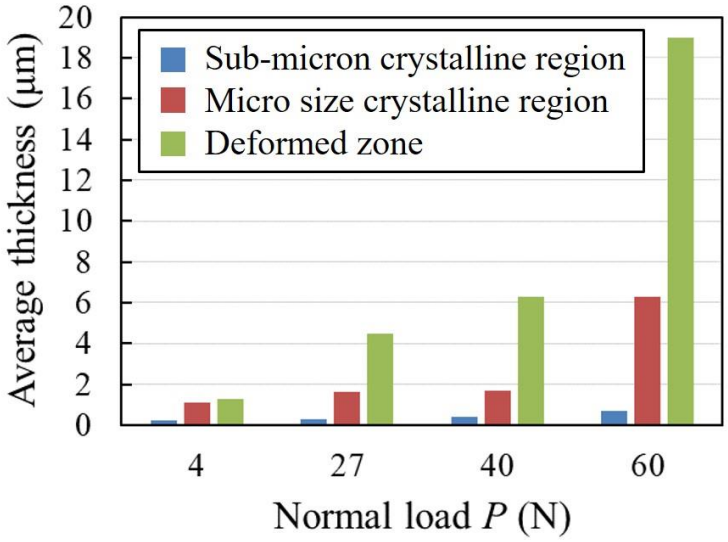


**Fig. 4-11 Relation between applied normal load *P* and average thicknesses of several regions.**

## 4.4 Relation between stress distribution and mechanical mixing

Subsequently, the stress applied to the powder particles was calculated to clarify what and how much stress is needed for deformation or bonding.

From the SEM fracture surface and SIM the cross-sectional observations (Fig. 4-3, Fig. 4-4, Fig. 4-8, Fig. 4-9), the powder particles of the uniaxial compressed samples were densely packed. It appears that the elastic deformation model can be used as the calculation method of the stress applied to the powder particles. The calculation method of stress field created by circular contact on the flat surface proposed by G.M. Hamilton and L. E. Goodman was used in this study [4-1]. Contact radius and maximum contact pressure were calculated by using Hertzian contact theory [4-2]. Young's moduli of Cu and $ZrO_2$ used in the calculation of the stress applied to the sample were 120 and 200 GPa, respectively. Poisson's ratios of them were 0.34 and 0.30, respectively. All these values were chosen to correspond with those of the samples used in the experiments. In addition, the coefficient of friction $\mu$ = 0.30 and 0.25 were chosen for the experiment with normal load $N$ = 4.0 and 27 N respectively from the results of the friction

experiments (Fig. 4-1 and Fig. 4-6).

Fig. 4-12 shows a schematic illustration of *xyz* Cartesian coordinates for Hamilton's model. A center of a contact surface is set as the origin. Fig. 4-13 shows a graph of a stress $\sigma_{xx}$ along the sliding direction ($y = z = 0$). $\sigma_{ij}$ is a Cauchy stress tensor applied to the sample. When there is no friction resistance (coefficient of friction $\mu = 0$), the $\sigma_{xx}$ inside the contact radius $a = 60$ μm is almost compressive and it is symmetrical shown as a black broken line in Fig. 4-13. With the certain $\mu$, the $\sigma_{xx}$ becomes unsymmetrical shown as a red solid line in Fig. 4-13. The most significant difference between the contact with and without sliding is an increase of a tensile stress at the edge of the contact zone ($x = -60$ μm). A compressive stress alone is not enough to bond the powder particles and shearing stress is indispensable. Therefore, this tensile stress can be thought as one of the important factors for the particle bonding.

In addition to $\sigma_{xx}$, although there are $\tau_{zx}$ and $\tau_{yx}$ as the stresses applied in the shearing direction, these of near the sample surface were small enough to be neglected in the calculation. In fact, $\tau_{yx}$ is constantly 0 regardless the tangential force applied or not. In contrast, $\tau_{zx}$ is 0 when the tangential force is not applied ($\mu = 0$), but it increases when the tangential force applied. Fig. 4-15 shows the stress $\tau_{zx}$ applied to pure Cu sample along *x*-axis ($P = 4.0$ N, $\mu = 0.30$) calculated by using Hamilton's model. $\tau_{zx}$ increased in the inner region of the sample. Nevertheless, the maximum tensile and compressive stress of $\tau_{zx}$ is about 70 MPa and -150 MPa and these are less than half of the maximum values of $\sigma_{xx}$. The shearing stress calculated by Hertzian theory reaches a maximum value at the half of the Hertzian contact radius from the sample surface. When normal load $P = 4.0$ N, it should be 160 MPa at 30 μm depth from sample surface. However, it was confirmed by the fracture surface observation that the powder particles didn't deform in that area. Fig. 4-16 shows the stress $\sigma_{zz}$ applied to pure Cu sample along *x*-axis ($P = 4.0$ N, $\mu = 0$ and 0.30) calculated by using Hamilton's model. The stress applied in the depth direction $\sigma_{zz}$ doesn't change even the coefficient of friction increased. Therefore, $\sigma_{xx}$ appears to be the leading parameter on the plastic deformation and bonding of the powder particles.

Fig. 4-14 shows $\sigma_{xx}$ applied to the pure Cu sample along *x*-axis ($P = 4.0$ N, $\mu = 0.30$) calculated by Hamilton's model. Even the depth *z* from the sample surface became deeper, the tendency of applied stress was similar. The most major change was the maximum tensile stress at $x = -60$ μm and it decreased when *z* increased. From above reasons, the maximum tensile stress $\sigma_{xx\,max}$ is focused in this study.

Fig. 4-17 shows the maximum tensile stress $\sigma_{xx\,max}$ at $y = 0$. When the normal load *P* was 27 N, larger stress was applied to the sample than $P = 4.0$ N at the same depth. The $\sigma_{xx\,max}$ decreased when the depth from the sample surface *z* increased. According to Ref. (4-2), the tensile yield stress (0.2% proof stress) of the pure Cu with 5.0 μm crystal grain size is 200 MPa. The depths where the 200 MPa or more stress was applied to the sample were up to 1.0 μm at 4.0 N and up to 4.0 μm at 27 N, respectively. These calculated values and the measured values almost same. The slight difference between calculated values and the measured values appears to be reasonable because the value of 0.2% proof stress (200 MPa) is one for pure Cu with relatively coarser crystal grain structure and it is different from that of the finer crystallized Cu [4-3]. Therefore, the relation between the applied stress and the plastic deformation of the powder particles was consistent between the observation results and the calculated values. This result suggests that Hamilton's model can successfully interpret the feature of the stress to powder particles

under the friction experiment. The tensile proof stress 200 MPa appears to be a threshold of the deformation of the pure Cu powder particle during the unidirectional friction experiment. In addition, the other repartitions of the applied stress other than $\sigma_{xx}$, $\tau_{zx}$ and $\sigma_{zz}$ does not reach this value (200 MPa). Thus, the tensile stress of $\sigma_{xx}$ appears to be the most effective stress to the inter particle bonding process during the unidirectional friction experiment. In contrast, the correlation between the bonding or the crystal grain refinement and the applied stress hasn't been clarified.

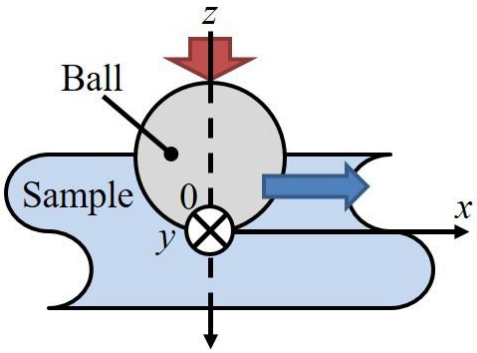


**Fig. 4-12 Cartesian coordinate for Hamilton and Goodman's model.**

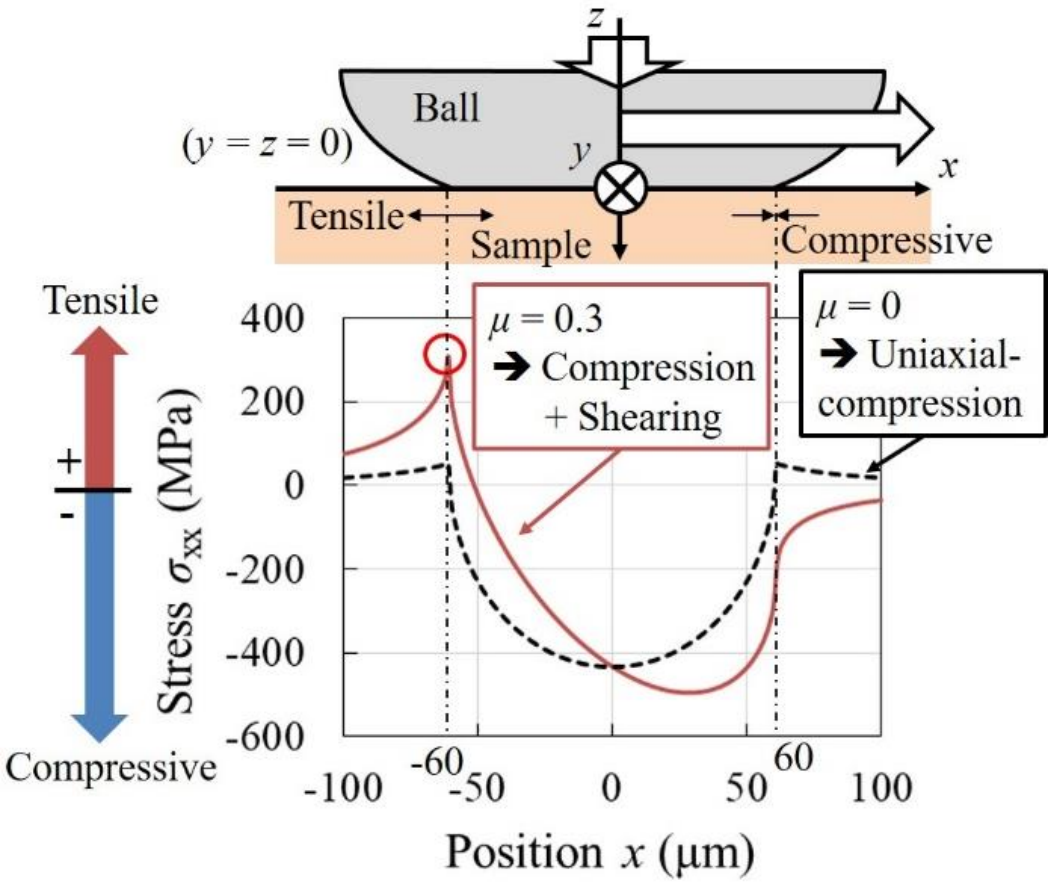


**Fig. 4-13 Stress $\sigma_{xx}$ along *x*-axis of circular contact for *P* = 4.0 N, $\mu$ = 0, 0.30.**

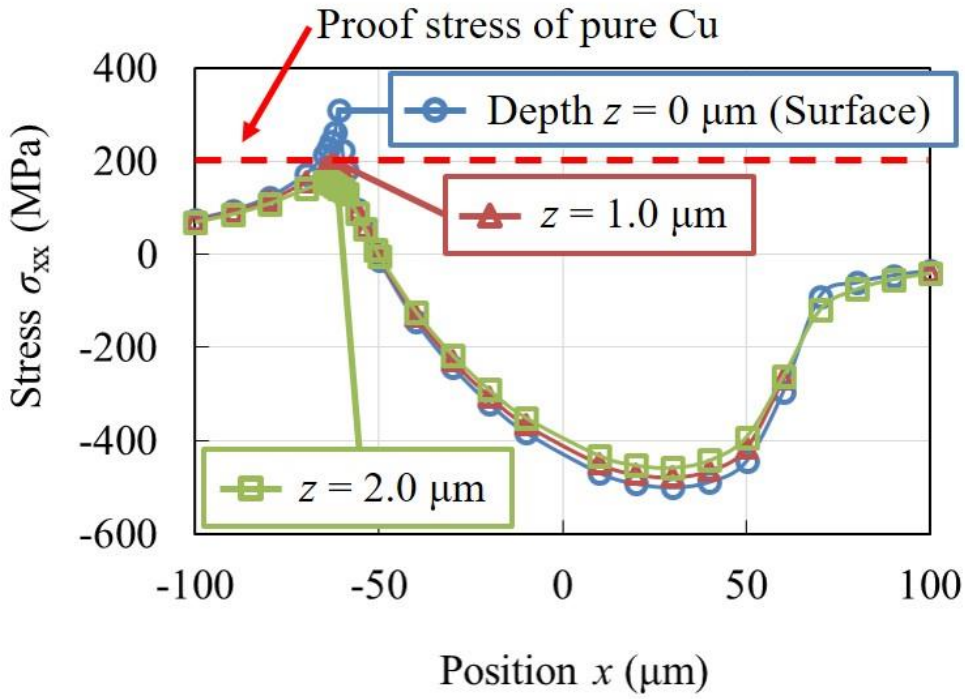


**Fig. 4-14 Stress $\sigma_{xx}$ applied to pure Cu sample along $x$-axis ($P$ = 4.0 N, $\mu$ = 0.30) calculated by using Hamilton's model.**

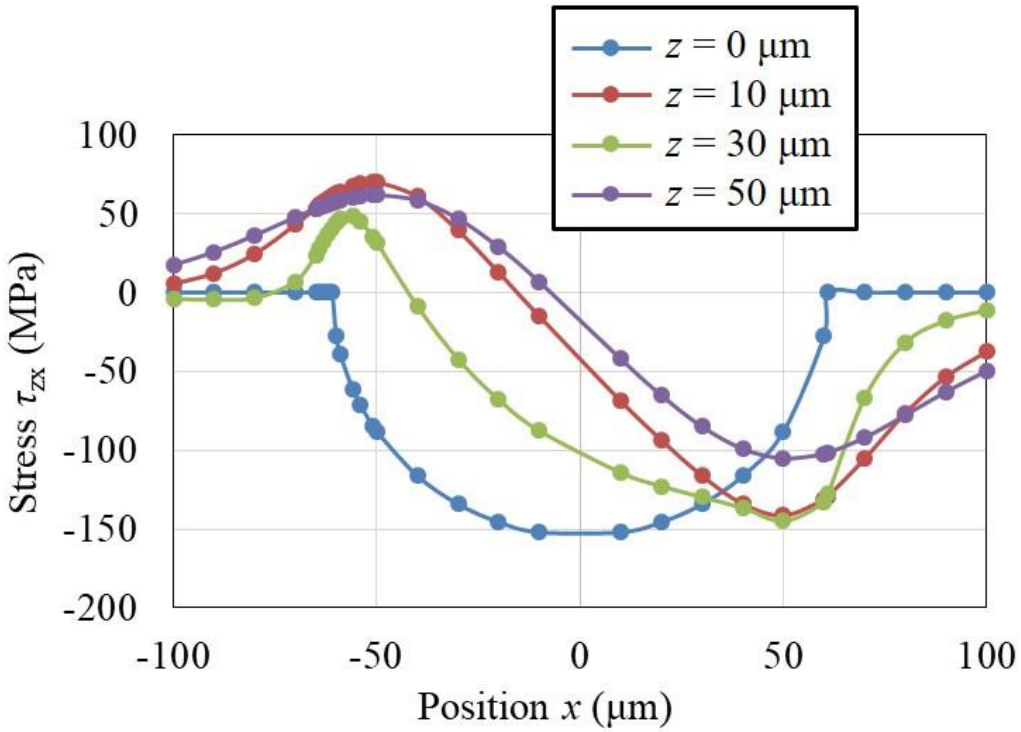


**Fig. 4-15 Stress $\tau_{zx}$ applied to pure Cu sample along $x$-axis ($P$ = 4.0 N, $\mu$ = 0.30) calculated by using Hamilton's model.**

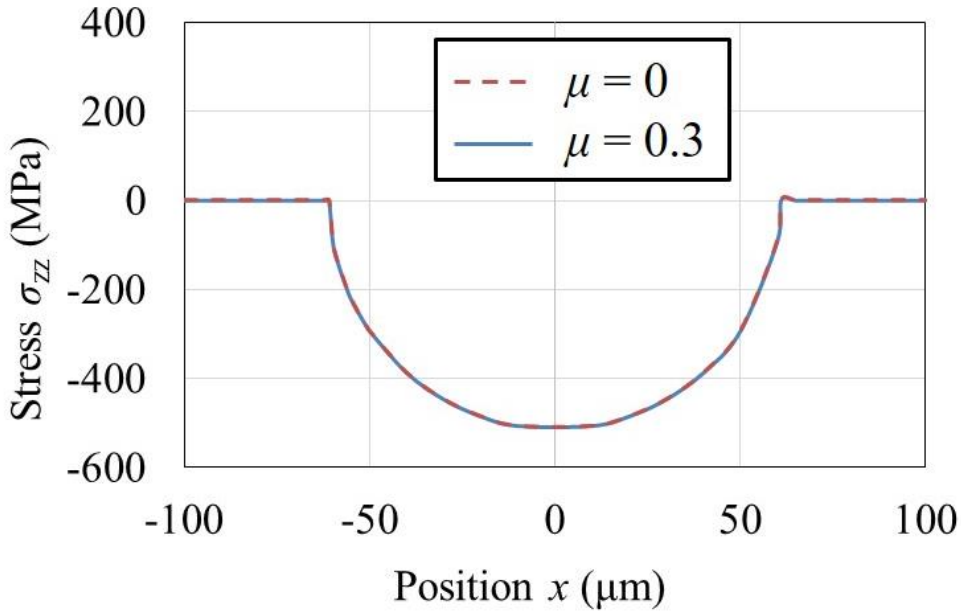


**Fig. 4-16 Stress $\sigma_{zz}$ applied to pure Cu sample along $x$-axis ($P$ = 4.0 N, $\mu$ = 0 and 0.30) calculated by using Hamilton's model.**

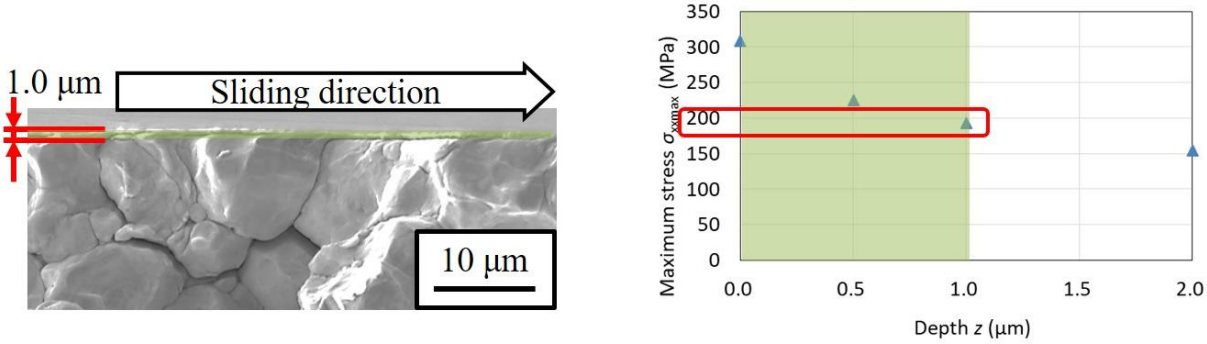


(a) $P$ = 4.0 N, $\mu$ = 0.30

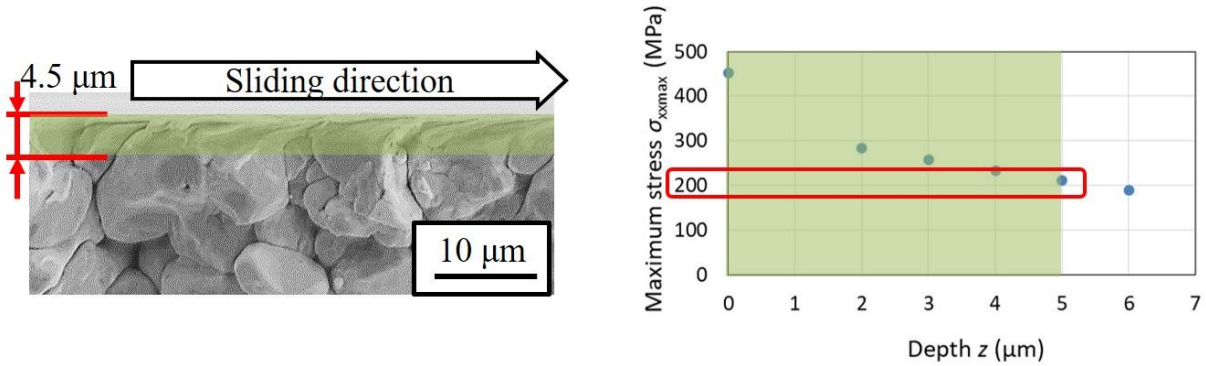


(b) $P$ = 27 N, $\mu$ = 0.25

**Fig. 4-17 Fracture surface of samples and relation between depth from pure Cu sample surface and maximum stress $\sigma_{xxmax}$.**

## 4.5 Conclusions

In this chapter, the unidirectional friction experiments were carried out to clarify the mechanism of interparticle bonding during the compression shearing process. The stability of the friction experiment is evaluated by measurement of coefficient of friction and observation of sample surfaces. The effect of applied stress to the powder particles is investigated by cross-sectional observations of the samples. Then, these experimental results are compared with the calculated stress distribution during the friction experiment to evaluate the experiment quantitatively.

The results are as follows.

1) The tangential force stably applied to the powder particles without any wear or oxidation
2) The surface of the powder particles were deformed and bonded each other under the repetitive unidirectional sliding experiment.
3) The range of applied stress enlarged with increasing the normal load while it was constant even the number of sliding cycles changed.
4) The relation between the applied stress and the plastic deformation of the powder particles was consistent between the observation results and the calculated values.
5) The tensile stress applied to the powder particles along the sliding direction appeared to be the most effective stress to the inter particle bonding process. When it reached the 0.2% proof stress of pure Cu (200 MPa), the powder particles deformed.

## References

(4-1) G. M. Hamilton, L. E. Goodman, The stress field created by a circular sliding contact, Journal of Applied Mechanics, (1996), pp. 371 - 376.

(4-2) K.L. Johnson, Contact Mechanics, Cambridge University Press, 1987.

(4-3) M. Mori, N. Yuki, Strength, ductility and electric conductivity pf copper and copper alloys and control of nanocrystalline structure, Journal of Japan Institute of Light Metals, Vol. 56, No. 11, (2006), pp. 615 - 620. (in Japanese)

# Chapter 5

# Understanding the Consolidation of Metal from Powder to Plate by Compression Shearing Method

The objective of this chapter is to connect the facts which have been clarified individually in each previous chapter, and to find out the new scientific knowledge. Firstly, the results of literary investigation of chapter 1 and these of the experimental approaches of chapter 3 and 4 are summarized. Then, these results are discussed to understand the consolidation of metal by COSME-RT.

## 5.1 Summary of the previous results

In the chapter 1, the problem of COSME-RT process and the approach to solve this problem were introduced by literature reviews. The problem is that the consolidation mechanism of the metal in the forming process by use of COSME-RT has not been clarified yet. The model which is built by Horita et al. suggested that the oxide films and contaminations around the powder particles are removed by the friction force between the particles due to the applied shearing force, and the clean surfaces of these particles make strong the metal bonding [5-1]. However, Horita's model is based on the observation of only the beginning and the end of the samples during the COSME-RT process. The objective of this thesis is to complete the consolidation mechanism of the COSME-RT process. I thus proposed to control the shearing force in order to understand the mechanism of consolidation process of material by COSME-RT.

In the chapter 2, the experiments to achieve the objective of this thesis were presented. To control the shearing force, two different approaches were attempted. First one is the suppression of the applied

shearing force by dispersing $MoS_2$ into the Cu matrix. Second one is the friction experiment, where the compression shearing process was applied to the uniaxial-compressed sample by the linear friction experiment. The mechanism of the COSME-RT apparatus was also introduced.

In the chapter 3, the result of the observations of $MoS_2$ dispersion were revealed and discussed. By dispersing $MoS_2$ that prevents the partial contacts between the Cu powder particles, it was suggested that the friction between the powder particles was needed to the particles bonding and the applied shearing strain caused by the friction force.

In the chapter 4, the result of the tribological approach was described and discussed. It was clarified that the unidirectional friction experiment can be used for interpret the COSME-RT process and the powder particles were bonded by the local compression shearing process of the friction experiment. In addition, it was indicated that the tensile stress applied to the particles along the shearing direction is the most effective stress to proceed the bonding process of the particles.

In this chapter, firstly the consolidation model of powder particles built by Horita et al. is considered again and its unresolved questions are made clear. Subsequently, the path to the bonding of the particles is discussed by investigating the result obtained in chapter 4. Then, how the friction between the particles is caused is discussed by considering the results of chapter 3 and 4. Finally, the new model of the bonding process of the powder particles by COSME-RT is proposed.

## 5.2 Unsolved issues on COSME-RT

### 5.2.1 Horita's model

Fig. 5-1 shows the simplified schematic illustration of the Horita's model [5-1]. Horita et al. clarified that the powder particles are partly bonded only by uniaxial compression. The refinement of crystal grain of the sample is occurred at boundary of the particles firstly, then grain refined area is enlarged with increasing applied shearing strain. Therefore, this model suggests that the local bonding is first happened in the COSME-RT process, and finally the crystal grain refinement of the sample is proceeded. However, two unresolved questions are still remained.

In the Horita's model, the middle process was not observed and it was only interpolated. Fig. 5-2 shows the schematic illustration of the order of the consolidation process of the powder particles by COSME-RT. In the middle process, there should be three steps, such as the deformation, the bonding, and the crystal grain refinement of the particles. However, the order of these processes are not clarified yet. In addition, it is considered that the bonding of the particles is caused by the friction force, but the detailed influence of this friction is not well explained yet.

In the following sections, above two unsolved issues are discussed.

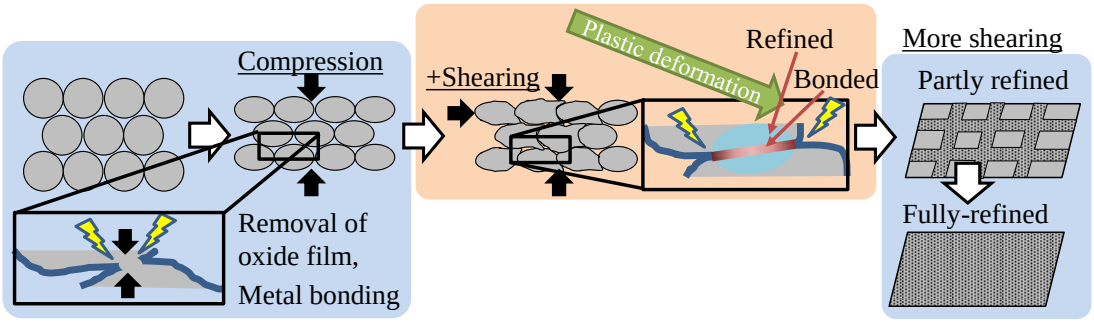


**Fig. 5-1 Simplified Horita's model.**

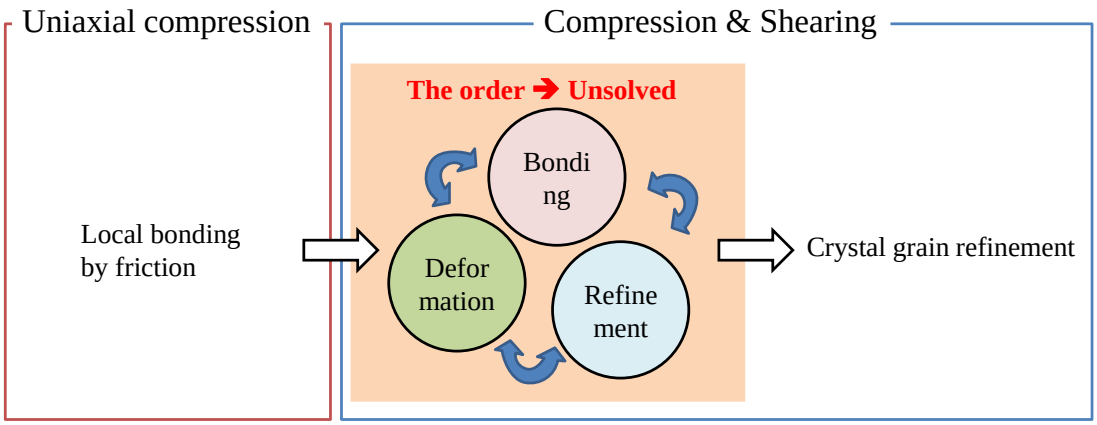


**Fig. 5-2 Schematic illustration of order of consolidation process by COSME-RT.**

## 5.2.2 Order of local bonding process

The process of the local bonding of the powder particles can be further discussed by the cross-section SIM image of pure Cu sample after the friction experiment observed in Chapter 4.In the sample after the friction experiment, the stress applied near the sample surface is larger than that applied to deeper region. Therefore, the bonding process of powder particles can be traced from inner part to the surface of the sample. In other words, the sample cross-section after the friction experiment shows a time-lapse in a process the powder particles along the depth direction. Therefore, the bonding process can be traced by observing SIM image of sample cross-section from deeper region to sample surface.

Fig. 5-3 shows the SIM image of the sample cross-section and the relation between the depth from the sample surface and the applied maximum tensile stress during the friction experiment ($P$ = 27 N, $N$ = 100) to the uniaxial-compressed pure Cu sample. The SIM image of Fig. 5-3 is same as Fig. 4-9(a), and the relation is same as Fig. 4-17(b). The powder particles deformed at the near-surface region, 4.6 to 1.7 μm from the sample surface. In contrast, the powder particles didn't deform at the region deeper than 4.6 μm from the sample surface. This result suggested that the powder particles firstly deformed

by applying shearing stress when the applied stress reached the proof stress of the sample.

At much shallower region, 1.7 to 0.33 μm from the sample surface, the crystalline structures of the particles became finer to micro meter size. The boundaries of the powder particles were disappeared at this micro size crystalline region, especially in the region where the boundaries of the particles were positioned generally parallel to the sliding surface. Therefore, the bonding of the powder particles appears to occur after crystal refinement because the boundaries of the particles disappeared in the middle areas of the micro size crystalline region rather than the edge. When the powder boundary became parallel to the sliding contact surface, the component parallel to the powder boundary of the tensile stress increases. It appears that the local sliding occurred by this tensile stress and the powder particles were bonded each other. At the region just below the sample surface, 0.33 μm from the sample surface to top of the sample surface, the crystal structures of the particles became sub-micro size.

From these results, the bonding process of the powder particle would be described as in the order of, (1) Plastic deformation, (2) Initial crystal grain refinement to micro size, (3) Bonding, (4) Crystal grain refinement to sub-micro size. A schematic illustration of this process is shown in Fig. 5-4.

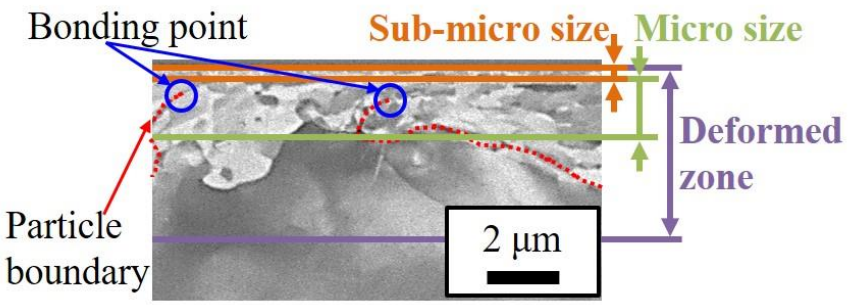


**Fig. 5-3 SIM image of sample cross-section after friction experiment (*P* = 27 N, *N* = 100) (Enlarged image of Fig. 4-9(a)).**

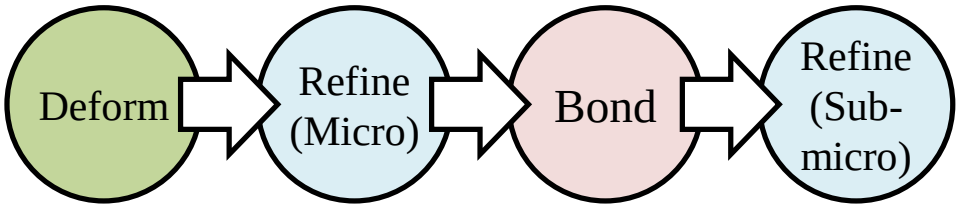


**Fig. 5-4 Schematic illustration of order of local bonding of pure Cu powder particles by compression shearing method.**

### 5.2.3 Applied force direction and friction of the powder particles

The shearing force is applied to the powder particles during the COSME-RT process. This shearing force appears to cause the friction behavior between the particles and the particles are bonded between powder boundaries. Nevertheless, the driving forces which cause the sliding of powder particles was not clarified yet. I would like to discuss this phenomenon by considering the direction of applied shearing force to the Cu powder particles during compression shearing process by the unidirectional friction experiment and COSME-RT.

Fig. 5-5 shows the schematic illustration of the direction of the applied shearing force to the Cu powder particles in the unidirectional friction experiment. The SIM image of Fig. 5-5 is the pure Cu sample cross-section after friction experiments with $P$ = 40 N, $N$ = 10, same as Fig. 4-9(b). During the friction experiment, the powder particles were deformed and bonded, and these crystal grains were refined along the sliding direction. This result suggests that the bonding process of the particles only proceeded to the sliding direction even though the bonding state of the particles changes in the depth direction. In addition, it appears that the shearing force only applied to the particles parallel to the sliding direction from the counter ball.

Fig. 5-6 shows the schematic illustration of the direction of the applied shearing force to the pure Cu powder particles in the COSME-RT process of Cu/$MoS_2$ sample. The SIM image of Fig. 5-6 is enlarged image of Fig. 3-20(c), the cross-section of Cu/$MoS_2$ sample when $L_S$ = 0.50 mm. $MoS_2$ reduces friction by intercepting between Cu powder particles and its lubricity, and Cu powder particles was not bonded and deformed except the top surface of the sample. In chapter 3, it was suggested that the sliding between the sample and the steel plate was occurred during the COSME-RT process and the top surface of the powder particles was deformed and bonded by this sliding.

Fig. 5-7 shows the schematic illustration of the direction of the applied shearing force to the Cu powder particles in the COSME-RT process of pure Cu sample. The SIM image of Fig. 5-7 is the cross-section of pure Cu sample when $L_S$ = 0.50 mm. This sample is same as Fig. 3-18(b), but its bottom side surface is shown. In the COSME-RT, the crystal grains of the pure Cu powder particles around the boundaries of the particles were refined by applying shearing force. Differs from the friction experiment, the partial crystal refinement was proceeded not only parallel to the shearing direction but also at boundaries in the depth direction. This result suggests that the force applied to the particles in both shearing and depth directions during the COSME-RT. Therefore, the resultant force behaves like as a rotational force applying to the sample as shown in Fig. 5-8.

From these results, it was demonstrated that the shearing force is necessary to cause the local sliding between the powder particles, and the local sliding causes the bonding of the particles. Even there is the difference in the direction of the applied shearing force, the local sliding between the powder particles is caused by the applied shearing force.

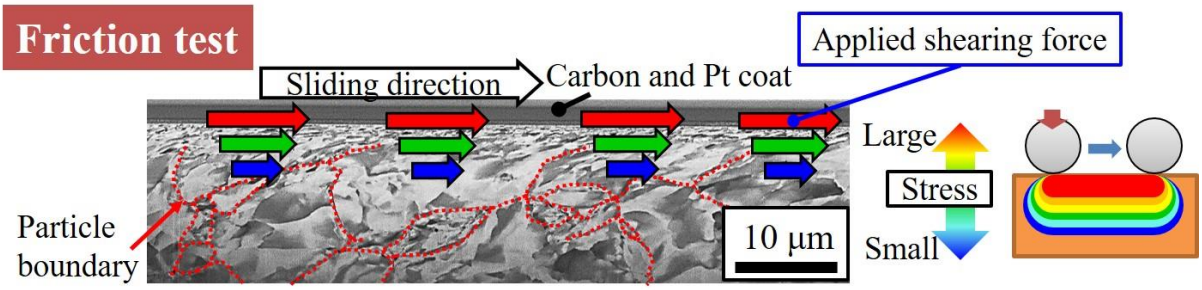


**Fig. 5-5 Direction of applied shearing force to pure Cu powder particles in friction experiment.**

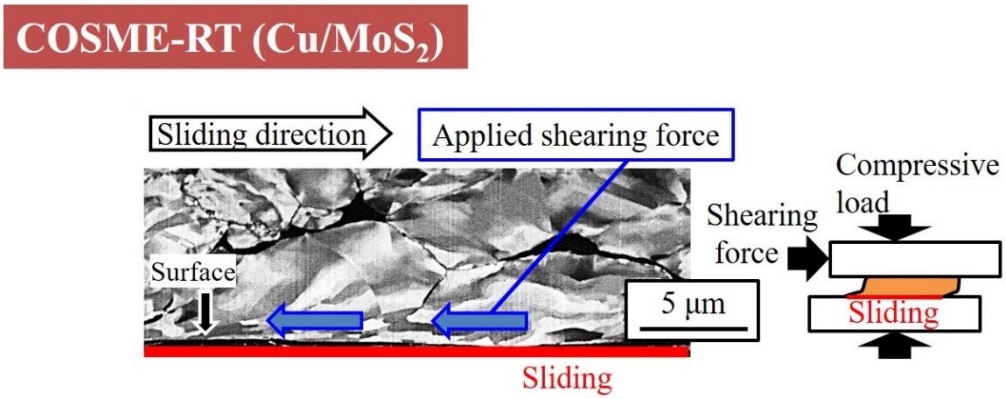


**Fig. 5-6 Direction of applied shearing force to pure Cu powder particles in COSME-RT process of Cu/$MoS_2$ sample.**

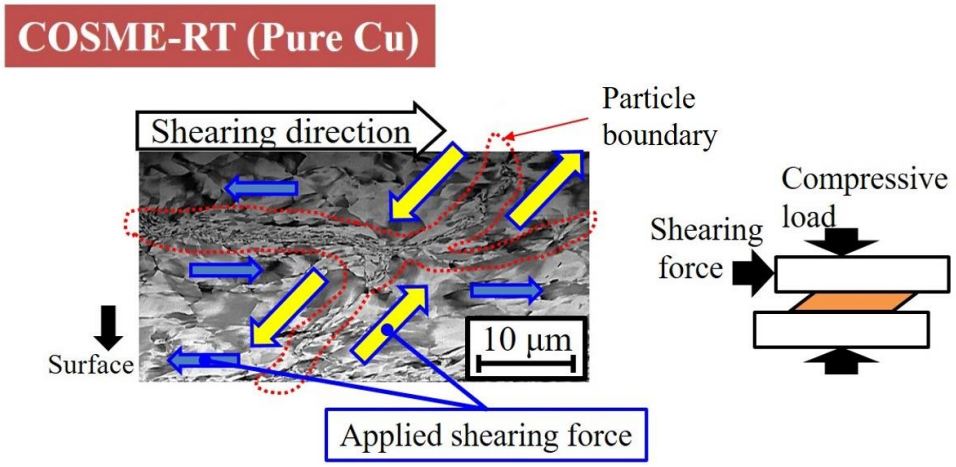


**Fig. 5-7 Direction of applied shearing force to pure Cu powder particles in COSME-RT process of pure Cu sample.**

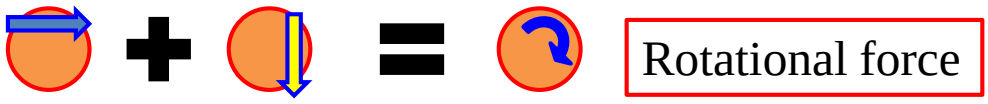


**Fig. 5-8 Rotational force applied to the powder particle during COSME-RT process.**

### 5.2.4 Local friction model

From above two discussions, how the frictions are caused in the friction experiment and COSME-RT is presented. Fig. 5-9 shows the schematic illustration of the bonding process of the powder particles by the unidirectional friction experiment and COSME-RT. In the friction experiment, the stress is applied to the powder particles from the counter ball, and the particles deformed. The contact angle of the powder particles become looser due to the plastic deformation of the particles. The amount of the stress applied to the two powder particles is different because the stress applied to the powder particles decreases from sample surface to the inside of the sample. It appears that this difference in the applied stress makes the local sliding between the powder particles in the process, so that the particles are bonded each other.

In the COSME-RT process, there is no stress distribution in the sample and an almost equivalent amount of stress is applied to each powder particle in the same direction. It appears that the rotational forces are applied to the all powder particles as shown in Fig. 5-9(b). At the boundary of the powder particles, the stresses in different directions apply to the particles. This difference of the direction of the stresses must cause local sliding between the powder particles and the particles are bonded each other.

Furthermore, in the solid state bonding techniques such as a surface activated bonding, the metal materials are bonded by the removal of their native oxide films and metal bonding [19]. In the compression shearing processes by the unidirectional friction experiment and COSME-RT, the oxide film around the powder particles appears to be removed by this local sliding and the particles are bonded each other.

Therefore, the powder particles were bonded by a local sliding at the powder boundary during the COSME-RT process, and the unidirectional friction experiment could interpret this process.

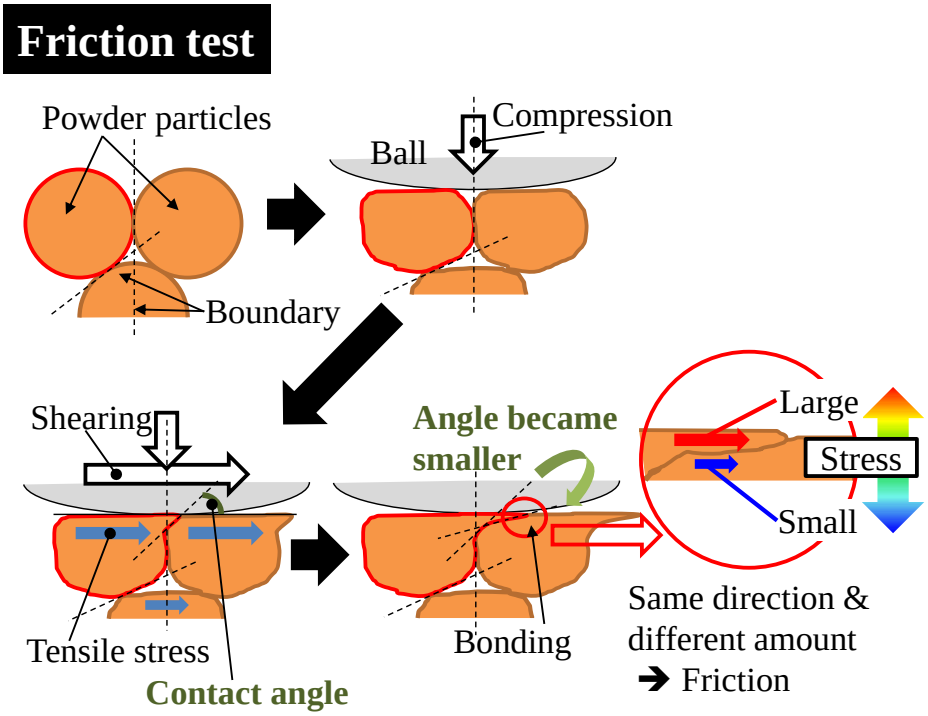


(a) Friction experiment

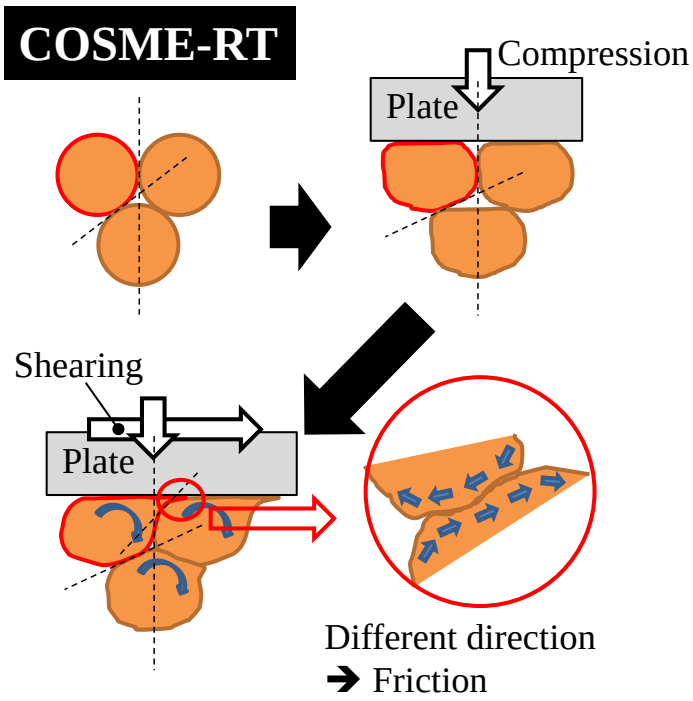


(b) COSME-RT

**Fig. 5-9 Schematic illustration of bonding process of powder particles by (a) unidirectional friction experiment and (b) COSME-RT.**

## 5.3 New model

From above two discussions, I propose the new model of COSME-RT. Fig. 5-10 shows the new model of consolidation process of metal from powder to plate by COSME-RT derived from this study. The step boxed by colored region is new result which was clarified in this study. Firstly, the powder particles partly bonded by applying compressive load. Subsequently, the shearing force is applied to the particles while maintaining the compression load. When the shearing force reached to the proof stress (it is about 200 MPa in the case of pure Cu), the powder particles are deformed. With increasing the applied shearing force, the local powder bonding process proceeds as (1) deformation, (2) initial grain refinement to micro size, (3) local bonding of the particles by the local sliding of the particles, and (4) grain refinement to sub-micro size. This sequence from (1) to (4) is happened several places in the whole sample simultaneously. By repeating this sequence, the powder particles of whole sample are bonded. After the bonding of powder particles, the grain refinement of particles proceeds around the boundaries of the powder particles as described in the Horita's model. Finally, the fully-refined sample was fabricated.

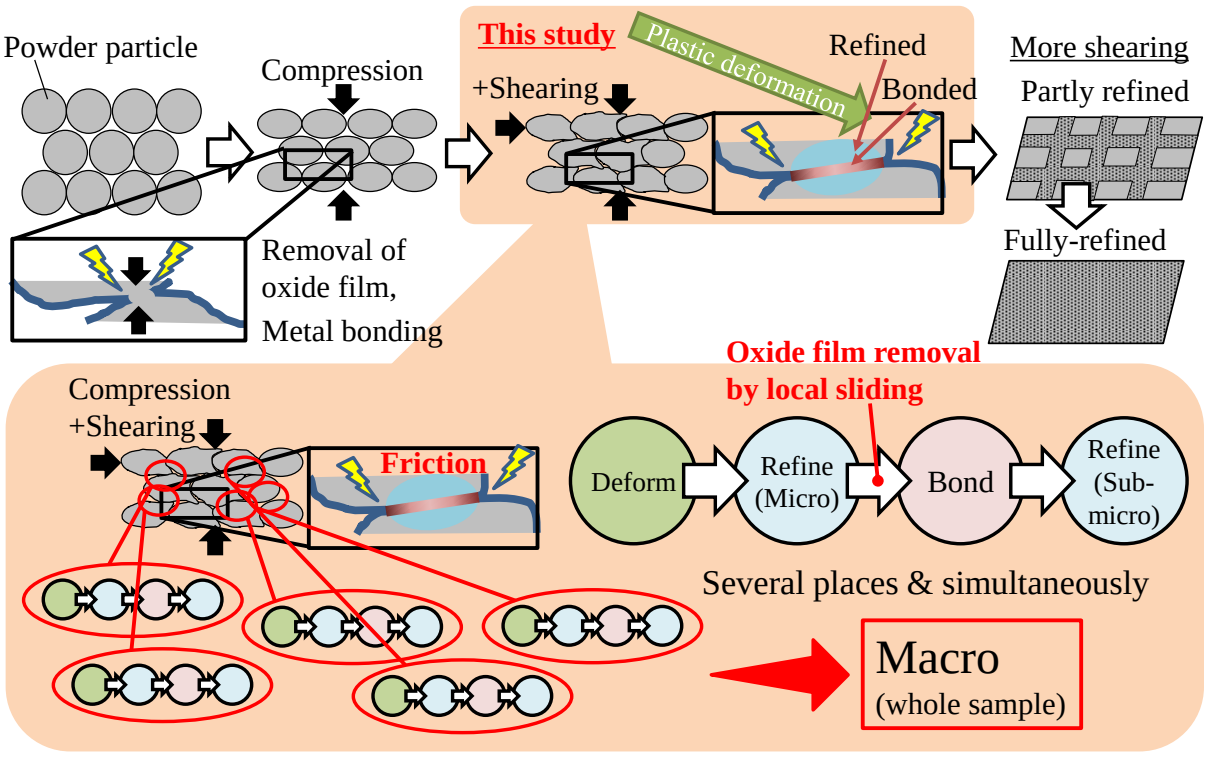


**Fig. 5-10 New model of consolidation process of metal from powder to plate by COSME-RT proposed in this study.**

## 5.4 Conclusions

In this chapter, the facts which have been clarified individually in each previous chapter was integrated and new consolidation model of metal from powder to plate by COSME-RT.

The results as follow,

1. It was clarified that the shearing force caused the local sliding between the powder particles and this sliding proceed the bonding process.
2. During the COSME-RT process, powder particles is applied the rotational force by shearing process.
3. The order of local bonding of powder particles is clarified. It proceeds in the order of, (1) Plastic deformation, (2) Initial crystal refinement to micro size, (3) Bonding, (4) Crystal refinement to sub-micro size.
4. New consolidation model of pure Cu from powder to plate by COSME-RT was built.

Finally, I obtained the new consolidation model of pure Cu from powder to plate by COSME-RT.

## References

(5-1) M. Horita, Doctor Thesis, Shinshu University, Japan, (2014). pp. 65 - 67.

# Chapter 6

# General Conclusions and Perspectives

## 6.1 General conclusions

The main objective of this study is to understand the consolidation of the metal powder to thin plate by the compression shearing method. Two experimental approaches had been attempted, and the new model of metal powder consolidation was proposed.

In chapter 1, the general overviews about materials and material molding methods were presented by reviewing the literatures.

In chapter 2, the detail of the experiments was highlighted. To achieve the objective of this thesis presented in the previous chapter, two different experimental approaches were attempted.

In chapter 3, Cu/$MoS_2$ samples were formed under the several shearing distances and their microstructures were observed. The microstructural change related to the decrease in applied shearing force was discussed.

In chapter 4, the unidirectional friction experiments were carried out to clarify the mechanism of interparticle bonding during the compression shearing process. The relationship between the normal loads applied, the number of sliding cycles, and the bonding condition of the powder particles was investigated by observing the surface structures and the fracture surfaces of the samples after the friction experiments.

In chapter 5, all the facts which have been clarified individually in each previous chapter were took consideration and new consolidation model of metal from powder to plate by COSME-RT was constructed.

From the results of these chapters, the new knowledges were obtained as follow,

1. Solid state metal molding methods has been expected to meet the requirements for metal materials, and a novel powder molding method, COSME-RT has many advantages with the conventional molding methods. If the metal consolidation mechanism by COSME-RT is clarified, it is expected to put it to practical use.
2. It was indicated that the shearing force makes friction force between powder particles and friction

motion proceed the bonding process. Therefore, the shearing force applied to the powder particles appears to be one of important factors on the metal consolidation by COSME-RT.

3. Unidirectional friction experiment can simulate the time axis information of metal consolidation process at COSME-RT. The microstructural change in depth direction which indicate time changes at COSME-RT was observed by changing applied normal load. Local tensile stress is the leading parameter on the bonding process of powder particles by COSME-RT.
4. With increasing the applied shearing force, the local powder bonding process proceeds as (1) deformation, (2) initial grain refinement to micro size, (3) local bonding of the particles by the local sliding of the particles, and (4) grain refinement to sub-micro size. During the step (3), it appears that the tensile stress caused the local sliding between the powder particles and the oxide film around the powder particles may be removed by this sliding proceed. Then, the powder particles are bonded. From these results, a new consolidation model of pure Cu from powder to plate by COSME-RT was constructed.

From above results, I succeeded to obtain new knowledge about the consolidation process of Cu plate from powder by COSME-RT.

## 6.2 Perspectives

In this thesis, the new model of the consolidation of Cu from powder to plate by COSME-RT was built. If the more investigation about threshold value to proceed the particle bonding such as applied stress or energy is progressed, the model will be much quantitative. Fortunately, it was clarified that the unidirectional friction experiment can interpret the COSME-RT process, and applied stress to the sample can be calculated. Therefore, additional investigations by using the unidirectional friction experiment is expected to clarify the threshold value of particle bonding.

The numerical model of the stress distribution during the friction experiment proposed by Hamilton et al. is for the elastic solid model. If another method such as an elasto-plastic finite element method is introduced for calculation, more precise estimation can be available because the unidirectional compressed sample has many voids and it was not a uniform material. In addition, the point of view of the granular mechanics appears to be required to understand the deformation and movement of powder particles during the COSME-RT process.

In this study, Cu is chosen as a feedstock powder, but Ti and Al were used in Horita's investigation and his model. In my experience, there are only few differences in the COSME-RT process depend on metal materials, and the model of the consolidation of Cu proposed in this study can be applied to other materials. Only differences appears to be oxide films and material strength. The general model for metal

material can be built by more investigation about the relation between oxide films and material strength by using several kinds of metals.

This thesis have been focusing on the COSME-RT, but the results obtained in this study can be applied to other dynamic molding methods of powder materials because these have same points on the mechanism of consolidation of powder particles.

In addition, COSME-RT can develop composite materials which cannot be consolidated by conventional methods like the combination of metal and non-metal materials. In the future, contribution to further development of society is expected by progress of development of various kinds of composite materials by COSME-RT. Especially Cu/$MoS_2$ has both high mechanical strength and good tribological property, and it should have good electrical conductivity. To improve formability of Cu/$MoS_2$, heating process under the chemical reaction temperature appears to be effective. In addition, the control of the sliding is one of the way to improve the formability of Cu/$MoS_2$. The Cu/$MoS_2$ sample slip during the COSME-RT process and shearing force applied to the sample was dissipated. The control of the roughness of steel plate is one of solutions to control the sliding of the sample against the steel plate.

# Appendix

## A.1 Summary of Hertzian elastic contact stress formulae

The contact stress of two elastic bodies with curved surfaces can be calculated by using Hertzian elastic contact theory.

Reduced Young's modulus $E^*$ is defined as

$$E^* = \left(\frac{1-{\nu_1}^2}{E_1} + \frac{1-{\nu_2}^2}{E_2}\right)^{-1} \quad \cdots (1)$$

$E_1$ and $E_2$ are Young's module of two elastic bodies. $\nu_1$ and $\nu_2$ are Poisson's ratio of two bodies.

Effective radius $R$ is defined as

$$R = \left(\frac{1}{R_1} + \frac{1}{R_2}\right)^{-1} \quad \cdots (2)$$

$R_1$ and $R_2$ are radiuses of curved surfaces of two bodies. Especially when contact of spherical and flat bodies, $R_2$ is considered as infinite and $1/R_2$ is neglected.

Radius of contact circle $a$ is

$$a = \left(\frac{3PR}{4E^*}\right)^{\frac{1}{3}} \quad \cdots (3)$$

$P$ is the normal load applied to the bodies.

Maximum contact pressure $p_0$ is

$$p_0 = \left(\frac{3P}{2\pi a^2}\right) = \left(\frac{6PE^{*2}}{\pi^3 R^2}\right)^{\frac{1}{3}} \cdots (4)$$

Maximum shear stress $\tau_{max}$ is

$$\tau_{\max} \cong 0.31p_0, \qquad \text{at} \quad r = 0, z = 0.48a \quad \cdots (4)$$

*r* is position and is defined as

$$r = \sqrt{x^2 + y^2} \quad \cdots (5)$$

## A.2 Summary of Hamilton and Goodman's model formulae

According to the Hamilton and Goodman's model, the quasi-static stress field generated on the flat surface by spherical contact is the sum of two stresses (6) which created by frictional force and (7) which created by indentation.

$$\sigma_{yz} = \sigma_{zz} = 0;\ \sigma_{xz} = -\frac{3fP}{2\pi a^3}\sqrt{a^2 - r^2},\ \ r < a \quad \cdots (6)$$

$$\sigma_{yz} = \sigma_{xz} = 0;\ \sigma_{zz} = -\frac{3P}{2\pi a^3}\sqrt{a^2 - r^2},\ \ r < a \quad \cdots (7)$$

*f*, and *a* are the coefficient of friction and the theoretical contact radius calculated by Hertzian elastic contact formula, respectively.

The Cartesian components of the stress field generated by (6) are the imaginary parts of

$$\sigma_{xx} = \frac{3fP}{2\pi a^3}\frac{x}{r^4}\left[\left(4\frac{x^2}{r^2} - 3\right)\left(H\nu - \frac{1}{2}z\frac{\partial H}{\partial z}\right) + y\frac{\partial H}{\partial y} + (1-\nu)x\frac{\partial H}{\partial x} + \frac{1}{2}xz\frac{\partial^2 H}{\partial x \partial z} - 2\nu r^2 F\right] \quad \cdots (8)$$

$$\sigma_{yy} = \frac{3fP}{2\pi a^3}\frac{x}{r^4}\left[\left(4\frac{y^2}{r^2} - 1\right)\left(H\nu - \frac{1}{2}z\frac{\partial H}{\partial z}\right) - \nu y\frac{\partial H}{\partial y} + \frac{1}{2}yz\frac{\partial^2 H}{\partial y \partial z} - 2\nu r^2 F\right] \quad \cdots (9)$$

$$\sigma_{zz} = \frac{3fP}{2\pi a^3}\frac{xz}{r^2}\frac{\partial F}{\partial z} \quad \cdots (10)$$

$$\sigma_{yz} = \frac{3fP}{2\pi a^3}\frac{xyz}{2r^4}\frac{\partial^2 H}{\partial z^2} \quad \cdots (11)$$

$$\sigma_{xz} = \frac{3fP}{2\pi a^3}\frac{1}{r^2}\left[2G + \frac{1}{2}\frac{\partial H}{\partial z} + z\frac{\partial}{\partial x}(xF) - 2\frac{zx^2}{r^2}F\right] \quad \cdots (12)$$

$$\sigma_{xy} = \frac{3fP}{2\pi a^3}\frac{y}{r^4}\left[\left(4\frac{x^2}{r^2} - 1\right)\left(H\nu - \frac{1}{2}z\frac{\partial H}{\partial z}\right) + \frac{1}{2}y\frac{\partial H}{\partial y} + \frac{1}{2}x(1-2\nu)\frac{\partial H}{\partial x} + \frac{1}{2}zx\frac{\partial^2 H}{\partial x \partial z}\right] \quad \cdots (13)$$

where

$$F = \frac{1}{2}(z - ia)R_2 + \frac{1}{2}r^2\ln(R_2 + z_2) \quad \cdots (14)$$

$$G = -\frac{1}{3}{R_2}^3 + \frac{1}{2}zz_2R_2 - \frac{1}{3}ia^3 + \frac{1}{2}zr^2\ln(R_2 + z_2) \quad \cdots (15)$$

$$H = \frac{4}{3}ia^3z - \frac{1}{6}z{R_2}^3 + \frac{1}{2}ia{R_2}^3 - \frac{1}{4}z_2R_2r^2 - \frac{r^4}{4}\ln(R_2 + z_2) \quad \cdots (16)$$

$$R_2 = \sqrt{{z_2}^2 + r^2} \quad \cdots (17)$$

$$z_2 = z + ia \quad \cdots (18)$$

$\nu$ is Poisson's ratio of flat surface. This is same as $\nu_2$ in the Hertzian formula.

The Cartesian components of the stress field generated by (7) are the imaginary parts of

$$\sigma_{xx} = \frac{3P}{2\pi a^3}\left[2\nu K + \frac{1-2\nu}{r^4}\left(y^2G - x^2G + xr^2\frac{\partial G}{\partial x}\right) + \frac{z}{r^4}\left(y^2F - x^2F + xr^2\frac{\partial F}{\partial x}\right)\right] \quad \cdots (19)$$

$$\sigma_{yy} = \frac{3P}{2\pi a^3}\left[2\nu K + \frac{1-2\nu}{r^4}\left(x^2G - y^2G + yr^2\frac{\partial G}{\partial y}\right) + \frac{z}{r^4}\left(x^2F - y^2F + yr^2\frac{\partial F}{\partial y}\right)\right] \quad \cdots (20)$$

$$\sigma_{zz} = -\frac{3P}{2\pi a^3}\left(-K + z\frac{\partial K}{\partial z}\right) \quad \cdots (21)$$

$$\sigma_{yz} = -\frac{3P}{2\pi a^3} z \frac{\partial K}{\partial y} \quad \cdots (22)$$

$$\sigma_{xz} = -\frac{3P}{2\pi a^3} z \frac{\partial K}{\partial x} \quad \cdots (23)$$

$$\sigma_{xy} = \frac{3P}{2\pi a^3} \frac{x}{r^4} \left[ (1-2\nu) \left( -2yG + r^2 \frac{\partial G}{\partial y} \right) + z \left( -2yF + r^2 \frac{\partial F}{\partial y} \right) \right] \quad \cdots (24)$$

where

$$K = z \ln(R_2 + z_2) - R_2 \quad \cdots (25)$$

# References

(1) G. M. Hamilton, L. E. Goodman, The stress field created by a circular sliding contact, Journal of Applied Mechanics, (1996), pp. 371 - 376.

(2) K.L. Johnson, Contact Mechanics, Cambridge University Press, 1987.

# Acknowledgements

Thank you very much for giving me your precious time, all juries, Prof. Toshiyuki Takagi, Prof. Kazuhiro Ogawa, Prof. Yutaka Sato, Prof. Hiroyuki Miki, Dr. Julien Fontaine, and Prof. Clotilde Minfray. The fruitful discussion with you increased the level of my thesis.

Thank you for your support, all laboratory members of Takagi laboratory, Miki laboratory, Uchimoto laboratory, and LTDS.

Extensive studies on the COSME-RT by Prof. Hiroyuku Takeishi of Chiba Institute of Technology, and Prof. Noboru Nakayama and Dr. Masaomi Horita of Shinshu University are gratefully acknowledged. I obtained many knowledges during the life of Nakayama laboratory even it was a short.

Thank you so much for your technical support, Dr. Takamichi Miyazaki.

I think this thesis cannot be carried out without not only scientific but also personal support from many people.

Thank you so much for everything, all other friends and my family, and all people who assisted me.

Thank you father and mother for believing me even when I couldn’t believe myself and times get rough.

Thank you a lot for all people.

January 16, 2018
Sendai, Japan
Sho TAKEDA